NEURONAL MECHANISM OF STATE CONTROL IN *DROSOPHILA MELANOGASTER*

Thesis by

Hidehiko K. Inagaki

In Partial Fulfillment of the Requirements for the degree

of

Doctor of Philosophy

CALIFORNIA INSTITUTE OF TECHNOLOGY

Pasadena, California

2014

(Defended October 22nd, 2013)

ACKNOWLEDGEMENTS

First and foremost, I would like to thank my thesis advisor, David Anderson, for his generous support throughout my graduate school years. I first visited him and his lab in the fall of 2006 as a collaborator for my undergraduate project at the University of Tokyo. He offered me an opportunity to give a presentation in his lab, and time to meet one-to-one to discuss the project. I was deeply impressed by his exuberant energy and passion for science. This was the moment I decided to come to Caltech to join his lab. He is not only curious and knowledgeable about broad topics in biology, but also creative, careful and a logical thinker. Both discussions with him and criticism by him, have always been helpful to elucidate my thoughts and figure out the right research direction. Unlike many of the big bosses in science, he never forced me to pursue a certain research direction. Instead, he always let me try my own ideas. He often told me, "Do whatever you think is important and fun." This freedom and self-responsibility helped me train myself to be an independent researcher. His broad interests are not only restricted to science, but also to Japanese culture, such as samurai movies, swords, sake, etc. Our trip to Kamakura visiting a sword smith is one of my most pleasant memories with him. I cannot think of anyone who could have been a better mentor than him, and I will always be grateful for his mentorship.

Besides David, I would like to thank all my committee members: Dr. Kai Zinn, Dr. Michael Elowitz and Dr. David Prober. Their divergent perspectives and opinions were always invaluable.

I am also thankful for all the members in the Anderson's lab. Special thanks to Allan M. Wong for lots of fun collaborations and for efforts teaching me calcium imaging. Shlomo Ben Tabou de Leon was another great collaborator who taught me electrophysiology. Thai Truong let me use his amazing microscope. I was incredibly lucky to have a chance to work with amazingly talented students, Yonil Jung, Ketaki Panse and Neeli Mishra. Kiichi Watanabe gave me a lot of insightful input on molecular biology. Robert Robertson was a great help in developing GUI for MATLAB programs. All the former and current members of fly-subgroup people in our lab were helpful and generous to share reagents: Allan, Kiichi, Shlomo, Eric Hoopfer,

Greg Suh, Timothy Tayler, Tim Lebestky, Anne Hergarden, Suzie Yorozu, Liming Wang, Rod Lim, Tyler Gibson, Kenta Asahina, Brian Duistermars, and Barret Pfeiffer. Discussions with lab members including mice subgroup were always enjoyable and productive: Sophia Vrontou, Haijiang Cai, Todd Anthony, Hyosang Lee, Li-Ching Lo, Prabhat Kunwar, Dong Wook Kim, Ryan Remedios, Moriel Zelikowsky and Weizhe Hong. I also would like to thank Gina Mancuso, Gaby Mosconi, Holly Oates-Barker, and Celine Chiu for their administrative help and with ordering.

I am grateful to the many teachers, mentors and friends during various stages of my education. I am especially thankful for my late grandfather, Katsuhiko Inagaki. He was a great medical doctor and a highly accomplished scientist, who invited me to the world of science. He taught me how to use microscopes when I was in primary school, and kept encouraging me to be a scientist. Hideki Ishikawa, my biology teacher in junior high and high school, introduced me even further into Biology. I do not think any other high school teachers in the world encourage kids to read "Molecular Biology of the Cell." Drs. Tatsuhiko Kodama, Juro Sakai, Toshiya Tanaka, and Tetsu Akiyama at the University of Tokyo were generous mentors to allow an undergraduate student work in their lab. It was an invaluable experience to do research in Dr. Kei Ito's lab and Dr. Hitoshi Sakano's lab for my undergrad thesis. I would like to say special thanks to Drs. Kei Ito, Azusa Kamikouchi, Hideo Otsuna and other Kei Ito's lab members. Without them it was impossible to publish a Nature article during my undergraduate years.

I deeply appreciate Nakajima Foundation for supporting me for five years.

Last but not least, I would like to thank my family members for continuous support throughout my life. My parents always believed in me and encouraged me to do what I believed I should do. I especially want to thanks my fiancé, Miho Suzuki, who has been patient during our long distance relationship. She has always supported me and given me a sense of relief. She has brought me happiness into my life. I am looking forward to our wedding and new life at Janelia Farm Research Campus. I would like to dedicate this dissertation to her.

ABSTRACT

The changes in internal states, such as fear, hunger and sleep affect behavioral responses in animals. In most of the cases, these state-dependent influences are "pleiotropic": one state affects multiple sensory modalities and behaviors; "scalable": the strengths and choices of such modulations differ depending on the intensity and imminence of demands; and "persistent": once the state is switched on the effects last even after the internal demands are off. These prominent features of state-control enable animals to adjust their behavioral responses depending on their internal demands. Here, we approached the neuronal mechanisms of state-controls by investigating energy-deprived state (hunger state) and social-deprived state of fruit flies, *Drosophila melanogaster*, as prototypic models.

Neuromodulators, such as biogenic amines and neuropeptides, play an important role in encoding or mediating internal states with their ability to change response properties of neurons. However, establishing the behavioral relevant, circuit level mechanisms of action of neuromodulators remains challenging. In the first chapter, I describe a novel, genetically based method to map, in an unbiased and brain-wide manner, sites of neuromodulation under different conditions in the *Drosophila* brain. This method, and genetic perturbations, reveal that the well-known effect of hunger to enhance behavioral sensitivity to sugar is mediated, at least in part, by the release of dopamine onto primary gustatory sensory neurons, which enhances sugar-evoked calcium influx. These data introduces a new methodology that can be extended to other neuromodulators and model organisms.

Following up the findings in the first chapter, we approached the neuronal circuits modulating feeding decision in hungry flies, in the second chapter. For feeding decisions, animals detect both attractive and aversive gustatory cues. We found that energy demands, or hunger state, modulates this decision making process by tuning sensitivities to sugar and toxic substances in opposite directions in *Drosophila melanogaster*. Moreover, we identified two distinct neuromodulatory pathways that regulate these two gustatory modalities during hunger. The neuropeptide F (NPF) – dopamine (DA) pathway increases sugar

sensitivity under mild starvation, while the adipokinetic hormone (AKH)- short neuropeptide F (sNPF) pathway decreases bitter sensitivity under severe starvation. Effects of both of the pathways are mediated by modulation of the gustatory sensory neurons, which reinforce the concept that sensory neurons constitute an important locus for state-dependent control of behaviors. These two pathways are recruited under different levels of energy demands without any cross interaction. Our data suggests that multiple independent neuronal pathways are underlying pleiotropic and scalable effects of the hunger state. Moreover, these findings added to a growing body of information indicating that neuromodulators are mediating the state-detection and the behavioral changes.

In the last chapter, we sought to approach persistent effects of state control by developing optogenetic tools in *Drosophila*. Optogenetics allows the manipulation of neural activity in freely moving animals with millisecond precision, but its application in *Drosophila* has been limited. Here we show that a recently described Red activatable Channelrhodopsin (ReaChR) permits activation of CNS neurons in freely behaving adult flies, at wavelengths that do not interfere with normal visual function. This tool affords the opportunity to control neural activity with millisecond time resolution over a broad dynamic range of stimulation intensities. Using such time-resolved activation, we show that the neural control of male courtship song can be separated into probabilistic/biasing, and deterministic/command-like components. The former, but not the latter, neurons are subject to functional modulation by social experience, supporting the idea that they constitute a locus of state-dependent influence. Interestingly, moreover, brief activation of the former, but not the latter, neurons trigger persistent behavioral response for more than 10 min. Although the mechanism is still unclear, this finding provides a new model system to study the neuronal mechanism of persistent activity.

Altogether, these findings and new tools described in this dissertation offer new entry points for future researchers to understand the neuronal mechanism of state control.

TABLE OF CONTENTS

LIST OF ILLUSTRATIONS

Chapter 1

Chapter 2

Chapter 3

Chapter I

VISUALIZING NEUROMODULATION IN VIVO: TANGO-MAPPING OF DOPAMINE SIGNALING REVEALS APPETITE CONTROL OF SUGAR SENSING

SUMMARY

Behavior cannot be predicted from a "connectome," because the brain contains a chemical "map" of neuromodulation superimposed upon its synaptic connectivity map. Neuromodulation changes how neural circuits process information in different states, such as hunger or arousal. Here we describe a genetically based method to map, in an unbiased and brain-wide manner, sites of neuromodulation under different conditions in the *Drosophila* brain. This method, and genetic perturbations, reveal that the well-known effect of hunger to enhance behavioral sensitivity to sugar is mediated, at least in part, by the release of dopamine onto primary gustatory sensory neurons, which enhances sugar-evoked calcium influx. These data reinforce the concept that sensory neurons constitute an important locus for state-dependent gain-control of behavior, and introduce a new methodology that can be extended to other neuromodulators and model organisms.

Inagaki HK, Ben-Tabou de-Leon S, Wong AM, Jagadish S, Ishimoto H, Barnea G, Kitamoto T, Axel R, Anderson DJ. Visualizing neuromodulation in vivo: TANGO-mapping of dopamine signaling reveals appetite control of sugar sensing. *Cell*. 2012 Feb 3;148(3):583-95. doi: 10.1016/j.cell.2011.12.022.

INTRODUCTION

The physiological responses of an animal's nervous system to sensory stimuli can differ, depending on internal states such as hunger or arousal (Chiappe et al., 2010; Dubner, 1988; Maimon et al., 2010; Niell and Stryker, 2010; Shea and Margoliash, 2010; Tsuno and Mori, 2009). Such state-dependent influences enable animals to adjust their behavioral response to metabolic, emotional, attentional or other demands. Neuromodulators, such as biogenic amines and acetylcholine, as well as neuropeptides, play a major role in encoding or mediating internal states (Harris-Warrick and Marder, 1991; Pfaff et al., 2008), by altering the input-output properties of specific neural circuits (Birmingham and Tauck, 2003; Marder and Bucher, 2007) .

Hunger and satiety represent a prototypic model for an internal state(s) that influences behavior. In the vinegar fly *Drosophila melanogaster*, for example, food deprivation is known to affect olfactory sensitivity (Root et al., 2011), formation and expression of food-associated memory (Krashes et al., 2009), the extent of feeding (Riemensperger et al., 2011) and locomotor activity (Lee and Park, 2004; Meunier et al., 2007) . In addition, in *Drosophila* (Scheiner et al., 2004) as well as in other species (Berridge, 1991; Dethier, 1976; Gillette et al., 2000; Moskowitz et al., 1976; Moss and Dethier, 1983; Page et al., 1998) starvation changes the consummatory response to tastants, typically by enhancing the acceptance of energy resources such as sugar, with an associated increased tolerance for bitter-tasting contaminants. This dramatic starvation-dependent shift in sensitivity to sweet vs. unpalatable and potentially toxic energy resources illustrates how state-dependent control of behavior is critical for survival.

Despite the importance of hunger for regulating animal behavior, we know relatively little about the circuit-level mechanisms underlying such regulation. Studies in blowflies and honeybees have demonstrated that biogenic amines can modulate feeding-related behaviors (Brookhart et al., 1987; Long et al., 1986; Scheiner et al., 2002). Whether such modulators actually mediate the effect of hunger on these behaviors, however, has been more difficult to establish in these systems due to the lack of genetic tools. It has also been challenging to identify the circuitry through which such modulators mediate behavioral responses to starvation. Modulatory neurons often exhibit widespread projections throughout the brain (Mao and Davis, 2009; Monastirioti, 1999) and act via multiple receptors. Identifying the behaviorally relevant circuitry on

which a given modulator acts, and demonstrating that such modulation is required for a specific state-dependent influence on a specific behavior *in vivo,* has been achieved in only a few cases (Crocker et al., 2010; Kong et al., 2010; Krashes et al., 2009; Lebestky et al., 2009; Root et al., 2011) .

Drosophila provides an attractive system to address the circuit-level mechanisms underlying neuromodulation of feeding behavior, because of the availability of powerful genetic tools and our growing understanding of the gustatory receptors and neural circuitry that control feeding in this species (Dahanukar et al., 2007; Gordon and Scott, 2009; Marella et al., 2006; Montell, 2009; Scott et al., 2001; Thorne et al., 2004; Wang et al., 2004; Weiss et al., 2011). Although several neuropeptides, as well as biogenic amines, have been implicated in mediating the influence of food-deprivation on feeding behavior in *Drosophila* (Nassel and Winther, 2010), with few exceptions (Root et al., 2011; Wu et al., 2005) the circuit-level mechanisms underlying their influences remains poorly understood.

Here we have developed and applied a method, called TANGO-map, to detect the release of endogenous neuromodulators *in vivo*, and identify the circuits on which they act. We have used this method to examine the mechanisms that underlie a starvation-induced change in a feeding behavior in *Drosophila.* Our results identify a hunger-dependent, dopamine-mediated gain-control of behavior at the level of primary gustatory sensory neurons. They also provide proof-of-principle for a methodology that may have general applicability in the genetic dissection of circuit-level neuromodulatory mechanisms.

RESULTS

Design and validation of a *Drosophila* Dopamine Receptor-Tango system *in vitro*

We sought to develop a genetically based tool that reports endogenous neuromodulator release and sites of action *in vivo,* with anatomic specificity. To do this, we adapted to *Drosophila* the Tango system (Barnea et al., 2008), which transforms a transient ligand/receptor interaction into a stable, anatomical readout of reporter gene expression. The reporter gene is activated by a "private," synthetic signal transduction pathway, using a bacterial transcription factor (lexA) that is covalently coupled (via a specific tobacco etch virus (TEV) protease-sensitive cleavage site) to the exogenous dopamine receptor expressed in the cells of interest (Fig. 1B). The transcription factor is cleaved from the dopamine receptor following ligand binding, by recruitment of an arrestin-TEV protease fusion protein, and translocates to the nucleus where it activates a lexAop-driven reporter. This system was originally developed to detect receptor activation in cultured mammalian cell lines (Barnea et al., 2008), but whether it could also be used to detect receptor activation *in vivo* was not clear.

To adapt this system to identify circuit-level sites of endogenous neuromodulator action in *Drosophila in vivo*, we generated a Tango system for dopamine (DA) (DopR-Tango), using the *Drosophila* DA receptor DopR1 (Gotzes et al., 1994; Sugamori et al., 1995) and *Drosophila* Arrestin1 (Figure 1A). Here, LexA is used as the tethered transcription factor. Stoichiometric co-expression of the Arrestin-TEV protease fusion was achieved using a 2A peptide (Szymczak and Vignali, 2005), which we have shown to permit bi-cistronic expression in *Drosophila* (Figure S1A-C).

To test whether DopR-Tango specifically reports cellular activation by DA, we co-expressed DopR-Tango in human embryonic kidney (HEK) 293 cells with a *lexAop-β-galactosidase* (*β-gal*) reporter. Treatment of these cells with DA or a DopR1 agonist (6,7-ADTN) resulted in a dose-dependent increase in reporter gene expression (Figure 1C). The EC_{50} of DopR1-Tango to DA and the D1 agonist are c.a. 1 μM in

this experiment, similar to values previously reported in insect cell lines (Sugamori et al., 1995). In contrast, neuromodulators that are not ligands for DopR1, such as 5-HT or Octopamine (OA), did not induce reporter gene expression (Figure 1C). Together, these results indicate that (1) a *Drosophila* DA receptor and arrestin can be successfully used to generate a functional Tango system; (2) *Drosophila* DopR-Tango can activate reporter expression in response to DA receptor ligands, in a dose-dependent manner and (3) DopR-Tango maintains the ligand specificity of the original DA receptor. Analogous results in HEK293 cells were obtained with a Tango system constructed using a *Drosophila* OA receptor (OctR-Tango) (data not shown).

DopR-Tango induces reporter expression in a ligand-specific manner in *Drosophila in vivo*

We chose *Drosophila* as a model to test whether the Tango system can report ligand activity *in vivo.* To do this, we generated transgenic flies that express DopR-Tango components under the control of *elav-GeneSwitch* (*elav-GS*), a pan-neuronally expressed, hormone- (RU486) inducible form of GAL4 (GAL4-PR) (Osterwalder et al., 2001). This transgenic line (referred to subsequently as "DopR-Tango flies"), also contains a *lexAop-mCD2::GFP* transgene that encodes a membrane-tethered form of GFP, as the Tango reporter. The use of an inducible GAL4 was based on the assumption that background signal would be minimized by restricting expression of the DopR-Tango system to a 24 hr period just prior to the experimental manipulation, thereby avoiding developmental accumulation of the reporter.

After feeding with RU486 for 12-24 hrs, widespread expression of DopR-Tango was detected throughout the brain by immunostaining with an antibody to an HA epitope-tag present on LexA (Figure $1D_2$). Importantly, widespread brain expression of the GFP Tango reporter was also observed (Figure $1D_1$), beginning at 12 hr and peaking at 36 hrs after the onset of Tango expression (Figure S1E). The pattern of reporter expression was not identical to that of the HA-tag, due to the different subcellular localization of the two markers (membrane vs. nuclear; Figure $1D_3$). Expression of the GFP reporter was not detected in control flies that expressed DopR fused to LexA without the Arrestin-TEV protease fusion protein (Figure S1D). These data indicate that GFP expression in DopR-Tango flies is Arrestin-TEV protease-dependent, and not due to basal transcription of the *lexAop-mCD2::GFP* reporter transgene, or TEV-protease independent cleavage of TEVcs-LexA.

To investigate if Tango reporter expression in flies can report changes in levels of endogenous DA signaling, we examined expression of the reporter after drug treatments. Feeding DopR-Tango flies with L-dopa, a precursor of DA that is known to increase DA levels in the fly brain (Bainton et al., 2000), for 2 days after RU486 treatment, caused a statistically significant increase in reporter expression in various neural structures including the antennal lobe (AL), the sub-oesophageal ganglion (SOG), and β and γ lobes of the mushroom body (MB) ((Figure $2A_{2-3}$, $2B_{1-4}$, S2E; see Figure S2A-C for details of GFP reporter quantification) . This increase, moreover, was reduced by SCH23390 (Sugamori et al., 1995), a D1 receptor antagonist, to a statistically significant extent in the AL (Figure $2B_1$) and MB β lobe (Figure $2B_3$), and exhibited a trend to reduction that did not reach significance in the SOG (Figure $2B_2$) and MB γ lobe (Figure $2B_4$). The dynamic range of this reporter (2-15 fold; Figure $2B_{1-4}$) is similar to that of the best currently available genetically encoded calcium indicators (GECIs) (Tian et al., 2009), although the signal-to-noise ratio (SNR; c.a. 4) is lower (see Supplemental Experimental Procedures). These data confirm that DopR-Tango can read out a statistically significant increase in reporter gene expression in response to an experimentally induced increase in DA levels *in vivo*.

We also investigated the source of the baseline expression of the Tango reporter observed in un-manipulated flies (Figure $2A_2$). Genetic elimination of DA in DopR-Tango flies was not feasible, as null mutations in *Tyrosine hydroxylase (Th)* are embryonic lethal (Riemensperger et al., 2011). Instead, we fed flies with SCH23390, or the DA synthesis inhibitor, 3-iodotyrosine (3IY) (Bainton et al., 2000). SCH23390 feeding significantly decreased, but did not abolish, Tango reporter expression in both the AL and SOG (Figure $2C_1$ and $3C_1$). 3IY feeding also decreased reporter expression in the AL (Figure $2C_2$) in statistically significant manner, but the decrease in the SOG did not reach significance (Figure $3C_2$). The incomplete effects of the antagonist to inhibit basal (as well as L-dopa-induced; Figure $2B_{1-4}$) expression of the reporter may reflect limits on the effective levels of the drug that can be achieved *in vivo*, due to instability, non-specific absorption or toxicity. Alternatively, it may reflect some level of DA-independent expression of the Tango reporter, for example due to ligand-independent binding of Arrestin-TEVp to DopR-Tango. Whatever the explanation, these results indicate that the level of baseline GFP reporter expression in DopR-Tango flies is, at least in part, a reflection of endogenous DA signaling in the brain.

DopR-Tango reporter expression also exhibited ligand specificity *in vivo*. When DopR-Tango flies were fed with either L-dopa or chlordimeform (CDM), an OA receptor agonist, only L-dopa feeding increased expression of the reporter in the SOG (Figure $2D_2$). L-dopa feeding also yielded an increase in DopR-Tango reporter signal in the AL (Figure $2D_1$), but in this case a smaller but still significant induction was observed using CDM. This difference may reflect an indirect effect of CDM to increase dopaminergic signaling in the AL, given that OA did not activate DopR-Tango *in vitro* (Figure 1C). In OctR-Tango flies fed with L-dopa or CDM, only CDM increased expression of the GFP reporter in the AL (Figure S2D). These data suggest that *in vivo*, as well as in HEK293 cells, DopR-Tango can specifically report an artificially induced increase in DA signaling

DopR-Tango reveals increased dopamine release onto primary gustatory neurons during starvation

To investigate whether DopR-Tango can identify neural circuits that are targets of modulation by endogenous DA, we exposed DopR-Tango flies to various treatments and looked for increases in reporter expression. Wet starvation of DopR-Tango flies for 2 days produced a statistically significant increase in GFP expression in the SOG, the primary gustatory center (Figure 3A and $3C_{1-2}$), but not in the MB β and γ lobes or the AL (Figure $3D_{1-3}$). Inclusion of the DopR antagonist SCH23390, or the DA synthesis inhibitor 3IY, abolished the starvation-induced increase in GFP expression in the SOG (Figure $3C_{1-2}$). Based on the time-course of Tango reporter expression, we estimate that the enhanced GFP expression likely reflects cumulative DopR-Tango activation integrated over the first 24 hrs of food deprivation (Figure S1E).

Two lines of evidence suggest that the starvation-induced increase in GFP expression in the SOG occurs, at least in part, in the terminals of primary gustatory receptor neurons (GRNs). First, the pattern of Tango reporter expression in the SOG resembled that of the projections of sugar-sensing GRNs, as visualized using a *Gr5-GAL4* transgene specifically expressed in these neurons (Wang et al., 2004) to drive mCD8::GFP expression (Figure $3B_1$). Second, surgical removal of the labellum (tip of proboscis, a mouth part of a fly; Figure S3A), which contains the cell bodies of GRNs, strongly reduced Tango reporter expression (Figure $3B_{2-3}$).

Starvation and L-dopa both increase behavioral sensitivity to sucrose

The proboscis extension reflex (PER; Figure S3A) (Dethier, 1976), is a simple feeding behavior elicited by presentation of sugar to Gr5a-expressing GRNs located in the labella or legs (Gordon and Scott, 2009; Marella et al., 2006). In *Drosophila*, the sucrose-sensitivity of the PER (elicited from the legs) has been reported to increase with the duration of food-deprivation (Scheiner et al., 2004), although a direct comparison to unstarved flies was not performed. Surprisingly, an effect of starvation to enhance the PER in response to activation of labellar sugar receptors has not previously been reported in this species. Therefore, to identify a behavioral correlate of the starvation-induced Tango signal on labellar sugar-sensing GRNs, we first investigated whether starvation indeed increases the sensitivity of the PER to sucrose applied to labellar taste receptors.

Wet starvation indeed increased the fraction of flies exhibiting a PER across a broad range of sugar concentrations (Figure $4A_1$), while decreasing sensitivity to bitter tastants (H.K.I. and D.J.A. unpublished result). In addition, the mean acceptance threshold (MAT; the sucrose concentration at which the probability of a PER response at the population level is 50%; see Figure S3B-D and Supplemental Experimental Procedures) (Long et al., 1986) significantly decreased as the starvation time was increased from 1 to 2 days (Figure $4A_2$; note that the y-axis/ordinate is inverted: when sensitivity increases the threshold decreases). This increase in sugar sensitivity is gradual and reversible (Figure S3E; significant changes observed as early as 6 hours of wet starvation). Thus, *Drosophila* exhibits a starvation-induced enhancement of PER behavior induced by sucrose applied to labellar GRNs, whose magnitude depends on the duration of food-deprivation.

Because our DopR-Tango results suggested that $Gr5a^+$ GRNs may be a target of dopaminergic regulation, we next asked whether experimental elevation of DA levels in fed flies would mimic the effect of food-deprivation to enhance the PER. We performed such an elevation in two ways: pharmacologically and genetically. After two days of L-dopa feeding, we observed a dose-dependent increase in PER sugar sensitivity similar to that produced by starvation (Figure $4B_{1-2}$). The sugar sensitivity of the PER was also increased in fed flies by artificial activation of dopaminergic neurons using dTRPA1, a *Drosophila* thermosensitive cation channel (Hamada et al., 2008), expressed under the control of *Th-GAL4* (Friggi-Grelin et al., 2003) (Figure $4C_{1-3}$). This behavioral phenotype was detectable within 10 min of the temperature shift

to 27^{o}C. Together, these data indicate that elevating endogenous levels of DA can increase behavioral sensitivity to sucrose in fed flies, mimicking the effect of starvation. Importantly, DopR-Tango flies also showed a starvation-induced increase in the sugar-sensitivity of the PER (Figure S3F$_{1-2}$), indicating that expression of this detector system in GRNs does not impair the physiological function of these neurons in feeding behavior.

The DA receptor DopEcR expressed in sugar sensing GRNs mediates the effect of L-dopa feeding to enhance the PER

Given that both starvation and the experimental elevation of endogenous DA levels increase DopR-Tango reporter levels on sugar-sensing GRNs, and also enhance the PER, we next investigated whether DA receptors expressed in GRNs mediate this behavioral effect. We approached this objective by: 1) identifying the DA receptors expressed in sugar-sensing GRNs; 2) testing whether genetic inactivation of any of these receptors blocks the effect of L-dopa feeding to enhance the PER; 3) testing whether the same genetic manipulations block the effect of starvation to enhance the PER.

In the absence of immune reagents specific for each of the DA receptor subtypes, we investigated whether GRNs normally express any of the 4 known *Drosophila* DA receptors (Gotzes et al., 1994; Han et al., 1996; Hearn et al., 2002; Srivastava et al., 2005), by carrying out Q-RTPCR experiments using RNA isolated from sugar-sensing GRNs via the "TU-tagging" method (See Supplemental Experimental Procedures; (Miller et al., 2009)). qPCR of cDNA synthesized from this RNA showed a 10-fold enrichment for *Gr5a* mRNA itself, relative to mRNA encoding the bitter sensing receptor, *Gr66*, which is not expressed in sugar sensing neurons (Figure S4A). This result implied successful synthesis of cDNAs enriched in sugar sensing neurons. qPCR analysis of this cDNA revealed that 3 of the 4 *Drosophila* DA receptors, namely *DopR1*, *D2R* and *DopEcR*, are expressed in *Gr5a* GRNs to varying levels, while *DopR2* mRNA was not detectable (Figure S4A).

We next asked whether any of the 3 DA receptors expressed in Gr5a GRNs is required for the effects of L-dopa feeding or starvation to enhance sugar sensitivity. In flies bearing a hypomorphic mutation in *DopEcR*, *DopEcR*^{c02142} (Fig. S4B; Ishimoto et al., *in prep*) (Thibault et al., 2004), L-dopa feeding failed to

produce an increase in sugar sensitivity (Figure $5A_{2-3}$). Moreover, expression of a *DopEcR* RNAi using pan-neuronal Gal4 driver, *neuronal synaptobrevin* (*nsyb*)-*GAL4* (Pauli et al., 2008) (Fig. S4C), similarly blocked the effect of L-dopa to enhance the PER (Figure $5B_{1-4}$). By contrast, flies bearing a hypomorphic mutation in *DopR1* (Lebestky et al., 2009) showed a normal L-dopa-dependent increase in sugar sensitivity (Figure S4D), as did flies with a pan-neuronal RNAi-mediated knock down of D2R (Figure $S4E_{1-3}$).

Importantly, cell-specific knock-down of DopEcR in *Gr5a* GRNs also prevented the L-dopa feeding-induced enhancement of the sugar sensitivity of the PER, while control flies expressing either *UAS-GFP* or *UAS-DopR2 RNAi* showed a statistically significant enhancement of PER behavior by L-dopa (Figure $5C_{1-4}$). The MAT of vehicle-fed flies of both the *DopEcR* RNAi and *DopEcR* mutant genotypes was not significantly different from that of the genetic control flies (Figure $5A_3$, $5B_4$ and $5C_4$), indicating that DopEcR is not necessary for baseline PER behavior *per se*, but rather for its enhancement by L-dopa feeding. Taken together, these data indicate that DopEcR expressed in *Gr5a* GRNs is necessary for the effect of L-dopa feeding to increase sugar sensitivity.

DopEcR expressed in sugar-sensing GRNs is required for the effect of starvation to enhance PER behavior

Having demonstrated that DopEcR in *Gr5a* neurons is necessary for the effect of L-dopa feeding to enhance the sugar sensitivity of the PER, we next tested whether DopEcR in *Gr5a* GRNs is also necessary for starvation to exert the same behavioral effect. Indeed, in flies wet-starved for 6 hours, *DopEcR* mutant flies failed to exhibit an increase in sugar sensitivity, in contrast to wild-type controls (Figure $5D_{1-2}$). Importantly, this phenotype could be rescued by specific expression in *DopEcR* mutant flies of a *UAS-DopEcR* transgene in *Gr5a* neurons (Figure $5D_3$). Over-expression of DopEcR, (but not of DopR1) in *Gr5a* neurons of $DopEcR^+$ flies also enhanced the sucrose sensitivity of the PER in starved, but not in fed, animals (Figure $S4H_{1-4}$ and $S4I_{1-3}$).

Finally, specific knock-down of *DopEcR* in sugar sensing neurons using RNAi also strongly attenuated the increase in sugar sensitivity caused by 6 hours of starvation (Figure $5E_{1-3}$). Thus, both selective rescue of the *DopEcR* mutant phenotype, and selective expression of RNAi, implicate Gr5a neurons as a site

of DopEcR action. Interestingly, although the *DopEcR* mutation and RNAi both impaired PER enhancement by 48 hrs of L-dopa feeding, they did not do so in flies wet-starved for 24 hrs or more (Figure $S4F_{1-3}$ and $S4G_{1-3}$). This observation suggests either a time-dependent recruitment of redundant DA receptors, or of DA-independent mechanisms, mediating enhanced sugar sensitivity at later stages of starvation. Flies lacking both *DopEcR* and *DopR1* did not show an impaired PER response after 24 hrs of starvation, suggesting the involvement of additional neuromodulators (data not shown). Whatever the explanation, at early times of starvation DA, acting through DopEcR expressed in *Gr5a* GRNs, is required for enhancement of PER behavior.

Cellular mechanism of the starvation-induced increase in behavioral sensitivity to sucrose

Lastly, we approached the cellular mechanism through which starvation and DA enhance the sugar-sensitivity of the PER. As a first step, we asked whether starvation and DA act to modify the activity of gustatory receptors (GRs) themselves, or rather on a downstream physiological process. To do this, we bypassed the requirement for GR activation in the PER response using Channelrhodopsin 2 (ChR2), a light sensitive cation channel (Zhang et al., 2006), to artificially activate sugar-sensing GRNs (*Gr5a-GAL4; UAS-ChR2*) (Zhang et al., 2007).

Increasing the strength of blue light illumination (from 1.6 to 2.9 mW/cm^2) increased the fraction of flies exhibiting a PER (Figure $6A_1$), similar to the effect of stimulating the labellum with increasing sugar concentrations. Strikingly, both wet-starved and L-dopa fed *Gr5a-GAL4;UAS-ChR2* flies showed an increased light sensitivity of the PER, compared to control non-starved flies (Figure $6A_2$). These data suggest that both starvation and DA enhance sugar sensitivity by acting downstream of the sugar sensing receptors themselves. Consistent with this idea, extracellular recordings from GRN somata in the labella indicated no change in the frequency of sucrose-evoked spiking in wet-starved vs. control fed flies (Figure S5A-B).

To pin down the physiological mechanism underlying starvation-dependent enhancement of PER behavior, we tested whether starvation and DA augment pre-synaptic Ca^{2+} influx in sugar-sensing GRNs. For this purpose, we performed calcium imaging, using two-photon microscopy, of sugar-sensing GRNs in flies expressing a genetically encoded calcium sensor (GCaMP3.0 (Tian et al., 2009)) under the control of *Gr5a-*

GAL4. Delivery of increasing concentrations of sucrose (from 0 mM to 400 mM) to the labellum yielded increasing GCaMP 3.0 fluorescence signal in *Gr5a*-expressing nerve fibers in the SOG (Figure 6B-D), consistent with a previous report (Marella et al., 2006). Strikingly, both wet-starved and L-dopa fed flies showed a statistically significant enhancement of sucrose-evoked GCaMP fluorescence, compared to non-starved control flies, at 100 mM sucrose, and a non-significant trend to enhancement at 400 mM sucrose (Nusbaum and Beenhakker, 2002) (Figure 6D).

A scatter-plot of integrated GCaMP fluorescence signal intensity vs. the fraction of flies showing a PER response at each sucrose concentration revealed a strong positive correlation between the two measures (R^2=0.969) (Figure 6E). The simplest interpretation of this correlation is that the starvation-induced enhancement of calcium influx in sugar-sensing GRNs underlies the parallel enhancement of PER behavior.

Finally, to examine more directly whether DA acts on $Gr5a^+$ GRNs to modulate Ca^{2+} influx, we compared the sugar responses of these GRNs before vs. after exposure to 1mM DA in the bath. Following 5 min of such exposure, there was a ~1.2 fold increase in basal Ca^{2+} influx, and a ~1.3-1.4 fold influx in Ca^{2+} influx caused by 400mM sucrose; the fold increase at 400mM sucrose was significantly higher than at 0mM sucrose ($p<0.05$, Wilcoxon matched pairs test) (Figure $6F_1$, 6G). Importantly, RNAi-mediated knockdown of DopEcR expression in sugar-sensing GRNs attenuated this increase in Ca^{2+} influx (Figure $6F_2$, and 6G). These data indicate that DA acts directly on Gr5a GRNs via DopEcR to enhance both baseline and sucrose-induced increases in intracellular free Ca^{2+}.

DISCUSSION

Drosophila is a potentially powerful model system for understanding how neuromodulators control state-dependent changes in behavior. However establishing the behaviorally relevant, circuit-level mechanisms of action of neuromodulators remains challenging. This is partially because standard methods used to measure the release of endogenous neuromodulators in vertebrates, such as fast-scan cyclic voltammetry (Phillips et al., 2003) or micro-dialysis (Benveniste and Huttemeier, 1990), are of limited applicability in *Drosophila*. Moreover, such methods cannot identify the neurons on which released neuromodulators act. The data presented here provide proof-of-principle for the utility of a new method, called TANGO-map, to identify, in a brain-wide and relatively unbiased manner, circuit-level substrates of neuromodulation relevant to a particular state-dependent influence on behavior.

Starvation regulates gustatory sensitivity in *Drosophila* and causes DA release onto sugar-sensing GRNs

We show here that sweet taste-sensitivity in the labellum is enhanced with increasing duration of food-deprivation in *Drosophila*. This observation confirms and extends previous reports in *Drosophila* (Meunier et al., 2007; Scheiner et al., 2004), and is consistent with observations in many other animal species (Dethier, 1976; Moskowitz et al., 1976; Page et al., 1998). We have used this phenomenon as a prototypic case of a state-dependent change in behavior, to investigate the ability of TANGO-map to identify underlying neuromodulatory mechanisms.

Our results indicate that starvation enhances endogenous DA release onto primary GRNs, as detected by increased expression of the DopR-Tango reporter *in vivo*. In contrast, starvation did not increase the DopR-Tango reporter in the MB or AL, although L-dopa feeding did so. These data indicate that DopR-Tango is capable of revealing selective sites of endogenous DA release in a brain-wide manner, under specific behavioral conditions.

DA release onto sugar-sensing GRNs is required for the behavioral effect of starvation to enhance PER sensitivity

Our results indicate that a mutation in the DA receptor *DopEcR,* as well as specific knock-down of this receptor in sugar-sensing GRNs, eliminates the effect of starvation to enhance the sucrose-sensitivity of the PER. However, this phenotype was only observed at 6 hr of starvation; after 24 hr of food deprivation these genetic manipulations no longer had an effect. This is not because these manipulations themselves became ineffective at later times, since the same manipulations did attenuate the increased PER sensitivity caused by L-dopa feeding for 24 hr. This suggests that at an early stage of starvation, DA is necessary to enhance the sugar sensitivity of the PER, while at later stages additional factors come into play (Figure 6H).

The slow kinetics of Tango reporter accumulation (Supplementary Figure S1E) preclude the detection of statistically significant increases in signal as early as 6 hr following an experimental manipulation. However, the level of reporter expression detected in animals examined after 48 hrs of treatment likely reflects the integration of increases in dopaminergic signaling occurring throughout the first 12-24 hr of the treatment period (Supplementary Figure S1E). Thus, although we detected an increase in DopR-Tango signal at a starvation timepoint when genetic reduction of *DopEcR* levels no longer impaired the behavioral effect of starvation, and observed a behavioral phenotype at a time point too early to be evaluated directly by the TANGO-map method, this should not be taken to imply that no DA release occurred after 6 hrs of starvation. Importantly, given the kinetics of the system, the DopR-Tango signals we detect *in vivo* are likely to reflect primarily changes in tonic levels of DA signaling, rather than brief episodes of phasic DA release. Further improvements of the TANGO-map method are required to increase its temporal resolution. Nevertheless, the present methodology provides a powerful method to identify sites where dopaminergic modulation of a given behavior may occur, even if it cannot reveal precisely how quickly such regulation is exerted.

Mechanism of dopaminergic regulation of GRN sensitivity

Several lines of evidence suggest that the dopaminergic modulation of sugar-sensing GRNs revealed here may involve an enhancement of Ca^{2+} influx at the nerve terminal. Both starvation and L-dopa feeding

increased sucrose-evoked Ca^{2+} influx, without changing the frequency of action potentials measured extracellularly at GRN somata (Figure S5), despite a previous report to the contrary (Meunier et al., 2007). Furthermore, we found that direct exposure of the brain to DA increased Ca^{2+} influx at the presynaptic terminals of sugar-sensing GRNs, in a DopEcR-dependent manner. A model consistent with these data is that starvation leads to increased DA release, which increases calcium influx into sugar-sensing GRNs via DopEcR, leading to increased neurotransmitter release. The fact that DopEcR signals via the cAMP/PKA pathway (Srivastava et al., 2005), and that this pathway has been reported to increase Ca^{2+} channel currents in *Drosophila* (Bhattacharya et al., 1999), is also consistent with this scenario. Nevertheless, our genetic data suggest that there are additional pathways through which starvation modulates feeding behavior in this system.

Our finding that DA modulates primary GRNs to control starvation-dependent changes in behavioral sensitivity to sugar echoes the observation of a similar influence of food-deprivation on odorant sensitivity in *Drosophila* (Root et al., 2011). Such neuromodulatory gain control at the level of primary sensory neurons has also been reported in variety of other invertebrate, as well as vertebrate, species (Bicker and Menzel, 1989; Hurley et al., 2004). While we cannot exclude the possibility that hunger also influences PER behavior at higher-order synapses in the circuit (Gordon and Scott, 2009), our data add to a growing body of information indicating that modulation of primary sensory neurons is a general mechanism for implementing state-dependent changes in behavioral responses to the stimuli detected by these neurons.

TANGO-map as a new tool to monitor neuromodulation at the circuit level

TANGO-map affords a number of unique advantages to study neuronal modulation in the brain (see Table S1 for comparison to other methods). Firstly, and most importantly, it permits the detection of increases in endogenous neuromodulator release *in vivo*, in an organism in which the application of conventional methods is not feasible. Secondly, it provides an anatomical readout of neuromodulation at the neural circuit level. The use of a pan-neuronal GAL4 driver to express the sensor permits, in principle, an unbiased survey of potential sites of neuromodulatory activity throughout the brain. Thirdly, the sensor has ligand-specificity. The modular design of the Tango system (Barnea et al., 2008) affords the ability to

develop *in vivo* Tango reporters for other biogenic amines and neuropeptides that work via GPCRs. Importantly, because the method employs a synthetic, "private" signal transduction pathway (Barnea et al., 2008), the readout of the reporter should be relatively insensitive to interference from conventional signal transduction pathways activated by other endogenous receptors. Systematic and comprehensive application of this approach could, in principle, provide an overview of anatomic patterns of neuromodulation in the brain in a given behavioral setting. Finally, since the Tango system is transcriptionally based, in principle it permits the expression not only of neutral reporters, but also of effectors such as RNAi's or ion channels, in the neurons receiving neuromodulatory input.

While the TANGO-map system can certainly benefit from improvements in its kinetics and signal-to-noise ratio, it affords a means of identifying points-of-entry for studying circuit-level mechanisms of behaviorally relevant neuromodulation, that are currently difficult to access in any other way. The extension of this methodology to other neuromodulators and model organisms should further our understanding of state-dependent control of neural activity and behavior.

EXPERIMENTAL PROCEDURES

Fly strains

Adult female *Drosophila melanogaster* were used for all experiments. All control genotypes were tested in the same genetic background as the experimental genotype. Construction of recombinant DNA, and descriptions of transgenic fly strains are described in the Supplemental Experimental Procedures.

TANGO-map

DopR-Tango flies or OctR-Tango flies were first dry-starved for 4 hr to make sure they consumed any drugs provided. Then, flies were moved into a vial containing 0.5 mM RU486 mixed in 89 mM sucrose and allowed to feed for 12 or 24 hr (for subsequent drug feeding or starvation experiments, respectively). After this RU486 feeding, flies were moved to either food vials (fed condition), vials containing a wet filter paper (wet-starved condition), or a drug dissolved in 89 mM sucrose (drug-fed condition). Two days later, fly brains were dissected and immunostained.

PER assays

For standard PER assays, 3-7 day-old female flies were wet-starved or fed in vials and tested as described previously (Shiraiwa and Carlson, 2007). In brief, 10-20 experimental flies were mounted into pipetman tips. After excluding flies that keep responding to water, fly response to stepwise increasing concentration of sucrose was tested. The same sets of flies were tested with all concentration of sucrose. For ChR2 experiments, flies were fed with 200 μM all trans-Retinal and tested for the response to blue light (emitted by a standard mercury lamp and filtered by GFP filter: 470/40 nm (center wavelength/ bandwidth)) under a fluorescent microscope. For details, see Supplemental Experimental Procedures.

Calcium imaging

Two-photon imaging was performed on an Ultima two-photon laser scanning microscope (Prairie Technology) with an imaging wavelength at 925nm. After a brief anesthesia on ice, flies were mounted on a

thin plastic plate with wax as shown in Figure 6B. The top side of the plate contained a well made with wax, and the fly head was immersed in saline. In this saline bath, the antennae and cuticle at the anterior side of the fly head capsule were surgically removed with sharp forceps, so that the SOG could be imaged. At the bottom side of the plate, a glass tube was mounted with the opening facing the proboscis of the mounted fly. A piece of twisted Kimwipe was placed just behind the fly. During imaging, a sucrose solution was delivered from the glass tubing to stimulate gustatory neurons in the proboscis and was removed by the Kimwipe. Details of the preparation and data processing are described in Supplemental Experimental Procedures.

ACKNOWLEDGMENTS

Drs. Shlomo Ben-Tabou de-Leon, Allan Wong, Smitha Jagadish, Hiroshi Ishimoto, Gilad Barnea, Toshihiro Kitamoto, Richard Axel, and David J. Anderson are collaborators and coauthor for this work.

We thank Dr. K. J. Lee for sharing Tango DNA constructs prior to publication. We also thank Dr. T. Lee, K. Deisseroth, A. Stathopoulos, and B. Pfeiffer for plasmids. Fly stocks were generously provided by the Bloomington Stock Center, the VDRC stock center, Drosophila RNAi Screening Center, Drs. G. M. Rubin, J. Simpson, L. L Looger, H. Keshishian, K. Scott, T. Lee, S. Birman, P. A. Garrity, C. Q. Doe, and K. Ito. We also thank Dr. H. Otsuna and Y. Wan for Fluorender, and members of the Anderson lab for helpful discussion and sharing of flies. H.K.I. is supported by the Nakajima Foundation. G.B. is a Pew scholar and is supported in part by NIH grant 5R01MH086920. D.J.A. is an investigator of the Howard Hughes Medical Institute. This work was supported in part by NIH grant 1RO1 DA031389 to D.J. Anderson.

REFERENCES

Bainton, R.J., Tsai, L.T., Singh, C.M., Moore, M.S., Neckameyer, W.S., and Heberlein, U. (2000). Dopamine modulates acute responses to cocaine, nicotine and ethanol in Drosophila. Curr Biol *10*, 187-194.

Barnea, G., Strapps, W., Herrada, G., Berman, Y., Ong, J., Kloss, B., Axel, R., and Lee, K.J. (2008). The genetic design of signaling cascades to record receptor activation. Proc Natl Acad Sci U S A *105*, 64-69.
Benveniste, H., and Huttemeier, P.C. (1990). Microdialysis--theory and application. Prog Neurobiol *35*, 195-215.

Berridge, K.C. (1991). Modulation of taste affect by hunger, caloric satiety, and sensory-specific satiety in the rat. Appetite *16*, 103-120.

Bhattacharya, A., Gu, G.G., and Singh, S. (1999). Modulation of dihydropyridine-sensitive calcium channels in Drosophila by a cAMP-mediated pathway. J Neurobiol *39*, 491-500.
Bicker, G., and Menzel, R. (1989). Chemical codes for the control of behaviour in arthropods. Nature *337*, 33-39.

Birmingham, J.T., and Tauck, D.L. (2003). Neuromodulation in invertebrate sensory systems: from biophysics to behavior. J Exp Biol *206*, 3541-3546.

Brookhart, G.L., Edgecomb, R.S., and Murdock, L.L. (1987). Amphetamine and reserpine deplete brain biogenic amines and alter blow fly feeding behavior. J Neurochem *48*, 1307-1315.

Chiappe, M.E., Seelig, J.D., Reiser, M.B., and Jayaraman, V. (2010). Walking modulates speed sensitivity in Drosophila motion vision. Current biology : CB *20*, 1470-1475.

Crocker, A., Shahidullah, M., Levitan, I.B., and Sehgal, A. (2010). Identification of a neural circuit that underlies the effects of octopamine on sleep:wake behavior. Neuron *65*, 670-681.

Dahanukar, A., Lei, Y.T., Kwon, J.Y., and Carlson, J.R. (2007). Two Gr genes underlie sugar reception in Drosophila. Neuron *56*, 503-516.

Dethier, V.G. (1976). The hungry fly : a physiological study of the behavior associated with feeding (Cambridge, Mass., Harvard University Press).

Dubner, R. (1988). The effect of behavioral state on the sensory processing of nociceptive and non-nociceptive information. Prog Brain Res *77*, 213-228.

Friggi-Grelin, F., Coulom, H., Meller, M., Gomez, D., Hirsh, J., and Birman, S. (2003). Targeted gene expression in Drosophila dopaminergic cells using regulatory sequences from tyrosine hydroxylase. J Neurobiol *54*, 618-627.

Gillette, R., Huang, R.C., Hatcher, N., and Moroz, L.L. (2000). Cost-benefit analysis potential in feeding behavior of a predatory snail by integration of hunger, taste, and pain. Proc Natl Acad Sci U S A *97*, 3585-3590.

Gordon, M.D., and Scott, K. (2009). Motor control in a Drosophila taste circuit. Neuron *61*, 373-384.

Gotzes, F., Balfanz, S., and Baumann, A. (1994). Primary structure and functional characterization of a Drosophila dopamine receptor with high homology to human D1/5 receptors. Receptors Channels *2*, 131-141.

Hamada, F.N., Rosenzweig, M., Kang, K., Pulver, S.R., Ghezzi, A., Jegla, T.J., and Garrity, P.A. (2008). An internal thermal sensor controlling temperature preference in Drosophila. Nature *454*, 217-220.

Han, K.A., Millar, N.S., Grotewiel, M.S., and Davis, R.L. (1996). DAMB, a novel dopamine receptor expressed specifically in Drosophila mushroom bodies. Neuron *16*, 1127-1135.

Harris-Warrick, R.M., and Marder, E. (1991). Modulation of neural networks for behavior. Annu Rev Neurosci *14*, 39-57.

Hearn, M.G., Ren, Y., McBride, E.W., Reveillaud, I., Beinborn, M., and Kopin, A.S. (2002). A Drosophila dopamine 2-like receptor: Molecular characterization and identification of multiple alternatively spliced variants. Proc Natl Acad Sci U S A *99*, 14554-14559.

Hurley, L.M., Devilbiss, D.M., and Waterhouse, B.D. (2004). A matter of focus: monoaminergic modulation of stimulus coding in mammalian sensory networks. Curr Opin Neurobiol *14*, 488-495.

Kong, E.C., Woo, K., Li, H., Lebestky, T., Mayer, N., Sniffen, M.R., Heberlein, U., Bainton, R.J., Hirsh, J., and Wolf, F.W. (2010). A pair of dopamine neurons target the D1-like dopamine receptor DopR in the central complex to promote ethanol-stimulated locomotion in Drosophila. PLoS One *5*, e9954.

Krashes, M.J., DasGupta, S., Vreede, A., White, B., Armstrong, J.D., and Waddell, S. (2009). A neural circuit mechanism integrating motivational state with memory expression in Drosophila. Cell *139*, 416-427.

Lebestky, T., Chang, J.S., Dankert, H., Zelnik, L., Kim, Y.C., Han, K.A., Wolf, F.W., Perona, P., and Anderson, D.J. (2009). Two different forms of arousal in Drosophila are oppositely regulated by the dopamine D1 receptor ortholog DopR via distinct neural circuits. Neuron *64*, 522-536.

Lee, G., and Park, J.H. (2004). Hemolymph sugar homeostasis and starvation-induced hyperactivity affected by genetic manipulations of the adipokinetic hormone-encoding gene in Drosophila melanogaster. Genetics *167*, 311-323.

Long, T.F., Edgecomb, R.S., and Murdock, L.L. (1986). Effects of substituted phenylethylamines on blowfly feeding behavior. Comp Biochem Physiol C *83*, 201-209.

Maimon, G., Straw, A.D., and Dickinson, M.H. (2010). Active flight increases the gain of visual motion processing in Drosophila. Nature neuroscience *13*, 393-399.

Mao, Z., and Davis, R.L. (2009). Eight different types of dopaminergic neurons innervate the Drosophila mushroom body neuropil: anatomical and physiological heterogeneity. Front Neural Circuits *3*, 5.

Marder, E., and Bucher, D. (2007). Understanding circuit dynamics using the stomatogastric nervous system of lobsters and crabs. Annu Rev Physiol *69*, 291-316.

Marella, S., Fischler, W., Kong, P., Asgarian, S., Rueckert, E., and Scott, K. (2006). Imaging taste responses in the fly brain reveals a functional map of taste category and behavior. Neuron *49*, 285-295.

Meunier, N., Belgacem, Y.H., and Martin, J.R. (2007). Regulation of feeding behaviour and locomotor activity by takeout in Drosophila. J Exp Biol *210*, 1424-1434.

Miller, M.R., Robinson, K.J., Cleary, M.D., and Doe, C.Q. (2009). TU-tagging: cell type-specific RNA isolation from intact complex tissues. Nat Methods *6*, 439-441.

Monastirioti, M. (1999). Biogenic amine systems in the fruit fly Drosophila melanogaster. Microsc Res Tech *45*, 106-121.

Montell, C. (2009). A taste of the Drosophila gustatory receptors. Curr Opin Neurobiol *19*, 345-353.

Moskowitz, H.R., Kumraiah, V., Sharma, K.N., Jacobs, H.L., and Sharma, S.D. (1976). Effects of hunger, satiety and glucose load upon taste intensity and taste hedonics. Physiol Behav *16*, 471-475.

Moss, C.F., and Dethier, V.G. (1983). Central nervous system regulation of finicky feeding by the blowfly. Behav Neurosci *97*, 541-548.

Nassel, D.R., and Winther, A.M. (2010). Drosophila neuropeptides in regulation of physiology and behavior. Prog Neurobiol *92*, 42-104.

Niell, C.M., and Stryker, M.P. (2010). Modulation of visual responses by behavioral state in mouse visual cortex. Neuron *65*, 472-479.

Nusbaum, M.P., and Beenhakker, M.P. (2002). A small-systems approach to motor pattern generation. Nature *417*, 343-350.

Osterwalder, T., Yoon, K.S., White, B.H., and Keshishian, H. (2001). A conditional tissue-specific transgene expression system using inducible GAL4. Proc Natl Acad Sci U S A *98*, 12596-12601.

Page, R.E., Jr., Erber, J., and Fondrk, M.K. (1998). The effect of genotype on response thresholds to sucrose and foraging behavior of honey bees (Apis mellifera L.). J Comp Physiol A *182*, 489-500.

Pauli, A., Althoff, F., Oliveira, R.A., Heidmann, S., Schuldiner, O., Lehner, C.F., Dickson, B.J., and Nasmyth, K. (2008). Cell-type-specific TEV protease cleavage reveals cohesin functions in Drosophila neurons. Dev Cell *14*, 239-251.

Pfaff, D.W., Kieffer, B.L., and Swanson, L.W. (2008). Mechanisms for the regulation of state changes in the central nervous system: an introduction. Ann N Y Acad Sci *1129*, 1-7.

Phillips, P.E., Robinson, D.L., Stuber, G.D., Carelli, R.M., and Wightman, R.M. (2003). Real-time measurements of phasic changes in extracellular dopamine concentration in freely moving rats by fast-scan cyclic voltammetry. Methods Mol Med *79*, 443-464.

Riemensperger, T., Isabel, G., Coulom, H., Neuser, K., Seugnet, L., Kume, K., Iche-Torres, M., Cassar, M., Strauss, R., Preat, T.*, et al.* (2011). Behavioral consequences of dopamine deficiency in the Drosophila central nervous system. Proc Natl Acad Sci U S A *108*, 834-839.

Root, C.M., Ko, K.I., Jafari, A., and Wang, J.W. (2011). Presynaptic facilitation by neuropeptide signaling mediates odor-driven food search. Cell *145*, 133-144.

Scheiner, R., Pluckhahn, S., Oney, B., Blenau, W., and Erber, J. (2002). Behavioural pharmacology of octopamine, tyramine and dopamine in honey bees. Behav Brain Res *136*, 545-553.

Scheiner, R., Sokolowski, M.B., and Erber, J. (2004). Activity of cGMP-dependent protein kinase (PKG) affects sucrose responsiveness and habituation in Drosophila melanogaster. Learn Mem *11*, 303-311.

Scott, K., Brady, R., Jr., Cravchik, A., Morozov, P., Rzhetsky, A., Zuker, C., and Axel, R. (2001). A chemosensory gene family encoding candidate gustatory and olfactory receptors in Drosophila. Cell *104*, 661-673.

Shea, S.D., and Margoliash, D. (2010). Behavioral state-dependent reconfiguration of song-related network activity and cholinergic systems. J Chem Neuroanat *39*, 132-140.

Shiraiwa, T., and Carlson, J.R. (2007). Proboscis extension response (PER) assay in Drosophila. J Vis Exp, 193.

Srivastava, D.P., Yu, E.J., Kennedy, K., Chatwin, H., Reale, V., Hamon, M., Smith, T., and Evans, P.D. (2005). Rapid, nongenomic responses to ecdysteroids and catecholamines mediated by a novel Drosophila G-protein-coupled receptor. J Neurosci *25*, 6145-6155.

Sugamori, K.S., Demchyshyn, L.L., McConkey, F., Forte, M.A., and Niznik, H.B. (1995). A primordial dopamine D1-like adenylyl cyclase-linked receptor from Drosophila melanogaster displaying poor affinity for benzazepines. FEBS Lett *362*, 131-138.

Szymczak, A.L., and Vignali, D.A. (2005). Development of 2A peptide-based strategies in the design of multicistronic vectors. Expert Opin Biol Ther *5*, 627-638.

Thibault, S.T., Singer, M.A., Miyazaki, W.Y., Milash, B., Dompe, N.A., Singh, C.M., Buchholz, R., Demsky, M., Fawcett, R., Francis-Lang, H.L.*, et al.* (2004). A complementary transposon tool kit for Drosophila melanogaster using P and piggyBac. Nat Genet *36*, 283-287.

Thorne, N., Chromey, C., Bray, S., and Amrein, H. (2004). Taste perception and coding in Drosophila. Curr Biol *14*, 1065-1079.

Tian, L., Hires, S.A., Mao, T., Huber, D., Chiappe, M.E., Chalasani, S.H., Petreanu, L., Akerboom, J., McKinney, S.A., Schreiter, E.R.*, et al.* (2009). Imaging neural activity in worms, flies and mice with improved GCaMP calcium indicators. Nat Methods *6*, 875-881.

Tsuno, Y., and Mori, K. (2009). Behavioral state-dependent changes in the information processing mode in the olfactory system. Commun Integr Biol *2*, 362-364.

Wang, Z., Singhvi, A., Kong, P., and Scott, K. (2004). Taste representations in the Drosophila brain. Cell *117*, 981-991.

Weiss, L.A., Dahanukar, A., Kwon, J.Y., Banerjee, D., and Carlson, J.R. (2011). The molecular and cellular basis of bitter taste in Drosophila. Neuron *69*, 258-272.

Wu, Q., Zhao, Z., and Shen, P. (2005). Regulation of aversion to noxious food by Drosophila neuropeptide Y- and insulin-like systems. Nat Neurosci *8*, 1350-1355.

Zhang, F., Wang, L.P., Boyden, E.S., and Deisseroth, K. (2006). Channelrhodopsin-2 and optical control of excitable cells. Nat Methods *3*, 785-792.

Zhang, W., Ge, W., and Wang, Z. (2007). A toolbox for light control of Drosophila behaviors through Channelrhodopsin 2-mediated photoactivation of targeted neurons. Eur J Neurosci *26*, 2405-2416.

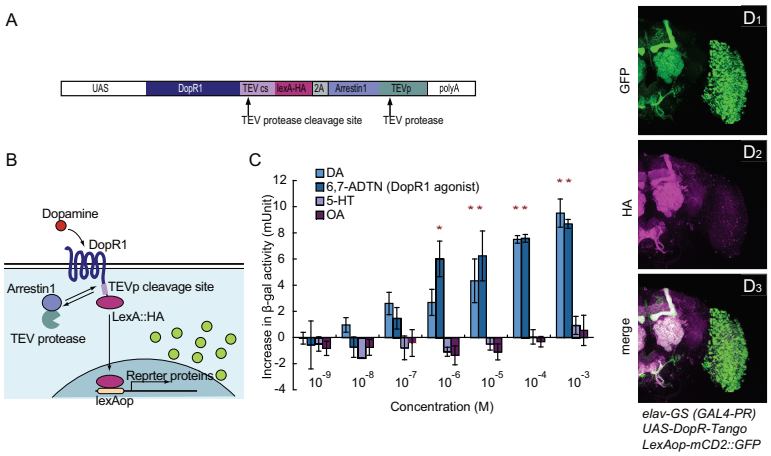
A
UAS
DopR1
TEV cs
lexA-HA
2A
Arrestin1
TEVp
polyA
TEV protease cleavage site
TEV protease
B
Dopamine
DopR1
Arrestin1
TEVp cleavage site
LexA::HA
TEV protease
Reprter proteins
lexAop
C
DA
6,7-ADTN (DopR1 agonist)
5-HT
OA
Increase in β-gal activity (mUnit)
Concentration (M)
GFP
HA
merge
D1
D2
D3
elav-GS (GAL4-PR)
UAS-DopR-Tango
LexAop-mCD2::GFP

Figure 1.

Figure 1. Characterization of DopR-Tango *in vitro* and in *Drosophila*

(A) Design of the DopR-Tango transgene; note HA epitope tag on LexA.

(B) Schematic illustrating DopR-Tango mechanism.

(C) DopR-Tango reporter (ß-gal) activity in response to indicated ligands in HEK293 cells co-transfected with *CMV-GAL4*, *UAS-DopR-Tango* and *LexAop-β-gal*. Increases in β-gal activity relative to background are shown. Error bars represent the standard error of mean (SEM). Asterisks represent statistically significant increases ($p<0.05$, t-test with Bonferroni correction, $n=3$).

(D) Representative confocal projections of whole-mount brains from DopR-Tango flies visualized with GFP native fluorescence (green) and anti-HA immunostaining (magenta).

See also Figure S1 and Table S1.

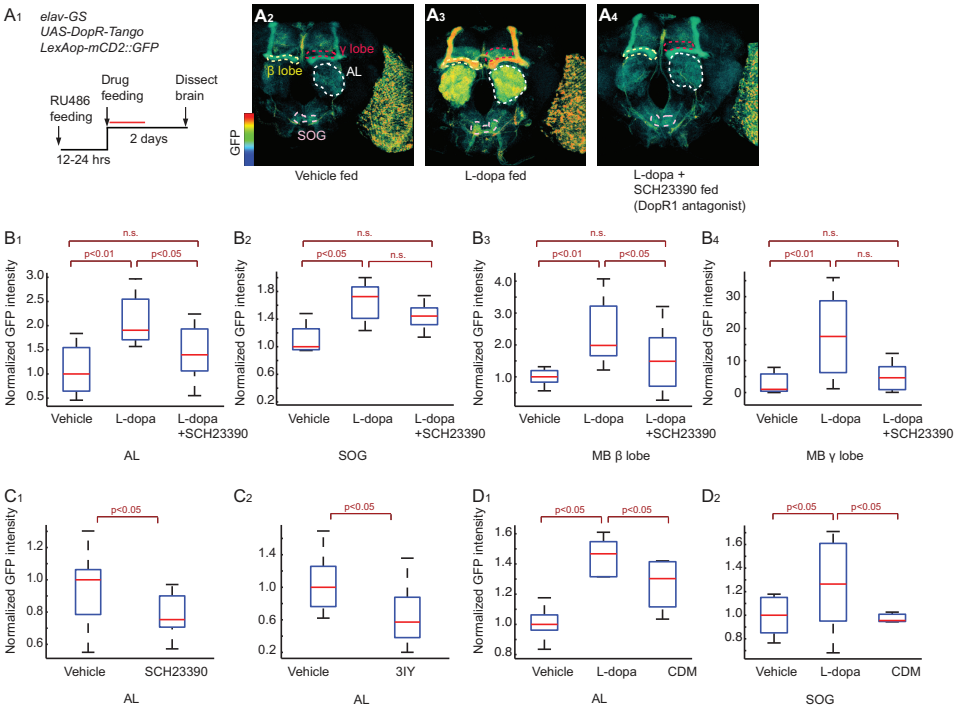
A1
elav-GS
UAS-DopR-Tango
LexAop-mCD2::GFP
RU486 feeding
Drug feeding
Dissect brain
2 days
12-24 hrs
A2
γ lobe
β lobe
AL
SOG
GFP
Vehicle fed
A3
L-dopa fed
A4
L-dopa + SCH23390 fed (DopR1 antagonist)
B1
B2
B3
B4
Normalized GFP intensity
n.s.
p<0.01
p<0.05
Vehicle
L-dopa
L-dopa +SCH23390
AL
SOG
MB β lobe
MB γ lobe
C1
C2
SCH23390
3IY
D1
D2
CDM

Figure 2.

Figure 2. Characterization of DopR-Tango in transgenic flies

(A). Specific activation of DopR-Tango by L-dopa *in vivo*. (A_1) experimental design. Red line represents 24 hr detection window for Tango reporter (see Figure S1E). (A_{2-4}) pseudocolor images of DopR-Tango reporter (GFP) expression; color scale to left. See Figure S2 for image processing details. Neuropils indicated by dashed outlines are: AL, Antennal Lobe (white); SOG, suboesophageal ganglion (pink); mushroom body (MB) β and γ lobes (yellow and red, respectively). (B-D). Quantification of reporter expression in the indicated neuropils. SCH23390, D1 receptor antagonist; 3IY (3-iodotyrosine, DA synthesis inhibitor). Unless otherwise indicated, p values in this and subsequent figures represent Kruskal-Wallis one-way ANOVA followed by Mann-Whitney U-tests with Bonferroni correction. n>5 for each experimental group. Boxplots: lower and upper whiskers represent 1.5 interquartile-range (IQR) of the lower and upper quartiles, respectively; boxes indicate lower quartile, median and upper quartile, from bottom to top.

See also Figure S2.

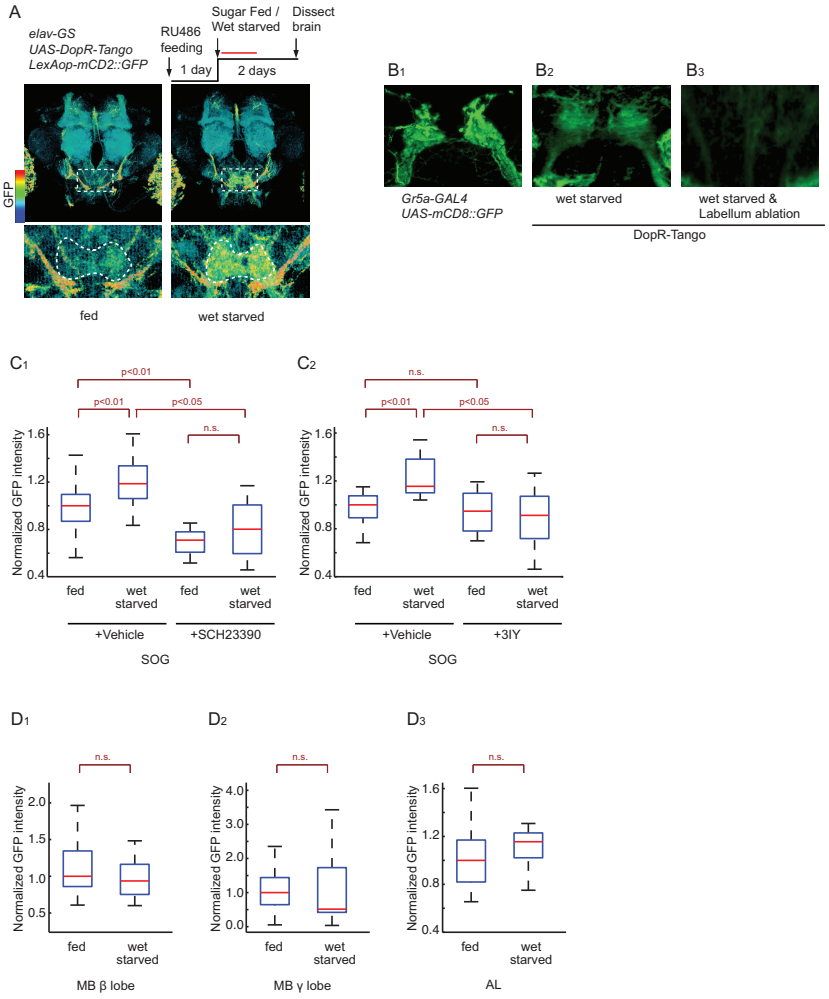
A
elav-GS
UAS-DopR-Tango
LexAop-mCD2::GFP
RU486 feeding
1 day
Sugar Fed / Wet starved
2 days
Dissect brain
GFP
fed
wet starved
B1
B2
B3
Gr5a-GAL4
UAS-mCD8::GFP
wet starved
wet starved & Labellum ablation
DopR-Tango
C1
C2
Normalized GFP intensity
p<0.01
p<0.05
n.s.
fed
wet starved
+Vehicle
+SCH23390
+3IY
SOG
D1
D2
D3
MB β lobe
MB γ lobe
AL

Figure 3.

Figure 3. DA release onto GRNs increases during starvation

(A) Experimental design and normalized Tango reporter (GFP) expression in brains of fed vs. 48-hr wet-starved flies; color scale to left. Laser scanning was performed at a higher gain setting to increase sensitivity. Dashed boxes delineate SOG (enlarged in lower panels). White dashed line in lower panels show ROIs used for quantification, based on *UAS-DsRed* expression in SOG neuropil.

(B) Representative confocal projections of sugar-sensing GRNs (B_1), and Tango reporter expression (B_2, B_3) in the SOG of normal (B_1, B_2) or labellum-ablated (B_3) flies.

(C, D) Normalized GFP expression in DopR-Tango flies quantified in the SOG ($C_{1\text{-}2}$), MB β lobe (D_1), MB γ lobe (D_2) and AL (D_3). n >6 for each experimental group.

See also Figure S3.

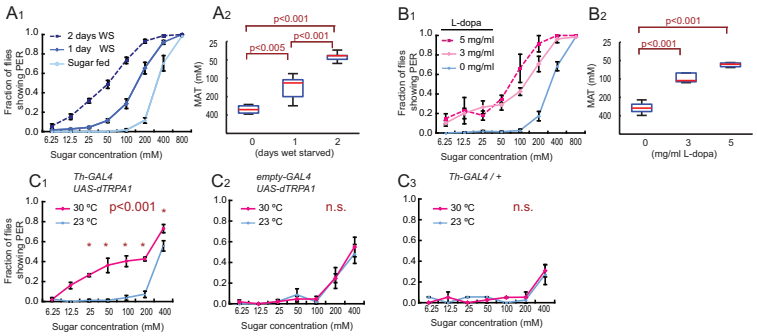
A1
2 days WS
1 day WS
Sugar fed
Fraction of flies showing PER
Sugar concentration (mM)
A2
p<0.001
p<0.001
p<0.005
MAT (mM)
(days wet starved)
B1
L-dopa
5 mg/ml
3 mg/ml
0 mg/ml
Fraction of flies showing PER
Sugar concentration (mM)
B2
p<0.001
p<0.001
MAT (mM)
(mg/ml L-dopa)
C1
Th-GAL4
UAS-dTRPA1
30 °C
23 °C
p<0.001
Fraction of flies showing PER
Sugar concentration (mM)
C2
empty-GAL4
UAS-dTRPA1
30 °C
23 °C
n.s.
Sugar concentration (mM)
C3
Th-GAL4 / +
30 °C
23 °C
n.s.
Sugar concentration (mM)

Figure 4.

Figure 4. Hunger and DA increase the sugar sensitivity of the PER

(A) Fraction of fed vs. wet-starved (WS) flies showing a PER at different concentrations of sucrose. (A_1). Average responses. Error bars represent S.E.M. (A_2) MAT (mean acceptance threshold; the sugar concentration where 50% of the flies show PER), plotted as a function of starvation time. One-way ANOVA followed by t-test with Bonferroni correction (n>4 for each experimental group).

(B) PER responses in non-starved flies fed with the indicated concentrations of L-dopa (n>4 for each experimental group).

(C) Genetic activation of DA neurons increases sugar sensitivity. PER vs. sugar concentration curves are shown for experimental *Th-GAL4;UAS-dTRPA1* (C_1) and genetic control flies (C_2 and C_3) at the permissive (red) and non-permissive (blue) temperatures for dTRPA1. Within-genotype differences between temperatures were analyzed using a two-way ANOVA with replication followed by post-hoc t-tests with the Bonferroni correction at each sugar concentration. *; $p<0.05$, n.s.; not significant (n>4 for each experimental group).

See also Figure S3.

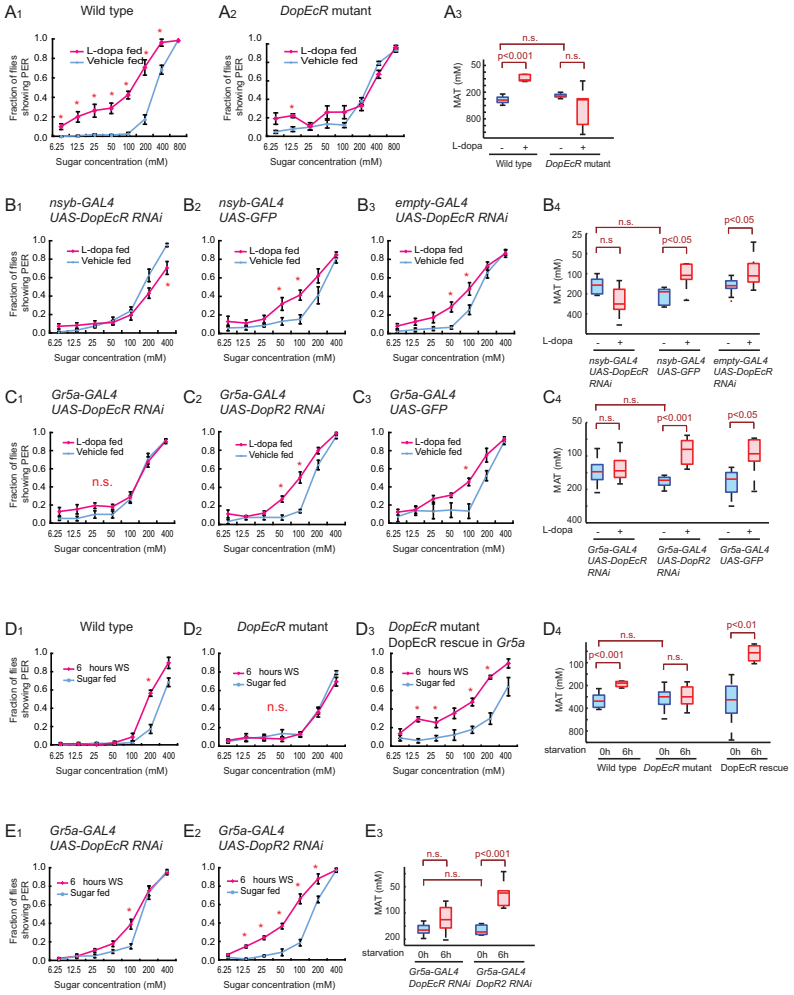
A1
Wild type
A2
DopEcR mutant
A3
L-dopa fed
Vehicle fed
Fraction of flies showing PER
Sugar concentration (mM)
MAT (mM)
L-dopa
Wild type
DopEcR mutant
n.s.
p<0.001
B1
nsyb-GAL4
UAS-DopEcR RNAi
B2
nsyb-GAL4
UAS-GFP
B3
empty-GAL4
UAS-DopEcR RNAi
B4
p<0.05
C1
Gr5a-GAL4
UAS-DopEcR RNAi
C2
Gr5a-GAL4
UAS-DopR2 RNAi
C3
Gr5a-GAL4
UAS-GFP
C4
D1
Wild type
D2
DopEcR mutant
D3
DopEcR mutant
DopEcR rescue in Gr5a
D4
p<0.01
6 hours WS
Sugar fed
starvation
0h
6h
DopEcR rescue
E1
Gr5a-GAL4
UAS-DopEcR RNAi
E2
Gr5a-GAL4
UAS-DopR2 RNAi
E3
Gr5a-GAL4
DopEcR RNAi
Gr5a-GAL4
DopR2 RNAi

Figure 5.

Figure 5. DopEcR expression in *Gr5a* GRNs is necessary and sufficient for L-dopa feeding- and starvation-induced increases in PER sugar sensitivity

(A) Sugar sensitivity of wild type, and *DopEcR* mutant flies after L-dopa (3 mg/ml) feeding. The wild-type data are identical to Figure $4B_1$ and are reproduced here for ease of comparison.

(B-E) Sugar sensitivity of RNAi flies or mutant flies after L-dopa feeding (B, C) or 6 hrs wet-starvation (WS; D, E). *UAS-DopEcR RNAi* and *UAS-DopR2 RNAi* are in the same genetic background. Note that DopR2 is not expressed in a detectable level in sugar-sensing GRNs (Figure S4A).

In PER curves, error bars represent SEM. Boxplots: lower and upper whiskers represent 1.5 interquartile-range (IQR) of the lower and upper quartiles, respectively; boxes indicate lower quartile, median and upper quartile, from bottom to top. The statistical significance of within-genotype differences between PER curves, or MAT values, for L-dopa vs. vehicle treatment or feeding vs. wet-starvation was analyzed using two-way ANOVA with replication followed by post hoc t-tests with Bonferroni correction. *; $p<0.05$, n.s.; not significant ($n>4$ for each experimental group). A significant interaction between genotype and feeding manipulation was revealed by a 2-way ANOVA in (A_3) $p<0.0001$; (B_4) $p<0.005$; (C_4) $p<0.01$; (D_4) $p<0.05$; and (E_3) $p<0.005$, indicating that the genetic manipulations interfered with the effect of wet-starvation or L-dopa feeding.

See also Figure S4.

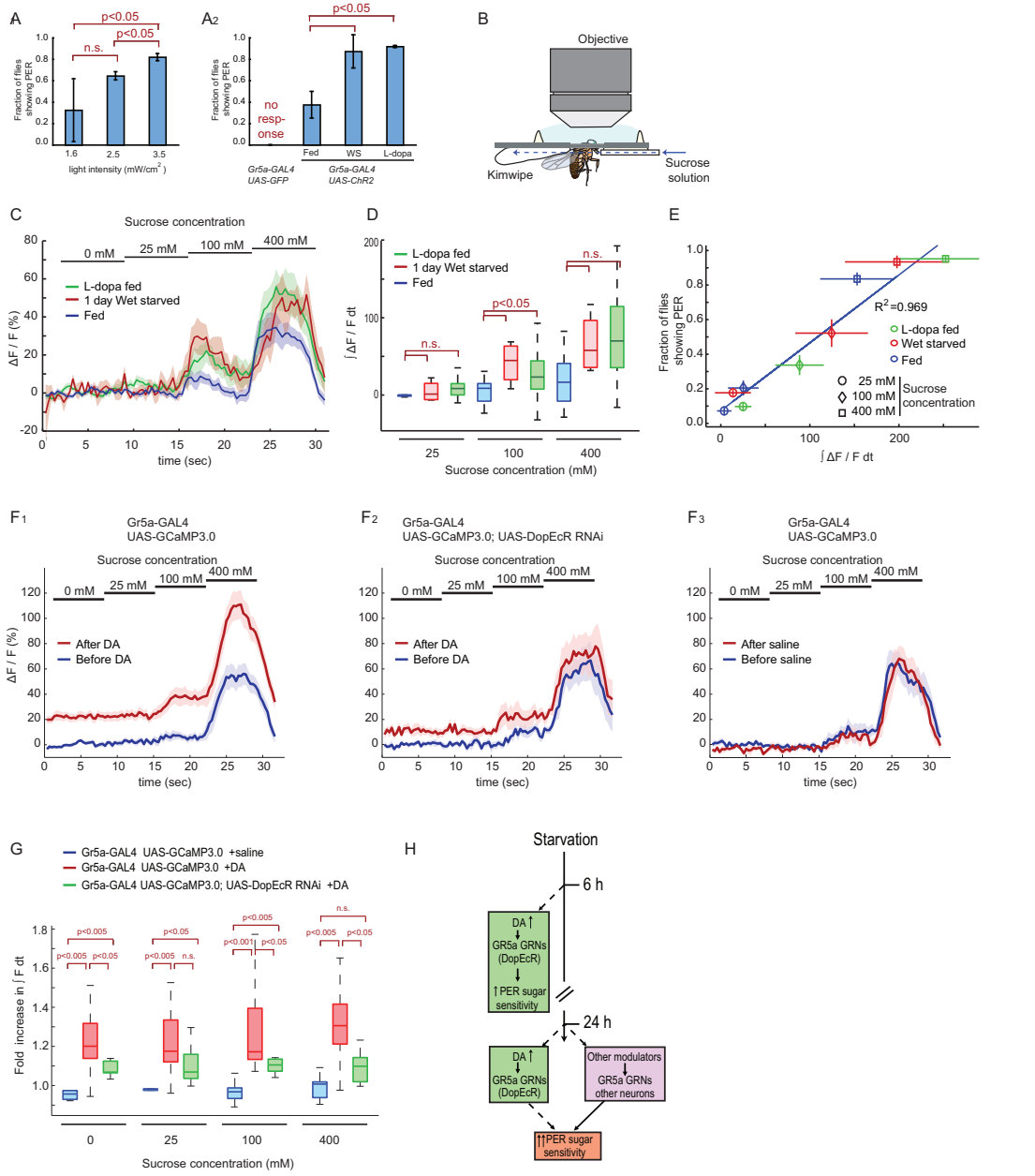
A
p<0.05
p<0.05
n.s.
Fraction of flies showing PER
light intensity (mW/cm²)
A2
p<0.05
no response
Fed
WS
L-dopa
Gr5a-GAL4 UAS-GFP
Gr5a-GAL4 UAS-ChR2
B
Objective
Kimwipe
Sucrose solution
C
Sucrose concentration
0 mM
25 mM
100 mM
400 mM
L-dopa fed
1 day Wet starved
Fed
ΔF / F (%)
time (sec)
D
L-dopa fed
1 day Wet starved
Fed
n.s.
p<0.05
n.s.
∫ ΔF / F dt
Sucrose concentration (mM)
E
R²=0.969
L-dopa fed
Wet starved
Fed
25 mM
100 mM
400 mM
Sucrose concentration
Fraction of flies showing PER
∫ ΔF / F dt
F1
Gr5a-GAL4
UAS-GCaMP3.0
Sucrose concentration
After DA
Before DA
ΔF / F (%)
time (sec)
F2
Gr5a-GAL4
UAS-GCaMP3.0; UAS-DopEcR RNAi
Sucrose concentration
After DA
Before DA
time (sec)
F3
Gr5a-GAL4
UAS-GCaMP3.0
Sucrose concentration
After saline
Before saline
time (sec)
G
Gr5a-GAL4 UAS-GCaMP3.0 +saline
Gr5a-GAL4 UAS-GCaMP3.0 +DA
Gr5a-GAL4 UAS-GCaMP3.0; UAS-DopEcR RNAi +DA
Fold increase in ∫ F dt
Sucrose concentration (mM)
H
Starvation
6 h
DA↑
GR5a GRNs (DopEcR)
↑PER sugar sensitivity
24 h
DA↑
GR5a GRNs (DopEcR)
Other modulators
GR5a GRNs other neurons
↑↑PER sugar sensitivity

Figure 6.

Figure 6. Starvation or L-dopa feeding enhance calcium transients in sugar sensing GRNs

(A) Channelrhodopsin-2-evoked PER. *Gr5a-GAL4;UAS-ChR2* or *Gr5a-GAL4;UAS-GFP* control flies were stimulated with blue (470/40 nm: centerwavelength/bandwidth) light at the indicated intensities (A1) or at 1.6 mW/cm^2 under the indicated conditions (A2). Error bars represent SEM.

(B) The setup for calcium imaging of sugar-sensing GRNs. Blue dashed arrow indicates direction of flow of sugar solution.

(C) Responses (ΔF/F) to different concentrations of sucrose in the central projections of sugar-sensing GRNs in *Gr5a-GAL4;UAS-GCaMP3.0* flies. The solid lines represent average trace, and envelopes indicate SEM (n>7 for each condition).

(D) Quantification of fluorescent changes. $\int \Delta F/F\ dt$, integrated ΔF/F during stimulus period. Data analyzed from (C). Mann-Whitney U-tests with Bonferroni correction.

(E) Correlation between GCaMP signals (analyzed in B, C) and behavioral responses (PER) of *Gr5a-GAL4;UAS-GCaMP3.0* flies (n>4). Error bars represent SEM.

(F) Responses (ΔF/F) to different concentrations of sucrose in the central projections of sugar-sensing GRNs before and after 5 min exposure of the brain to saline with or without 1mM DA. The solid lines represent average trace, and envelopes indicate SEM (n>7 for each condition).

(G) Fold increase in $\int F\ dt$ ($\int F\ dt_{[After\ DA]}/\int F\ dt_{[Before\ DA]}$) during each stimulus period, calculated from the data in (F). Mann-Whitney U-tests with Bonferroni correction.

(H) Schematic illustrating mechanisms controlling starvation-induced increases in the sugar sensitivity of PER behavior.

See also Figure S5.

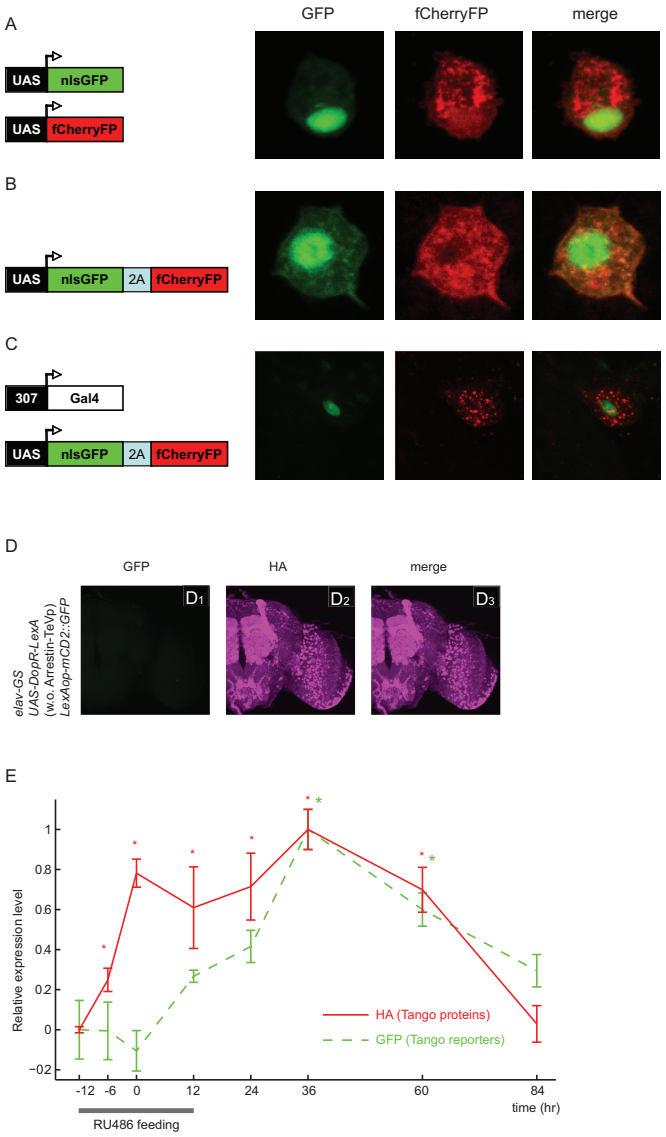

Supplemental figure 1.

Supplemental figure 1. Bi-cistronic expression using a 2A peptide in *Drosophila* and kinetics of DopR-Tango activation *in vivo*, related to Figure 1

(A-B) Characterization of 2A peptide in *Drosophila* Schneider 2 (S2) cells. nls::GFP (GFP tagged with nuclear localization signal; green) and fCherryFP (mCherry tagged with farnesylation signal; red) were expressed from two separate co-transfected vectors (*UAS-nls::GFP* and *UAS-fCherryFP*; A), or from a single vector with a 2A peptide (*UAS-nlsGFP-2A-fCherryFP*; B). *Actin promoter-Gal4* driver was used to induce the expression. The nuclear-cytoplasmic segregation of GFP and fCherry expression, respectively, in (B) indicates that the 2A peptide is functional in S2 cells.

(C) The 2A peptide is functional in the *Drosophila* brain *in vivo*. *UAS-nlsGFP-2A-fCherryFP* was expressed in a giant fiber neuron using the *307-GAL4* driver. The nuclear-cytoplasmic segregation of GFP and fCherry signals implies cleavage of the 2A sequence *in vivo*.

(D) DopR Tango reporter expression is dependent on co-expression of Arrestin-TEVp. Representative confocal projections of a whole mount brain from DopR-Tango flies expressing *UAS-DopR-TEVcs-LexA* without Arrestin1-TEVp co-expression, visualized using GFP native fluorescence (green; D_1) and anti-HA immunostaining (magenta; D_2). Note absence of GFP reporter expression.

(E) Time course of DopR-Tango and GFP reporter expression in DopR-Tango flies co-expressing *elav-GeneSwitch* after RU486 feeding. X-axis/abcissa (time) represents the time after DopR-Tango expression (determined by anti-HA antibody staining) reached steady-state levels (RU486 was fed for 24 hrs between -12 to 12 hrs). Fluorescent pixel intensities were quantified in the antennal lobe, and are expressed relative to baseline values determined at t= -12hrs. One-way ANOVA was followed by t-test with Bonferroni correction (*: signal is significantly different from that of time point 0). Error bars represent standard deviation, n=2-4 for each experimental group.

A time course of DopR-Tango and GFP reporter expression (Figure S1E) indicated that the expression of the former starts within 6-12 hrs after the initiation of RU486 feeding, while the level of GFP reporter expression reaches a statistically significant increase 36-48 hrs after that time. This implies that it takes >24 hrs for the GFP reporter to accumulate to significant levels after DopR-Tango expression. This

interval likely reflects the sum of the times required for (1) LexA to be cleaved after the expression of DopR-Tango, (2) LexA to be transported to the nucleus and activate GFP transcription, and (3) translation and transport of GFP to various neuropils. Therefore, in order to ensure a detectable change in GFP reporter expression following experimental manipulations of DopR-Tango flies, such as drug feeding, we chose to dissect fly brains 48 hrs after the starting point of manipulation. The level of GFP reporter expression measured at this end-point likely reflects the integration of DA signal over the first 24 hr of the manipulation (Figure 2A and 3A, red line). Based on our data, additional signaling in the second 24 hr period likely does not yield a sufficient additional increase in reporter expression to contribute significantly to the signal detected at the 48 hr end-point.

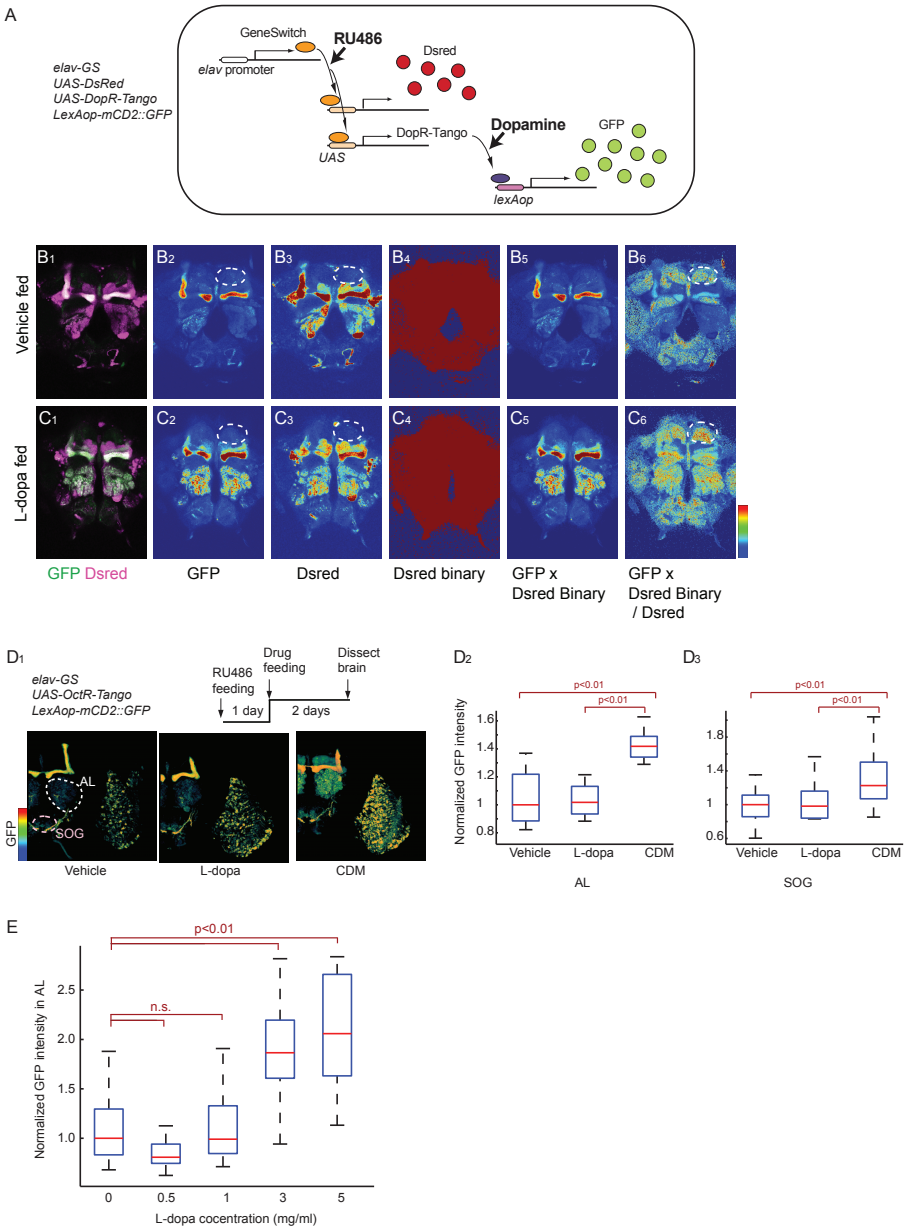

Supplemental figure 2.

Supplemental figure 2. Normalization and image processing of DopR-Tango reporter signal *in vivo*, related to Figure 2

(A) Schematic illustrating the transgenically encoded DopR-Tango signal transduction cascade. GeneSwitch (GS)-Gal4 (orange oval) induces the expression of both DsRed and DopR-Tango. DA-dependent cleavage of DopR-Tango results in translocation of LexA (purple oval) to the nucleus, where it activates expression of the lexAop-GFP Tango reporter. The level of GFP reporter expression reflects not only the ambient level of DA, but also the expression level of the DopR-Tango cassette itself. Since both DsRed and DopR-Tango are under the control of GS, the signal intensity of DsRed should proportionately reflect the expression level of DopR-Tango, in a given region of the brain in a given specimen. Therefore, dividing the GFP signal by the DsRed signal on a pixel-to-pixel basis corrects for within- or between-specimen variations in the level of DopR-Tango expression, and provides a normalized measure of GFP reporter expression that should primarily reflect ambient levels of DA activation of the DopR-Tango cassette. Native fluorescence rather than antibody staining was used to avoid non-linear signal amplification. This method permitted quantification of the normalized GFP signal in various regions of interest (ROIs).

(B and C) Representative examples of image normalization process. Single optical sections from a whole mount DopR-Tango fly brain (Vehicle fed: $B_{1\text{-}3}$, L-dopa fed: $C_{1\text{-}3}$). Signal intensity of native GFP (B_2 and C_2) and DsRed (B_3 and C_3) are represented in pseudo color. After noise filtering using the Wiener method (Lim, 1990), DsRed signals were converted into binary data using a threshold that cuts off noise outside the brain (B_4 and C_4). The GFP signal was multiplied by these binary data (B_5 and C_5) on a pixel-by-pixel basis. This process eliminates GFP signals in pixels lacking any DsRed signal, thereby avoiding division by zero in the subsequent normalization step. Finally, this processed GFP signal was divided by the signal intensity of DsRed (B_6 and C_6) on a pixel-by-pixel basis. Note how this processing facilitates comparison of GFP signals in many brain areas, such as the dorsal protocereberum (indicated by white dashed circle), in which DsRed expression levels are low.

(D) Specific activation of OctR-Tango by CDM *in vivo*. Pseudocolor images of OctR-Tango reporter (GFP) expression are shown (D_1). Quantification of reporter expression in the indicated neuropil

structures(D_{2-3}). p-values in this figure represents the results of Kruskal-Wallis ANOVA followed by Mann-Whitney U-test with Bonferroni correction for multiple comparisons. n>5 for each experimental group.

(E) Dose-response profile of reporter expression in DopR-Tango flies. Reporter expression in the antennal lobe (AL) was quantified as described above after feeding with the indicated concentration of L-dopa. p-values in this figure represents the results of Kruskal-Wallis ANOVA followed by a Mann-Whitney U-test with the Bonferroni correction for multiple comparisons. n>10 for each experimental group.

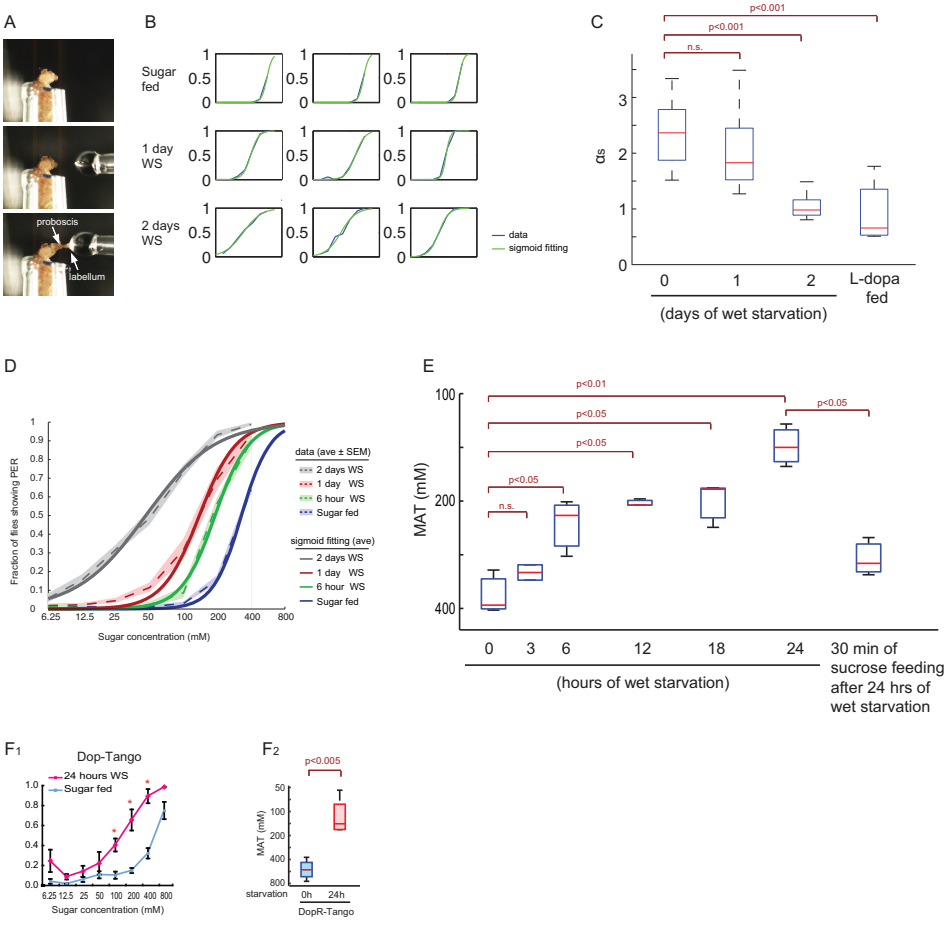

Supplemental figure 3.

Supplemental figure 3. Analysis of PER, related to Figure 3 and 4

(A) PER assay. Presentation of sucrose solution to the tip of proboscis (labellum) causes full extension of proboscis.

(B) A response curve to the sugar (PER curve) can be fitted into a sigmoid curve. Representative examples of PER curve (3 examples each for sugar fed, 1day wet-starved, and 2 days wet-starved wild-type flies). Raw data, blue; sigmoid fitting, green. In all cases, fitting of sigmoid to the data was confirmed with two-way ANOVA. See also Supplemental Experimental Procedures.

(C) α_s decreases with two-day wet-starvation or L-dopa feeding. α_s is slope of the sigmoid curve (see Supplemental Experimental Procedures). One-way ANOVA was followed by t-test with Bonferroni correction.

(D) Average curves of the fitted sigmoid curves (solid lines), fit well to the average curves of the raw data (dotted lines. Envelopes indicate SEM). Raw data are pooled from Figure $4A_1$ and $5D_1$ ($n>4$ for each). Fitting was confirmed with two-way ANOVA.

(E) Time course of changes in MAT during starvation. MATs were measured 0, 3, 6, 12, 18, and 24 hour after wet-starvation, and 30 min after sucrose feeding of 24 hr wet-starved flies ($n>3$, each). While increase in sugar-sensitivity during starvation is gradual, the decrease in sugar-sensitivity after feeding is abrupt, suggesting different mechanisms controlling sugar-sensitivity under states of starvation and satiety. One-way ANOVA was followed by t-test with Bonferroni correction (n.s.: $p>0.05$).

(F) Sugar sensitivity of sugar fed and wet starved DopR-Tango flies tested using the PER assay. As in wild type flies (Figure $4A_1$), DopR-Tango flies showed normal PER behavior and starvation-dependent increase in sugar sensitivity. (F_1) average response. See Figure S4 for the statistical method to test the difference between two PER curves. Error bars represent SEM. (F_2) MAT. t-test ($n>4$ for each experimental group).

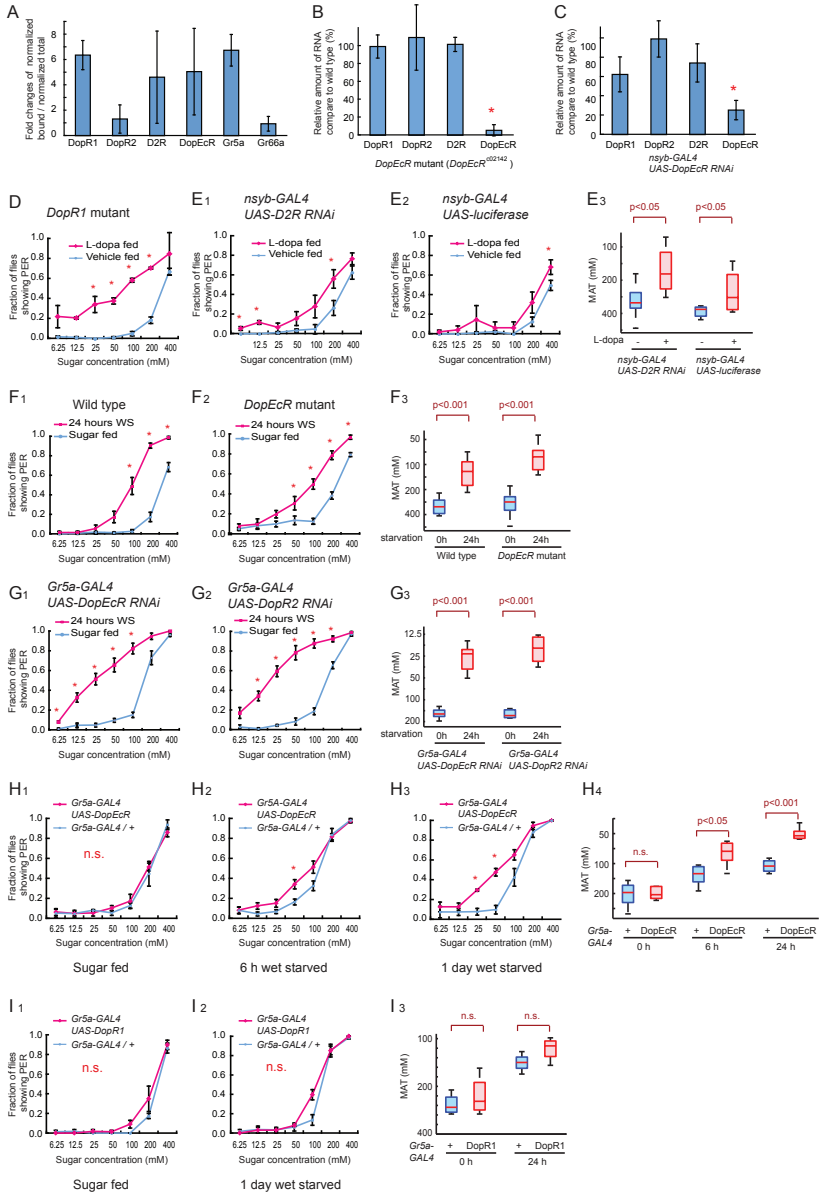

Supplemental figure 4.

Supplemental figure 4. Quantification of DA receptor mRNA expression and validation of RNAi, related to Figure 5

(A) DA receptor expression in RNA isolated from sugar-sensing GRNs by the TU-tagging method (Miller et al., 2009) and quantification by qRT-PCR. Error bars represent standard deviation (n=2).

(B-C) The effect of the *DopEcR* mutation and *DopEcR* RNAi on the amount of *DopEcR* RNA was quantified using qRT-PCR. Error bars represent standard deviation (n=3). One-way ANOVA was followed by t-test with Bonferroni correction (*: $p<0.05$).

(D-E) Sugar sensitivity of *DopR1* hypomorph mutant (D), pan-neuronal *D2R* RNAi (E_1) and its genetic control flies (E_2) with or without L-dopa feeding. All genotypes exhibited a significant increase in sugar sensitivity by feeding L-dopa. Data in D are directly comparable to wild-type data in Figure $5A_1$ for the same genetic background.

(F-G) Sugar sensitivity of *DopEcR* RNAi or mutant after 24 hrs of starvation.

(H) Over-expression of DopEcR in sugar-sensing GRNs boosts the increase in sugar sensitivity caused by food-deprivation. The sugar sensitivity of flies over-expressing DopEcR in sugar-sensing GRNS (*Gr5a-GAL4;UAS-DopEcR*; red lines) was compared to the sensitivity of its genetic control flies (*Gr5a-GAL4*/+; blue lines).

(I) Over-expression of DopR1 in sugar-sensing GRNs did not influence sugar sensitivity. The sugar sensitivity of flies over-expressing DopR1 in sugar GRNs (*Gr5a-GAL4;UAS-DopR1*; red lines) was compared to the sensitivity of its genetic control flies (*Gr5a-gal4*/+; blue lines). $DopR^{f02676}$ was used as *UAS-DopR1*(Lebestky et al., 2009).

As in Figure 5, in PER curves, error bars represent SEM. Boxplots: lower and upper whiskers represent 1.5 interquartile-range (IQR) of the lower and upper quartiles, respectively; boxes indicate lower quartile, median and upper quartile, from bottom to top. The difference between PER curves for each pair of experimental groups (red vs. blue lines in all panels) was analyzed by two-way ANOVA with replication followed by a post hoc t-test with Bonferroni correction. *; $p<0.05$, n.s.; non-significant ($n>4$ for each experimental group).

Differences between MATs were analyzed by two-way ANOVA with replication followed by post hoc t-test with Bonferroni correction. Interactions between genotyopes and feeding conditions (Genotypes×Conditions), which were calculated by the two-way ANOVA, were not significant for all cases listed below, implying that the genetic manipulations (mutation or RNAi) did not interfere the effect of feeding manipulations (wet-starvation or L-dopa feeding); $p=0.5275$ (non significant) (E_3), $p=0.2876$ (F_3), $p=0.3478$ (G_3).

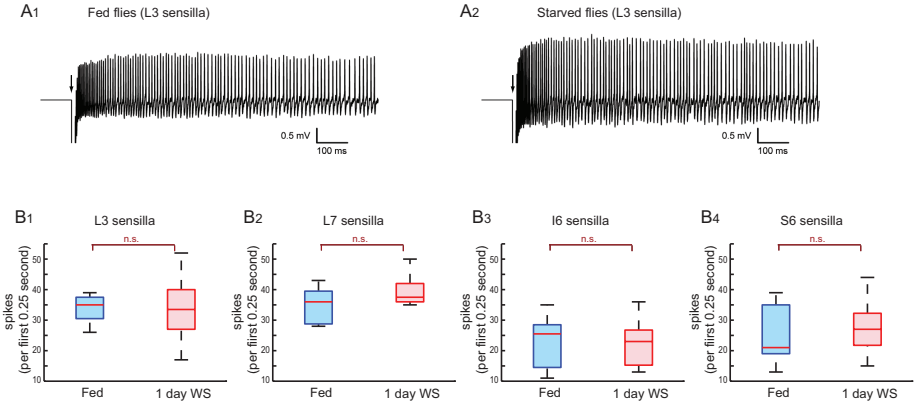

Supplemental figure 5.

Supplemental figure 5. Extaracellular recording of GRNs in labellum, related to Figure 6

(A) Sample traces of electrophysiological recordings made from L3 sensilla of fed (A_1) and starved flies (A_2). The electrophysiological responses of labellar sugar-sensing GRNs to 100 mM sucrose were recorded extracellularly by using the tip recording method (see Supplemental Experimental Procedures). Recording electrode filled with sucrose solution touched the sensilla at the time pointed by the arrow. Contact artifacts are observed at the beginning of each trace.

(B) Effect of starvation on the action potential frequency of sugar-sensing GRNs in response to 100 mM sucrose. The spike number in the first 0.25 sec ($B_{1\text{-}4}$) and the first 1.0 sec (data not shown) of the response to sucrose was measured. No change in action potential frequency was observed between fed and starved flies in any of the sensilla tested (Man-Whitney U-test). In case of the L-type sensilla, we observed statistically significant increase in action potential amplitude in starved flies, compared to fed flies (data not shown). Since the action potential shape and amplitude, measured by extracellular recording, depend on extracellular factors, such as the distance and position of the recording electrode and the resistance of the environment around the cell, we could not conclude whether this increase in the action potential amplitude is due to a change in the sugar-sensing GRNs themselves.

Supplemental table1.

Comparison of TANGO-map with other methods to monitor nueromodulators *in vivo*, related to Figure 1

		Direct measurements		Indirect measurements			
	TANGO-map	HPLC, ELISA[1)]	*In vivo* voltammetry	IEG	Ca2+ [2)]	cAMP [3)]	Electro-physiology
Cellular resolution	+	-	-	+	+	+	+
Ligand-specificity	+	+	+	-	-	-	-
Unbiased [4)]	+	N.A.	N.A.	+	-	-	+/- [5)]
Non-invasive [6)]	+	N.A.	-	+	-	-	-
Temporal resolution	12-24 hrs[7)]	N.A.	100 msec	1 hr	100 msec	100 msec	msec level

[1)] HPLC or ELISA of homogenized nervous system (Bainton et al., 2000).

[2)] Measured using organic Ca^{2+} sensor or genetically encoded Ca^{2+} sensor such as GCaMP (Tian et al., 2009) and TN-XXL (Mank et al., 2008).

[3)] Measured using genetically encoded cAMP sensor, Epac1-camps (Shafer et al., 2008).

[4)] Meaning that the method does not require specific Gal4 lines.

[5)] Gal4-UAS system is often used to visualize neurons to record (Wilson et al., 2004).

[6)] Non-invasive means the method does not require surgical manipulation before or during the behavior of interest, so that there is no interference with the behavior.

[7)] By changing the time-point of dissection, in principle, temporal resolution can be improved.

Supplemental Experimental Procedures

Recombinant DNA construction

Plasmids were constructed by standard DNA cloning and PCR methods. All PCR reactions were performed using PrimeStar® HS DNA polymerase (Takara). PCR-amplified DNA fragments were inserted into the pCRII Vector (Invitrogen). After amplification all sequences were verified by DNA sequencing.

Completed vectors for expression in *Drosophila* (UAS-DopR-Tango, UAS-OctR-Tango, UAS-DopEcR, and UAS-ChR2(C128T)) were inserted into either the attP2 site or attP40 site (Pfeiffer et al., 2010) using attB/attP and C31-mediated recombination (Genetic Services, Inc.) (Groth et al., 2004; Markstein et al., 2008).

Plasmids containing UAS-DopR-Tango and UAS-OctR-Tango were created in several steps as shown below. The "Valium" vector was used as the backbone for all constructions (Ni et al., 2008).

pCRII-2A

A DNA fragment encoding the F2A peptide (Donnelly et al., 2001) was amplified by PCR using primers 2A-f (CCTAGGGAGCAGAAGGGCCCCGGGCTAAGAGATCAGGTTC) and 2A-r (GCTAGCGAGCAGGGCCGGCCTGGCCCTGGGTTGGACTCC), and a plasmid generously provided by Dr. Pin Wang. The pCRII vector containing this DNA fragment was named pCRII-2A.

Valium-2A-TEVp

The DNA fragment encoding TEV protease (TEVp) was amplified by PCR using primers TEVp-f (GAATTC CCTAGGGAGCAG GCTAGCTTGTTTAAGGGACCACG) and TEVp-r (GTCTAGATCAAGCGTAATCTGGAACATCA), and a vector generously provided by Dr. Kevin J Lee (Barnea et al., 2008). This fragment was subcloned into the C-terminal side of 2A in pCRII-2A using AvrII and NheI. Subsequently, the DNA fragment containing both 2A and TEV protease was subcloned into a Valium vector (Ni et al., 2008), a vector containing both UAS and attB sequence, using EcoRI and XbaI.

Valium-TEVcs-LexA-HAtag-2A-TEVp

A DNA fragment encoding the TEV cleavage site (TEVcs) and a hemagglutinin (HA) epitope tag sequence was created by PCR and inserted into the pCRII vector. For the initial version of DopR Tango (used only in Figure 2D and S2D, E), GGSGGENLYFQLGGSGG was used as a cleavage sequence, where GGSGG at both ends are linkers. Subsequent experiments showed that the S/N *in vitro* was better using a different cleavage sequence with shorter linkers, GENLYFQLG. Therefore, a modified DopR-Tango containing this TEVcs sequence was used for the remainder of the study. The constructed sequence is shown below (the TEVcs is GENLYFQLG):

GCCTAGGACGAGTCCGCGGCCGCGGAGAAAATCTCTATTTCCAGCTAGGACCCGGGTTGGTTCC
CATATGATGGACCTGCACCGTGGTGGCGGTCGTATCTTTTATCCGTATGACGTGCCGGACTATG
CCGGCTATCCATACGATGTCCCCGACTACGCTGGATCCTACCCCTACGACGTCCCAGATTATGC
CGCTCATGGCGGAGGGCCCG .

A DNA fragment encoding LexA::VP16 (LexA) (Lai and Lee, 2006) was amplified by PCR using primers LexA-f (GCCCGGGAAAGCGTTAACGGCCAGG) and LexA-r (GCATATGCCCACCGTACTCGTCAATT), and a plasmid generously provided by Dr. Tzumin Lee. This DNA fragment was subcloned in between the TEVcs and the HA tag by using XmaI and NdeI, to create a fusion sequence, TEVcs-LexA-HAtag. This DNA fragment was in turn subcloned 5' to the 2A sequence in Valium-2A-TEVp using AvrII and ApaI. This vector was named Valium-TEVcs-LexA-HAtag-2A-TEVp.

Valium-TEVcs-LexA-HAtag-2A-Arrestin-TEVp

A *Drosophila Arrestin1* coding sequence was amplified by PCR using primers Arrestin-f (GGGCCGGCCCATGGTGGTCAATTTCAAGGTG) and Arrestin-r (GCTAGCGCCTCCGCTGCCACCGTAGGCCTCAATGGAGCCC), and a cDNA template synthesized

from the heads of wild-type (Canton-S) flies. This DNA fragment was subcloned into Valium-TEVcs-LexA-HAtag-2A-TEVp between the 2A and TEVp sequences using FseI and NheI.

UAS-DopR-Tango (Valium-DopR1- TEVcs-LexA-HAtag-2A-Arrestin-TEVp)

A *Drosophila DopR1* coding sequence was amplified by PCR using primers DopR1-f (GCCTAGGCAAAATGTACACACCACACCCATTTG) and DopR1-r (GGCGGCCGCCGCAAATCGCAGACACCTGCTC), and a cDNA template synthesized from the heads of Canton-S flies. This DNA fragment was subcloned into Valium-TEVcs-LexA-HAtag-2A-Arrestin-TEVp using AvrII and NotI, to produce the final product Valium-DopR1-TEVcs-LexA-HAtag-2A-Arrestin-TEVp. For simplicity this vector was re-named UAS-DopR-Tango.

UAS-OctR-Tango (Valium-OctR1- TEVcs-LexA-HAtag-2A-Arrestin-TEVp)

A *Drosophila OctR1* coding sequence was amplified by PCR using primers OctR-f (CCTAGGCAAAATGAATGAAACAGAGTGCGAGG) and OctR-r (GCGGCCGCCCCTGGGGTCGTTGCTCAT), and a cDNA template synthesized from the heads of Canton-S flies. This DNA fragment was subcloned into Valium-TEVcs-LexA-HAtag-2A-Arrestin-TEVp using AvrII and NotI, to produce Valium-OctR1-TEVcs-LexA-HAtag-2A-Arrestin-TEVp. For simplicity this vector was named UAS-OctR-Tango.

UAS-DopEcR

A *Drosophila DopEcR* coding sequence was amplified by PCR using primers DopEcR-f (GGCGGCCGCCAAAATGCAGGAAATGAGCTACCTAC) and DopEcR-r (GTCTAGACTAGTCATCTGGGTCCAACC), and a cDNA template synthesized from the heads of Canton-S flies. This DNA fragment was subcloned into pJFRC-MUH (Pfeiffer et al., 2010) using NotI and XbaI.

UAS-ChR2(C128T)

DNA fragment of ChR2(C128T)::eYFP (Berndt et al., 2009) was amplified by PCR using primers chr2-f (AGAGAACTCTGAATAGATCTCACCatggactatggcggcgctttg) and chr2-r (TTCCTTCACAAAGATCCTCTAGAttacttgtacagctcgtcca), and a plasmid generously provided by Dr. Karl Deisseroth. The amplified PCR products were subcloned into pJFRC-MUH using SLIC cloning (Li and Elledge, 2007).

Fly strains

Th-GAL4 (Friggi-Grelin et al., 2003), *Gr5a-GAL4* (Scott et al., 2001), *elav-GenesSwitch* (Osterwalder et al., 2001), *empty promoter-GAL4* (a *GAL4* line with a *Drosophila* synthetic core promoter but no enhancer 5' to this promoter, which has been shown to have no detectable expression in the adult CNS (Pfeiffer et al., 2008)), and *n-synaptobrevin-GAL4* (*nsyb-GAL4*) (Pauli et al., 2008) were obtained from Dr. Serge Birman, Dr. Kristin Scott, Dr. Haig Keshishian, Barret Pfeiffer and Dr. Gerald M. Rubin, and Dr. Julie Simpson, respectively. *UAS-mCD8::GFP* (pJFRC2 described in (Pfeiffer et al., 2010)), *UAS-DsRed* (Verkhusha et al., 2001), *UAS-GCaMP3.0* (Tian et al., 2009), *UAS-dTRPA1* (Hamada et al., 2008) , *UAS-UPRT* (Miller et al., 2009) and *LexAop-mCD2::GFP* (Lai and Lee, 2006) were generously provided by Dr. Gerald M. Rubin, Dr. Kei Ito, Dr. Loren L Looger, Dr. Paul A. Garrity, Dr. Chris Q. Doe, and Dr. Tzumin Lee, respectively. RNAi lines (Dietzl et al., 2007) were generously provided by Dr. Barry J. Dickson via the VDRC stock center (*UAS-DopEcR RNAi* (KK 103494), *UAS-DopR2 RNAi* (KK 105324), *UAS-GFP*, and *UAS-Dicer2* (on X chromosome)), or the *Drosophila* RNAi Screening Center (*UAS-D2R RNAi* (JF02025) and *UAS-luciferase*) (Dietzl et al., 2007). *UAS-Dicer2* on X chromosome are combined with *nsyb-GAL4* and called *nsyb-GAL4* in this paper. *UAS-dTRPA1* on second chromosome and third chromosome are combined to make a fly strain with two copies of *UAS-dTRPA1*, which are described as *UAS-dTRPA1* in this paper. For DopEcR rescue in *Gr5a* GRNs in *DopEcR* mutant (Figure $5D_3$), *Gr5a-GAL4*(II); $DopEcR^{c02142}$(III) and *UAS-DopEcR*(II); $DopEcR^{c02142}$(III) were crossed (Loss of DopEcR expression was checked with qRT-PCR).

Cell culture

HEK293 cells were maintained in Dulbecco's Modified Eagle Medium (DMEM) (Invitrogen) supplemented with 4mM L-glutamate (Invitrogen), 10% fetal bovine serum (Invitrogen), and 100 units/ml penicillin and streptomycin. Cells were grown at 37°C with 5% CO_2. Cells in 24 well plates were transfected with 0.8 μg each of three plasmids (*CMV-Gal4*, *UAS-DopR-Tango*, and *LexAop-βgal*) by using Lipofectamin2000 (Invitrogen). 12 hours after the transfection, the medium was changed into medium containing one of the following drugs: Dopamine hydrochloride (Sigma); 6,7-ADTN (Sigma); Serotonin hydrochloride (Sigma); or Octopamine hydrochloride (Sigma), and cultured for 24 hours. Cells were harvested and the activity of β-galactosidase was measured using "β-Galactosidase Enzyme Assay System with Reporter Lysis Buffer" kit (Promega) .

Schneider cells (S2 cells) were maintained in fresh complete Schneider's *Drosophila* Medium (Invitrogen). Effecrene™ transfection reagenet (QIAGEN) was used for transfection.

TU-tagging and qPCR

500 transgenic flies carrying *Gr5a-GAL4* and *UAS-UPRT* were fed with 1mM 4-TU solved in sucrose solution for 8 hours. The proboscis of each fly was excised and collected, and TU-tagged RNA was purified from this tissue as described previously (Miller et al., 2009). cDNA was synthesized using Super Script® VILO™ cDNA Synthesis kit (Invitrogen). Real Time PCR was performed using EXPRESS SYBR® GreenER™ (Invitrogen) and a 7300 Real Time PCR system (Applied biosystems). *Cyclophilin1* (*Cyp1*), a housekeeping gene, was used as a standard (*TATA binding protein* (*tbp*) was also used as a standard to give similar results; data not shown). Using melting temperature analysis, each primer pair was confirmed to produce a single PCR product. Primers listed below were used;

Cyp1-f : AGTCTGGCAAGACCTCCAAG

Cyp1-r : TTGCATCGCACCTTCTTAAA

DopR1-f : GAAGTCCATCAAGGCGGTAA

DopR1-r : AGCCAGGTGAGGATCTTGAA

DopR2-f : GAGGATCTCTGAGCCACTCG

DopR2-r : GCAGGCGTAAATCACAGGAT

D2R-f : CACAAGGCCTCGAAAAAGAA

D2R-r : GCGAAACTCGGGATTGAATA

DopEcR-f : TTTGACCGGAGAATGGATGT

DopEcR-r : ATGCAAATGTGCGTCATGTT

Gr5a-f : CCTTCGTGCTGCTGGTAGTT

Gr5a-r : CTTCTTCGTGGGCAGAAGTC

Gr66a-f : ATCTGGTTCGCTGTTTCGTT

Gr66a-r : TTATGCTTCTCGTGCGTGTC

qRT-PCR of mutant or RNAi was performed by synthesizing cDNA from the heads of >10 flies and performing Real Time PCR using the same sets of primers described above.

TANGO-map and confocal imaging

DopR-Tango flies or OctR-Tango flies (*UAS-DsRed* (X)*; LexAop-mCD2::GFP* (II)*; elva-GeneSwitch/ UAS-DopR-Tango* (III; or *UAS-OctR-Tango*)) were collected using CO_2 anesthesia and allowed to recover for 2 days. Flies were first dry-starved for 4 hours to make sure they consumed any drugs provided. Then, flies were moved into a vial containing 0.5 mM RU486 mixed in 89 mM sucrose and allowed to feed for 12 or 24 hours (for subsequent drug feeding or starvation experiments, respectively). After this RU486 feeding, flies were moved to either food vials (fed condition), vials containing a wet filter paper (wet-starved condition), or a drug dissolved in 89 mM sucrose (drug-fed condition). Two days later, fly brains were dissected and immunostained. Drugs used for feeding were L-dopa precursor (Sigma, 3 mg/ml), Chlordimeform (CDM) (Sigma, 0.5 mg/ml), SCH23390 (Sigma, 5 mg/ml), and 3-Iodo-L-tyrosine (3IY) (Sigma, 10mg/ml). In the case of 3IY and SCH23390, feeding was started 5 days before RU486 feeding, or on the day of RU486 feeding, respectively, to achieve effective levels of the drugs. All food vials containing drugs were freshly prepared and drug-fed flies were transferred to fresh drug vials daily for the duration of any feeding period.

Dissected brains were fixed in 4% formaldehyde in PEM (0.1M PIPES, pH 6.95, 2mM EGTA, 1mM $MgSO_4$) for 2 hours at 4 °C. After three 15 min rinses with PBS, brains were incubated with primary antibodies overnight. Following three 15 min rinses with PBS, brains were incubated with secondary antibody overnight. Following three rinses, brains were incubated in 50% glycerol in PBS for 2 hours and cleared with VECTASHIELD® (VECTA). All procedures were performed in 4 °C. For observation of native fluorescence, incubation with primary and secondary antibodies was omitted. An LSM 510 confocal microscope (Carl Zeiss) was used to obtain confocal serial optic sections.

The antibodies used were: Rat anti-HA High Affinity monoclonal antibody (Roche Applied Science), Mouse Tyrosine Hydroxylase Antibody (ImmunoStar) , Cy™5-conjugated AffiniPure Goat Anti-Mouse IgG (H+L) (Jackson ImmunoResearch), and DyLight™549-conjugated AffiniPure Donkey Anti-Rat IgG (H+L) (Jackson ImmunoResearch). Image processing methos are described in Figure S2. Fluorender software (Wan et al., 2009) was used to make 3D reconstructed images of these processed images. ROIs were identified based on the signal of the co-expressed UAS-DsRed; in this way, the expression level of the GFP reporter does not affect the size or identification of the ROI. ROIs were measured in single optical sections in the Z-plane and not in the projection images.

For labellum ablation experiments, the labellum (not including other parts of the proboscis) was surgically ablated using sharp forceps 24 hour after RU486 feeding. The brains were dissected two days after this manipulation.

Signal-to-Noise ratio of DopR-Tango

The Signal-to-Noise ratio (SNR) is defined as SNR=μ/σ, where μ is the mean signal (signal in a given experimental condition) and σ is the standard deviation of the noise (deviation in signal level of control flies). In case of L-dopa feeding (Figure $2B_{1-4}$) the measured SNR was 4.1, 4.0, 3.9 and 1.5 in the AL, SOG, MB β lobe and MB γ lobe, respectively. The SNR in the γ lobe is low due to one outlier point in the control sample, which increased σ. The relatively low SNR may due to variability among flies in endogenous factors (e.g.,

differences in levels of endogeneous baseline DA release) and/or exogenous factors (e.g., differences in the expression level of DopR-Tango, or the extent of DA-independent cleavage).

PER assays

All PER tests were performed by an experimenter blind to genotype or experimental condition. All of experimental flies were maintained on a 12 hour day-night cycle. Newborn female flies were CO_2 anesthetized and allowed to recover for more than 3-7 days prior to the assay at 25°C (or 10-14 days at 27°C in the case of RNAi flies, to boost the effect of RNAi). For standard PER assays, 10-20 flies were pre-incubated for the indicated times in a vial containing a piece of filter paper soaked with 1 ml of water, in the case of wet-starved flies, or with 1 ml of 89mM sucrose solution in the case of sucrose-fed flies. For L-dopa feeding experiments, L-dopa precursor (Sigma) was dissolved in the sucrose solution, and flies maintained with this solution for 2 days (In all experiments with L-dopa feeding, a concentration of 3 mg/ml was used unless otherwise indicated. Higher concentrations of L-dopa was not used because of side-effects such as changes in body coloration or death).

Prepared 10-20 experimental flies were mounted into 200 μl pipetman tips as described previously (Shiraiwa and Carlson, 2007). After mounting, the backs of flies were glued to the pipetman tip to avoid their escape. Flies were allowed 3 min for acclimation prior to testing. A 10μl pipetman (Gilson) was used to present 0.5μl drops of water or sucrose solutions to the labellum of the flies. All flies were initially checked for responses to water. If flies showed a PER to water, they were allowed to drink until they stopped. This procedure was repeated twice, and flies still responding to water were excluded from subsequent testing. Next we tested the responses to stepwise increasing concentrations of sucrose, ranging from 6.25 mM to 400 mM (or 800 mM). The same sets of flies were tested with all concentrations of sucrose. We presented the same concentration of sucrose twice to each fly, and if they extended their proboscis to either of the two presentations, we scored a positive response. Only full extensions of the proboscis, but not partial extensions, were scored as positive. We withdrew the drop as soon as possible after touching it to the labellum, so that flies could not drink the sucrose solution. The fractions of flies showing a PER response as a function of

sucrose concentration was calculated. For each experimental condition, an experimental trial using 10-20 flies was repeated independently at least 5 times to perform statistics (the number of repetitions is the n shown in legends. E.g. n=5 means the curve represents data from 5 such independent experiments. Thus the total number of flies used for the curve is 50-100). The standard PER assay was performed at room temperature (23±2°C). Mean Acceptance Thresholds (MATs) (Long et al., 1986) were calculated as described in Supplemental Experimental Procedures.

For TrpA1 experiments, flies were raised at 21°C. Flies were mounted at 23°C, and PER assays performed at either 23°C or 30°C. The PER test was performed immediately after transferring the flies to different temperature and finished within 10 min. *Th-GAL4*; *UAS-dTRPA1* flies showed partial proboscis extensions without sugar stimulation at 30°C, but rarely showed full extensions without the stimulation. Only full extensions were scored as positive responses.

Calculation of MAT

In order to calculate MAT, sugar concentration where 50% of flies show PER, sigmoid interpolation was performed (PER response curves were fitted into sigmoid curves). The sigmoid curves can be described as below:

$$S_s = \frac{1}{1 + e^{(-\alpha_s \log_2 \frac{S_{con}}{MAT})}}$$

Ss : Fraction of flies showing PER on different sugar concentration

Scon : Sugar concentration (mM)

MAT: Sugar concentration where 50% of flies show PER

αs : slope of the sigmoid curve

For all experimental data, polynomial curve fitting, which finds the coefficients that fit the data by the least squares method, was done with Matlab (MathWorks). Goodness-of-fit was tested by two-way ANOVA between the actual PER response curves, and the sigmoid curve with the calculated coefficients (Figure S3B). All wild-type sucrose response data were well-fit by a sigmoid curve (two-way ANOVA). The value of MAT decreased with starvation time, while αs shows a statistical significant decrease after 2 days of starvation or L-dopa feeding ($p<0.05$ by one-way ANOVA followed by a post hoc t-test with Bonferroni correction; Figure S3C). Decrease in MAT indicates the increase in behavioral sugar sensitivity, and decrease in αs implies either (1) increase in distinguishability between two sugar concentration or (2) increase sugar sensitivity at lower sugar concentration. Since we are interested in the changes in behavioral sugar sensitivity, MAT was used for data analysis. It should be noted that the use of MAT as a metric for comparison does not require that the PER response be titrated to saturation for each experimental or control condition, because MAT is a probabilistic measure (i.e., it measures the sucrose concentration at which 50% of the flies in a population are likely to show a PER response), whose value by definition therefore ranges between 0 and 1 (Long et al., 1986). The values of MAT are normally distributed among the data obtained from wild-type flies under the same condition of food-deprivation (Lillifors test and Jarque-BARA test, and also checked by linearity in a probability plot). Thus parametric statistical tests were used for analysis of MAT data. With the exception of the data from the *TH-Gal4; UAS-TrpA1* experiment at 30°C (Figure $4C_1$), and the *DopEcR* mutant fed with L-dopa (Figure $5A_2$), all of the experimental curves were well-fit by sigmoid curves (two-way ANOVA). Therefore, the value of MAT (50% probability of a PER response) was interpolated from the experimental data based on the sigmoidal curve-fitting. In case of the *DopEcR* mutant fed with L-dopa (Figure $5A_{2,3}$), the MAT was estimated by linear interpolation between the two nearest data points above and below a 50% response. In addition, to the comparison of MAT values, these experiments were also analyzed using two-way ANOVA of experimental vs. control curves.

ChR2 assay

All *trans*-Retinal powder (Sigma) was stored in -20°C as 20mM solution dissolved in ethanol. After overnight wet starvation, *Gr5a-GAL4*;*UAS-ChR2(C128T)* flies were transferred into a vial with 200μM all *trans*-Retinal

diluted in 89mM sucrose, and allowed to feed for 24 hours. These vials were maintained in the dark to avoid photo-isomerization of all *trans*-Retinal. After retinal feeding, flies were either fed or wet-starved for 1 day, or fed with L-dopa precursor (3 mg/ml) for 2 days.

Flies were mounted into pipet tips, as in the standard PER assay, and placed under a fluorescent microscope (Lecia MZ FLIII Fluorescence Stereomicroscope). Light emitted by a standard mercury lamp (HBO® 100w/2, OSRAM) equipped with a GFP filter (Leica, 470/40nm: centerwavelength/bandwidth) was used to stimulate ChR2-expressing flies. The light was switched on by moving the filter manually. The fraction of flies showing a full proboscis extension in response to light in the first 5 seconds was scored. The intensity of the light was controlled by changing the magnification of the microscope. The light power density at 488nm was measured with Power meter (Model 1931, New port). Each fly was tested only at a single intensity of light, because repeated exposure to light decreased the behavioral response.

Calcium imaging

The protocol for calcium imaging was modified from that described in (Marella et al., 2006). After a brief anesthesia on ice, flies were mounted on a thin plastic plate with wax as shown in Figure 6B. The top side of the plate contained a well made with wax, and the fly head was immersed in ice-cold Ca^{2+} free saline (108mM NaCl, 5mM KCl, 8.2mM $MgCl_2$, 4mM $NaHCO_3$, 1mM NaH_2PO_4, 15mM Ribose, 5mM HEPES, pH 7.5; note that Ribose, which does not stimulate *Drosophila* sugar sensing neurons, is used instead of other sugars). In this saline bath, the antennae and cuticle at the anterior side of the fly head capsule were surgically removed with sharp forceps, so that the SOG could be imaged. The fat body, air sacs, and esophagus were gently removed to give a clear view of the brain and to minimize its movement. At the bottom side of the plate, a glass tube was mounted with the opening facing the proboscis of the mounted fly. A piece of twisted Kimwipe was placed just behind the fly. During imaging, a sucrose solution was delivered from the glass tubing to stimulate gustatory neurons in the proboscis and was removed by the Kimwipe.

Following dissection, the ice-cold Ca^{2+} free saline was removed and the fly brain was immersed in 1 ml of room-temperature imaging saline (108mM NaCl, 5mM KCl, 2mM $CaCl_2$, 8.2mM $MgCl_2$, 4mM $NaHCO_3$,

1mM NaH_2PO_4, 15mM Ribose, 5mM HEPES, pH 7.5). This setup was moved under an Ultima two-photon laser scanning microscope (Prarie Instruments, Inc) with a 40× 0.8 N.A. objective (Olympus, Inc). The glass tubing was connected to four silicon tubes with a plastic manifold (MP-4, Warner Instruments). Each silicon tube was connected to 50 ml syringes filled with either 15 ml of 0mM, 25mM, 100mM, or 400mM sucrose dissolved in the imaging saline solution. The flow of sucrose solution was controlled using electrically triggered pinch valves (ALA-VM8, ALA Scientific Instruments) that compressed the silicon tubes between the syringes and the manifold. The timing of valve opening was controlled by the two-photon acquisition system and its software (Prairie view and Trigger Sync, Prairie) so that the timing was linked with the image acquisition. $\int \Delta F/F \, dt$, the integral of $\Delta F/F$ during the period of exposure to each stimulus, was calculated using MatLab (MathWorks).

Since the behavioral effect of L-dopa feeding was smaller in *Gr5a-GAL4*; *UAS-GCaMP3.0* flies compare to other flies with different genetic backgrounds, we fed these flies with 5 mg/ml of L-dopa precursor (rather than the standard 3 mg/ml) for both imaging and the PER. PER assays of *Gr5a-GAL4*; *UAS-GCaMP3.0* flies were performed as described in the PER assay.

For direct DA exposure during imaging (Figure $6F_{1-3}$), firstly the GCaMP response to sugar was measured as described above. Then 10 μl of 100 mM dopamine chloride (dissolved in the imaging saline) was added to 1 ml of imaging saline in which the fly brain was immersed using a pipetman, so that the final concentration of DA became 1mM. The 100× DA stock solution was prepared freshly just before each experiment to avoid oxidation. After 5 min of incubation, the same brain was scanned before and during stimulation with different concentrations of sucrose. These responses were imaged in the same presynaptic terminals that were imaged prior to DA addition, and a comparison of the calcium signal in each condition (0 mM, 25 mM, 100 mM and 400 mM sucrose) was made pre- vs. post-DA addition. To do this, the average fluorescence signal in the absence of sucrose (0 mM), prior to DA addition, was used as F to calculate $\Delta F/F$ both before and after DA addition ($\Delta F/F_{\text{before DA}}=(F_{t\_before}-F_{0\_before})/ F_{0\_before}$ and $\Delta F/F_{\text{after DA}}=(F_{t\_after}-F_{0\_before})/ F_{0\_before}$, where F_t is F at time t). From these values, we calculated the fold-increase in F as the ratio of the integrated signals post/pre DA

addition (Fig. 6G). This analysis could be performed because the signals both before and after addition of DA were scanned from the same neurons in the same fly. To eliminate the contribution of motion artifacts, we ensured that scans were performed on the same focal plane for each measurement. To further control for non-specific changes in fluorescence due to movement during addition of the concentrated DA solution to the imaging bath, we imaged a series of flies in which we added 10 μl of imaging saline (without DA) to the bath.

Electrophysiology

The tip recording method was used for the recording of the electrophysiological responses of labellar taste neurons (Hodgson et al., 1955; Weiss et al., 2011). Briefly, the fly was mounted and immobilized for recording by inserting a pulled glass capillary (BF150-86-10, Sutter instruments) from the dorsal surface of the thorax to the tip of the labellum, passing through the cervical connective and the head. The mounting glass capillary was filled with recording solution (7.5 g/L NaCl, 0.35 g/L KCl, 0.279 g/L $CaCl_2 \cdot 2H_2O$ and 11.915 g/L HEPES (Sigma-Aldrich)) and served as indifferent electrode. Another glass capillary, pulled to a tip diameter of 10 to 20 micrometers and filled with tastant solution, was used for both introducing the taste molecules to the tip of the relevant sensillum and for the recording of the electrophysiological responses of the gustatory neurons innervating this sensillum. Sucrose was dissolved in water solution containing 30 mM tri-choline chloride (TCC; Sigma-Aldrich), as an electrolyte. TCC solution was used as a control to monitor the spontaneous activity of the sugar neurons in the absence of sucrose.

In each recording, the relevant sensillum was exposed to the tastant solution or to the control solution for 7 seconds. The recordings were made by using MultiClamp 700B amplifier and Digidata 1440A A/D converter (Molecular Devices). The recorded data were sampled at a rate of 10 KHz, filtered (band pass filter between 100 Hz and 3 KHz) and stored on a PC hard drive with Clampex 10 software (Molecular Devices). The data were analyzed by sorting the action potentials and measuring their frequency in the indicated time windows along the trace with Clampfit software (Molecular Devices). Only the first exposure of sensilla that responded to high concentrations of sucrose (100 mM) were included in the analysis. In every experiment, several sensilla from the same fly were tested.

Supplemental References

Berndt, A., Yizhar, O., Gunaydin, L.A., Hegemann, P., and Deisseroth, K. (2009). Bi-stable neural state switches. Nat Neurosci *12*, 229-234.

Dietzl, G., Chen, D., Schnorrer, F., Su, K.C., Barinova, Y., Fellner, M., Gasser, B., Kinsey, K., Oppel, S., Scheiblauer, S.*, et al.* (2007). A genome-wide transgenic RNAi library for conditional gene inactivation in Drosophila. Nature *448*, 151-156.

Donnelly, M.L., Hughes, L.E., Luke, G., Mendoza, H., ten Dam, E., Gani, D., and Ryan, M.D. (2001). The 'cleavage' activities of foot-and-mouth disease virus 2A site-directed mutants and naturally occurring '2A-like' sequences. J Gen Virol *82*, 1027-1041.

Friggi-Grelin, F., Coulom, H., Meller, M., Gomez, D., Hirsh, J., and Birman, S. (2003). Targeted gene expression in Drosophila dopaminergic cells using regulatory sequences from tyrosine hydroxylase. J Neurobiol *54*, 618-627.

Groth, A.C., Fish, M., Nusse, R., and Calos, M.P. (2004). Construction of transgenic Drosophila by using the site-specific integrase from phage phiC31. Genetics *166*, 1775-1782.

Hodgson, E.S., Lettvin, J.Y., and Roeder, K.D. (1955). Physiology of a primary chemoreceptor unit. Science *122*, 417-418.

Lai, S.L., and Lee, T. (2006). Genetic mosaic with dual binary transcriptional systems in Drosophila. Nat Neurosci *9*, 703-709.

Li, M.Z., and Elledge, S.J. (2007). Harnessing homologous recombination in vitro to generate recombinant DNA via SLIC. Nat Methods *4*, 251-256.

Lim, J.S. (1990). Two-dimensional signal and image processing (Englewood Cliffs, N.J., Prentice Hall).

Mank, M., Santos, A.F., Direnberger, S., Mrsic-Flogel, T.D., Hofer, S.B., Stein, V., Hendel, T., Reiff, D.F., Levelt, C., Borst, A.*, et al.* (2008). A genetically encoded calcium indicator for chronic in vivo two-photon imaging. Nat Methods *5*, 805-811.

Markstein, M., Pitsouli, C., Villalta, C., Celniker, S.E., and Perrimon, N. (2008). Exploiting position effects and the gypsy retrovirus insulator to engineer precisely expressed transgenes. Nat Genet *40*, 476-483.

Ni, J.Q., Markstein, M., Binari, R., Pfeiffer, B., Liu, L.P., Villalta, C., Booker, M., Perkins, L., and Perrimon, N. (2008). Vector and parameters for targeted transgenic RNA interference in Drosophila melanogaster. Nat Methods *5*, 49-51.

Pfeiffer, B.D., Jenett, A., Hammonds, A.S., Ngo, T.T., Misra, S., Murphy, C., Scully, A., Carlson, J.W., Wan, K.H., Laverty, T.R.*, et al.* (2008). Tools for neuroanatomy and neurogenetics in Drosophila. Proc Natl Acad Sci U S A *105*, 9715-9720.

Pfeiffer, B.D., Ngo, T.T., Hibbard, K.L., Murphy, C., Jenett, A., Truman, J.W., and Rubin, G.M. (2010). Refinement of tools for targeted gene expression in Drosophila. Genetics *186*, 735-755.

Shafer, O.T., Kim, D.J., Dunbar-Yaffe, R., Nikolaev, V.O., Lohse, M.J., and Taghert, P.H. (2008). Widespread receptivity to neuropeptide PDF throughout the neuronal circadian clock network of Drosophila revealed by real-time cyclic AMP imaging. Neuron *58*, 223-237.

Verkhusha, V.V., Otsuna, H., Awasaki, T., Oda, H., Tsukita, S., and Ito, K. (2001). An enhanced mutant of red fluorescent protein DsRed for double labeling and developmental timer of neural fiber bundle formation. J Biol Chem *276*, 29621-29624.

Wan, Y., Otsuna, H., Chien, C.B., and Hansen, C. (2009). An interactive visualization tool for multi-channel confocal microscopy data in neurobiology research. IEEE Trans Vis Comput Graph *15*, 1489-1496.

Wilson, R.I., Turner, G.C., and Laurent, G. (2004). Transformation of olfactory representations in the Drosophila antennal lobe. Science *303*, 366-370.

Chapter II

INDEPENDENT NEUROMODULATORY CONTROL OF ATTRACTIVE AND AVERSIVE TASTE SENSING IN STARVED *DROSOPHILA MELANOGASTER*

SUMMARY

Adjusting behavioral decisions to internal demands is critical for an animal's survival. Here, we find that the hunger state modulates feeding decisions by reciprocally regulating attractive and aversive gustatory sensing in *Drosophila melanogaster*. Genetic manipulations revealed that two distinct neuromodulatory pathways control these two gustatory modalities during hunger: The neuropeptide F (NPF) – dopamine (DA) pathway enhances sugar sensitivity under mild starvation, while the adipokinetic hormone (AKH)- short neuropeptide F (sNPF) pathway attenuates bitter sensitivity under severe starvation. The influences of these pathways are exerted, at least in part, via modulation of peripheral taste sensitivity. Moreover, these two pathways are recruited without any detectable crosstalk at all levels of regulation examined, from interoceptive receptors, to mediating neuromodulators and target sites of modulation, implying parallel rather than unitary mechanisms regulating starvation state. Independent and inverse regulation of bitter and sugar sensing yield adaptive feeding-decisions with a high dynamic range at different hunger levels.

INTRODUCTION

Changes in internal states, such as defensive arousal, starvation and sleep, affect behavioral choices in animals (Blanchard and Blanchard, 1989; Sternson et al., 2013; Taghert and Nitabach, 2012). Typically, these state-dependent influences are "multi-dimensional": one state affects multiple sensory modalities and behaviors; "scalable": the strength of such modulation differs depending on the intensity of the state; and time-varying. These prominent features of state-control enable animals to adjust their behavioral responses properly according to context or internal demands. However, understanding how these features are instantiated is challenging because it requires a comprehensive analysis of state-control pathways, including the identification of interoceptive mechanisms, neuromodulatory influences, targets of neuromodulation, and consequent behavioral changes.

The control of feeding in starved *Drosophila melanogaster* provides an attractive model for state-dependent control of behavior, because of the organism's relatively simple nervous system, a quantitative feeding response, and our growing understanding of the gustatory, interoceptive, and neuromodulatory systems in this species. *Drosophila* detects gustatory cues in foods with their taste bristles on the labellum and other parts of the body (Montell, 2009; Thorne et al., 2004). Sugar, low concentrations of salt, fatty acids and other attractive tastants are detected by gustatory receptor 5a (Gr5a)-expressing gustatory receptor neurons (GRNs), while toxic compounds, such as bitter substances and high concentrations of salt, are detected by Gr66-expressing GRNs (Marella et al., 2006; Masek and Keene, 2013; Scott et al., 2001; Wang et al., 2004; Weiss et al., 2011; Zhang et al., 2013). Multiple candidate interoceptive receptors and cells have been also identified in *Drosophila* (Dus et al., 2013; Kim and Rulifson, 2004; Kreneisz et al., 2010; Miyamoto et al., 2012). As in mammals (Andrews et al., 2008; Luquet et al., 2005; Sternson et al., 2013), some of these interoceptive neurons express neuropeptides/neurohormones, such as adipokinetic hormone (AKH) and *Drosophila* insulin-like peptides (DILPs) (Kim and Rulifson, 2004; Kreneisz et al., 2010). In addition, various other neuromodulators have been shown to regulate feeding responses in starved adult *Drosophila* (Itskov and Ribeiro, 2013; Nassel and Wegener, 2011; Taghert and Nitabach, 2012). In particular, NPF and sNPF, distinct functional orthologues of NPY, modulate multiple feeding related behaviors, including the formation and

expression of food-associated memory, enhancement of food-related olfactory sensitivity, and control of food intake during starvation (Beshel and Zhong, 2013; Hergarden et al., 2012; Krashes et al., 2009; Lee et al., 2004; Root et al., 2011).

Many animal species become less selective in their food choices during periods of energy deficit. They do so by enhancing their sensitivity to nutritious resources, such as sugar (Berridge, 1991; Dethier, 1976; Gillette et al., 2000; Inagaki et al., 2012; Kawai et al., 2000; Moss and Dethier, 1983; Page et al., 1998; Sengupta, 2013). In *Drosophila*, starvation enhances behavioral sensitivity to sugar, at least in part, via increased dopamine release onto Gr5a-expressing sugar-sensing GRNs, which increases calcium responses to GR activation (Inagaki et al., 2012; Marella et al., 2012). Starvation also decreases sensitivity to unpalatable compounds, such as bitter tastants. The prevailing view is that this decrease in bitter sensitivity is not independently controlled, but rather is an indirect consequence of the "masking effect" of enhanced sugar sensitivity (Figure $1A_1$) (Moss and Dethier, 1983). Here we identify a pathway in *Drosophila* controlling the reduction of bitter taste sensitivity during starvation that is mechanistically independent of the increase in sweet tastant sensitivity. This pathway combines with the masking effect of enhanced sugar sensitivity to increase acceptance of resources containing unpalatable contaminants, during periods of energy deficit (Figure $1A_3$). Thus the multi-dimensional features of the "hunger" state reflect parallel regulatory mechanisms, rather than a unitary control process.

RESULTS

Bitter sensitivity decreases during starvation independently from the change in sugar sensitivity

To quantify feeding behavior, we presented a drop of solution containing sugar and/or bitter tastants to the labellum, where GRNs are located. When sugar is presented, *Drosophila* extend their proboscis, a reaction known as the proboscis extension reflex (PER) (Dethier, 1976). We selected this method over others because only this method provides quantification of gustatory sensitivity independently of food intake. As previously reported (Inagaki et al., 2012; Meunier et al., 2007), when flies are wet starved (WS; deprived of food but not water; see Experimental Procedures), dose-response curve for fraction of flies showing PER to each

concentration of sucrose shifted to the left, indicating an increase in sugar sensitivity (Figure $1B_1$). In addition, the mean acceptance threshold to sugar, S_{50} (the sucrose concentration at which 50% of the flies show a PER; see Experimental Procedures) (Inagaki et al., 2012) is decreased (Figure $1B_2$; note that the y-axis is inverted: as sensitivity increases, S_{50} decreases). Importantly, the magnitude of both effects increased significantly with longer starvation times (1 day vs. 2 days), suggesting a scalable underlying state change (Fig. $1B_{1\text{-}2}$). These analyses confirm that starvation increases behavioral sensitivity to sucrose in *Drosophila*.

Next, we tested behavioral sensitivity to unpalatable tastants by presenting a sugar solution mixed with various concentrations of bitter substances. Consistent with a previous report (Meunier et al., 2003), the admixture of bitter substance (lobeline) suppressed the PER to sugar in a dose dependent manner. We quantified this effect by measuring the fraction of flies <u>not</u> showing a PER; thus a higher value of this metric reflects a stronger suppression of the PER to a fixed amount of sucrose (Figure $1C_1$,"Fed"). Genetic silencing experiments indicated that Gr66a GRNs are required for the effect of bitter substances to suppress the PER (Figure S1A), consistent with earlier studies (Gordon and Scott, 2009; Wang et al., 2004). Interestingly, during starvation the dose-response curve for this parameter was shifted to the right, indicating a progressive reduction in bitter sensitivity (Figure $1C_1$,"WS"). Consistent with this, the mean acceptance threshold to bitter, B_{50} (the bitter concentration required to inhibit the PER in 50% of flies that showed response to sugar: Figure S1B), significantly increased with starvation duration (Figure $1C_2$; note that the y axis is inverted). Similarly sensitivity to other bitter substances (caffeine and coumamine) decreased during starvation (data not shown). Therefore, during starvation behavioral sensitivity to sugar increases, while sensitivity to bitter tastants is reduced (c.f. Fig. $1B_2$ vs. $1C_2$).

Because bitter sensitivity was quantified as the suppression of a behavioral response to sucrose, it was possible that when flies are starved, their absolute bitter sensitivity does not change, but is relatively reduced due to the increased sugar sensitivity. Studies in the blowfly, *Phormia regina*, support this idea (Moss and Dethier, 1983). Indeed, higher concentrations of sugar shifted the dose-response curve for bitter inhibition of the PER to the right (Figure S1C). In order to quantify behavioral sensitivity to bitter independently of the increase in sugar sensitivity, we tested the effect of lobeline to suppress PER responses in fed, 1 day WS, 2 day WS flies, at concentrations of sugar that yielded the same sub-saturating PER responses (50-60 %), i.e.

800mM, 300mM and 200mM (see red dotted boxes in Figure $1B_1$ and $1D_1$). Using such a "sugar-normalized PER assay" in starved vs. fed flies, we still observed a statistically significant, albeit smaller magnitude, decrease in bitter sensitivity following food deprivation (Figure $1D_{1,2}$).

We next compared the kinetics of these gustatory sensitivity changes. Sugar sensitivity increased most strongly during the first 6 hours of starvation and continued more gradually from 6 to 48 hours (Figure $1E_1$). In contrast, sugar-normalized PER assays did not reveal any decrease in bitter sensitivity until after 24 hours of starvation (Figure $1E_2$).

Taken together, these data reveal that, in contrast to the prevailing view, bitter sensitivity decreases independently from the increase in sugar sensitivity during starvation, at least in *Drosophila*. Moreover, these changes occur at different levels of food deprivation. Different models may explain these results (Fig. $1A_{1-3}$). In order to distinguish between them, we investigated the cellular and molecular mechanisms underlying these changes.

NPF acts upstream of dopamine to control sugar but not bitter sensitivity

We first asked whether the neuromodulatory pathway that regulates sugar sensitivity also modulates bitter sensitivity during starvation. The effect of dopamine to increase sugar sensitivity during mild starvation (Inagaki et al., 2012; Marella et al., 2012) is mediated by the receptor DopEcR (Srivastava et al., 2005), expressed on Gr5a GRNs (Inagaki et al., 2012). To test whether dopamine reciprocally regulates bitter sensitivity, we fed non-starved flies with L-dopa, a precursor of dopamine, that is known to increase dopamine levels in the fly brain (Bainton et al., 2000). As previously reported, L-dopa feeding increased sugar sensitivity in non-starved wild-type flies, mimicking the effect of starvation (Figure $2A_{1-2}$) (Inagaki et al., 2012). In contrast, L-dopa feeding did not cause a decrease in bitter sensitivity (Figure $2B_{1-2}$). Thus, dopamine modulates sugar but not bitter sensitivity during starvation.

NPF, an orthologue of mammalian neuropeptide Y, has been shown to promote ingestion of unpalatable foods in both larval and adult *Drosophila* (Hergarden et al., 2012; Wu et al., 2003; Wu et al., 2005). To determine whether NPF might directly suppress bitter sensitivity in adult flies, we artificially stimulated NPF-expressing neurons using dTrpA1 (Hamada et al., 2008) and performed PER assays at 31 °C.

Activation of NPF neurons enhanced the sugar sensitivity of fed flies, as if they were starved, in comparison to flies of the same genotype tested at 21ºC (Figure $2C_{1-2}$). None of the genetic control flies exhibited different sugar sensitivities at the permissive and non-permissive temperatures (Figure $S2A_{1-4}$: Note that genetic background has a significant effect on baseline gustatory sensitivities. For genetic manipulations using the GAL4-UAS system below, GAL4/UAS-effector, +/ UAS-effector, GAL4/+, and genetic background-matched +/+ controls were always performed in parallel to show that the effects were specific to the GAL4/ UAS-effector genotype). In contrast, activation of NPF did not affect behavioral bitter sensitivity in sugar-normalized PER assay (Figure $2D_{1-2}$ and $S2B_{1-4}$). Conversely, genetic silencing of NPF-GAL4 neurons inhibited the starvation-dependent increase in sugar sensitivity, but it did not interfere with the starvation-dependent decrease in bitter sensitivity (Supplementary Figure $S2C_{1-6}$ and S2D). Thus, as in the case of DA, activation of NPF neurons enhances sugar sensitivity, but does not independently influence bitter sensitivity.

Since both NPF neurons and DA enhance sugar sensitivity during starvation, we sought to determine whether NPF neurons and DA function in the same or in parallel neuronal pathway(s). Immunostaining experiments indicated that NPF and DA neurons are distinct (Figure $S2E_{1-3}$). We reasoned that if NPF and DA act in the same pathway to modulate sugar sensitivity, then NPF neurons would likely function upstream of DA neurons because the latter directly modulates sugar-sensing GRNs (Inagaki et al., 2012). To test this idea, we combined thermogenetic activation of NPF neurons (*NPF-GAL4/UAS-dTrpA1*) with a hypomorphic mutation in *DopEcR*, which is expressed in sugar-sensing GRNs and mediates the influence of DA on these cells (Inagaki et al., 2012). A homozygous *DopEcR* mutation completely blocked the increase in sugar sensitivity caused by activation of NPF neurons in heterozygous fed flies (Figure $2E_{1-2}$). These data suggest either that 1) NPF neurons act upstream of DA neurons to increase sugar sensitivity, or that 2) both DA and NPF neurons act on the same targets, but DA is somehow permissive for the action of NPF neurons. In either case, the results imply that NPF and DA neurons act in an inter-dependent manner to modulate sugar sensitivity (Figure 2F). This NPF-DA pathway is necessary and sufficient to enhance sugar sensitivity during starvation, but does not affect bitter sensitivity.

sNPF is necessary and sufficient to modulate bitter sensitivity during starvation without affecting sugar sensitivity

Next, we sought to identify neuromodulatory systems that mediate the decrease in bitter sensitivity during starvation. sNPF, an NPY-related protein in *Drosophila*, has been implicated in many hunger related behaviors (Nassel and Wegener, 2011), including the control of food intake in larvae (Lee et al., 2008; Lee et al., 2004) and food-related olfactory sensitivity in adults (Root et al., 2011). To ascertain whether sNPF is also involved in starvation-mediated control of gustatory sensitivity, we tested the behavioral sensitivity of *sNPF* mutant flies to sugar and bitter using the PER assay. We used a hypomorphic mutant of *sNPF*, $sNPF^{c00448}$ (Lee et al., 2008), which has a piggyBac transposon insertion (Thibault et al., 2004) in the first intron of the *sNPF* locus (Figure S3A: These *sNPF* mutant flies were backcrossed into a wild type background for at least six generations). Homozygous *sNPF* mutant flies did not show any difference from controls in their sugar sensitivity, at any starvation time (Figure $3B_1$ and $S3B_{1-3}$). In contrast, these homozygous mutants showed an attenuated decrease in bitter sensitivity during starvation (Figure $3A_{2-3}$ and $3B_2$, red curves/bars). Interestingly, *sNPF*/+ heterozygotes also showed a similar phenotype (Figure $3B_2$, green curves/bars), indicating haploinsufficiency of this neuropeptide gene. Importantly under fed conditions, *sNPF* mutant flies did not show any change in bitter sensitivity (Figure $3A_1$). Similar results were obtained with a different *sNPF* hypomorphic PiggyBac insertion allele, $sNPF^{f07577}$ (Figure S3A and $S3C_{1-2}$). When we used normalized-sugar PER assays to compare the bitter sensitivity between 1-day wet-starved and unstarved flies, homozygous *sNPF* mutant flies showed no change in bitter sensitivity (Figure $3C_2$), unlike wild type flies (Figure $3C_1$). Flies trans-heterozygous for $sNPF^{c00448}$ and $sNPF^{f07577}$ also showed the same loss of bitter sensitivity decrease (Figure $3C_3$). Together, these data suggest that *sNPF* is necessary for the starvation-induced decrease in bitter sensitivity, but not for baseline bitter detection.

In larvae, sNPF regulates food intake and growth (Lee et al., 2008; Lee et al., 2004). To show that the loss of bitter sensitivity change in adult flies is not a developmental byproduct of sNPF function in larvae, we rescued the expression of sNPF specifically in the adult nervous system. We expressed sNPF protein in neurons of *sNPF* hypomophic mutant flies using *UAS-sNPF* under the control of *elav-GeneSwitch* (*elav-GS*), a pan-neuronally expressed, hormone (RU486) inducible form of GAL4 (Osterwalder et al., 2001). Rescue of

sNPF expression by RU486 feeding in adult flies resulted in a recovery of the starvation-induced decrease in bitter sensitivity (Figure $3D_2$ and $3E_2$), without affecting sugar sensitivity (Figure $3E_1$ and $3SD_2$). RU486 feeding did not affect bitter sensitivity in control flies lacking *elav-GS*, showing this is not an artifact caused by the inducer (Figure $3D_1$, $3E_{1-2}$, and $S3D_1$). Altogether these results indicate that, 1) sNPF expression is necessary for the decrease in bitter sensitivity during starvation, 2) this effect is not due to a developmental function, and 3) neuronal sNPF regulates bitter sensitivity. Importantly, none of the genetic manipulations of *sNPF* described above affected sugar sensitivity, suggesting that sNPF independently modulates bitter sensitivity (Figure 3H).

To test whether sNPF-expressing neurons (sNPF neurons) play a role in the control of bitter sensitivity, we genetically silenced subsets of sNPF neurons by expressing KIR2.1 under the control of different GAL4 lines each driven by different DNA fragments from the *sNPF* gene (Lee et al., 2009; Pfeiffer et al., 2008). Expression of KIR2.1 was restricted to adulthood using $Gal80^{ts}$, and bitter sensitivity was analyzed after 1 day of wet starvation. Among 6 lines tested, only one line, *GMR21B10-GAL4*, exhibited an attenuated change in bitter sensitivity (Figure $3F_1$ and $3F_3$). Importantly, silencing of neurons labeled by this GAL4 line did not affect sugar sensitivity (Figure $3F_2$ and S3E). The *GMR21B10-GAL4* line does not label GRNs in the labellum (Figure S3F), indicating that the behavioral phenotype is not due to silencing of sugar-sensing or bitter-sensing GRNs. Instead, this line labels a small number of neurons in the central brain (not including the optic lobes), some of which also exhibited anti-sNPF immunoreactivity (Figure 3G): 7-9 lateral neurosecretory cells (LNCs) and 5-7 S3 interneurons in the SOG (Nassel et al., 2008). Anti-sNPF immunocreactivity of these neurons was reduced in *sNPF* mutant flies (Figure $S3G_{1-2}$).

To confirm further that the sNPF-expressing neurons labeled by *GMR21B10-GAL4* regulate bitter sensitivity, we rescued sNPF expression under the control of *GMR21B10-GAL4* in the *sNPF* hypomorphic mutant background. This rescue restored the starvation-dependent decrease in bitter sensitivity (Figure $3C_5$). Driving *UAS-sNPF* expression in a different subset of neurons using *sNPF-GAL4* did not rescue the mutant phenotype (Figure $3C_4$ and S3H). Therefore, while there is a large number of sNPF positive neurons, including ~4000 Kenyon cells and c.a. 280 other neurons in the brain (Nassel et al., 2008; Nassel and Wegener, 2011), a specific subset (~15 neurons per hemisphere) is necessary and sufficient to regulate bitter

sensitivity. Importantly, none of the neurons labeled by *GMR21B10-GAL4* co-expressed NPF or DA (Figure S3I and S3J). These data, and the lack of any effect of *sNPF* mutations or neuronal silencing on sugar sensitivity, suggests that the NPF-DA sugar-regulating pathway and sNPF bitter-regulating pathway are distinct at the neuronal circuit level (Figure 3H).

sNPFR is necessary for bitter sensitivity control

If sNPF controls the starvation-dependent decrease in bitter sensitivity, one might predict that its receptor should have a similar function. sNPF receptor (sNPFR) is the only identified G-protein coupled receptor for sNPF in *Drosophila* (Feng et al., 2003; Mertens et al., 2002; Reale et al., 2004). Over-expression of sNPFR using *UAS-sNPFR* under the control of the pan-neuronal *nsyb-GAL4* driver (Pauli et al., 2008) enhanced the starvation-dependent decrease in bitter sensitivity (Figure $4A_{1-2}$, B_2, and $S4B_{1-2}$). Conversely, pan-neuronal knock-down of sNPFR using *sNPFR RNAi* attenuated the starvation-dependent decrease in bitter sensitivity (Figure $4C_{1-3}$, and $4D_2$: these transgenic flies also contained *UAS-Dicer2* to enhance the effects of RNAi). Importantly, neither of these manipulations affected sugar sensitivity (Figure $4B_1$, $4D_1$, $S4A_{1-3}$ and $S4C_{1-3}$), nor did they affect bitter sensitivity in fed flies (Figure $4A_1$ and $4C_1$). Therefore, neuronal expression of sNPFR 1) is necessary for the starvation-dependent decrease in bitter sensitivity, 2) does not affect basal bitter sensitivity in fed flies, 3) can enhance the starvation-induced decrease in bitter sensitivity, and 4) is independent of the control of sugar sensitivity. Given that sNPF and sNPFR are implicated in the regulation of insulin -producing cells (IPCs) both in adults and in larvae (Kapan et al., 2012; Lee et al., 2008), we tested whether IPCs may constitute a target of modulation by sNFP/sNPFR in the control of bitter sensitivity. However, neither IPC-specific knock-down of sNPFR expression, using an *Ins3P-GAL4* driver (Buch et al., 2008), nor ablation of IPCs using *UAS-hid* (Grether et al., 1995), affected bitter sensitivity in starved flies (Figure $S4D_{1-2}$ $S4E_{1-4}$; cell ablation was histologically confirmed; see Figure $S4F_{1-2}$). Therefore IPCs are unlikely to serve as direct targets of the modulatory influence of sNPF/sNPFR on bitter sensitivity during starvation.

Next, we asked whether the sNPF-sNPFR pathway might modulate primary bitter-sensing GRNs. To test this hypothesis, we performed functional calcium imaging of bitter-sensing GRNs in wild type and *sNPF* hypomorphic mutant flies. To monitor calcium transients in bitter-sensing GRNs, we expressed a genetically

encoded calcium indicator, GCaMP3.0 (Tian et al., 2009), under the control of *Gr66-GAL4* (Scott et al., 2001). Consistent with previous reports (Marella et al., 2006), the axonal terminals of bitter-sensing GRNs in the subesophageal ganglion (SOG) exhibited increased GCaMP3.0 fluorescence in response to increasing concentrations of lobeline applied to the labellum (Figure 4E and F_1, blue line). Strikingly, 2 day wet starved wild-type flies showed a statistically significant reduction in GCaMP3.0 fluorescence evoked by application of 0.07mM lobeline, and a non-significant decrease at 0.31 mM lobeline (Figure $4F_1$ and G, red line/box). Importantly, this reduction was attenuated in heterozygous $sNPF^{c00448}$ mutant flies (Figure $4F_2$ and G), consistent with the effect of this mutation to reduce behavioral sensitivity to bitter tastants in starved flies. These data indicate that the starvation-dependent decrease in bitter sensitivity is reflected in a decreased responsiveness of Gr66 GRNs to bitter tastants, and that *sNPF* is necessary for this decrease. However, neither overexpression nor knock-down of *sNPFR* in bitter-sensing GRNs, using Gr66 and Gr33-GAL4 drivers (Moon et al., 2009) and *UAS-Dicer2,* affected bitter sensitivity in starved flies (Figure $S4G_{1-2}$, $S4H_{1-2}$ and $S4I_{1-2}$). Thus, the effect of sNPF to modulate the activity of bitter sensing GRNs during starvation is likely indirect (Figure 4H).

AKH interoceptive neuroendocrine cells act with sNPF to control bitter sensitivity

Since energy demands trigger changes in gustatory sensitivities, we wondered whether any known interoceptive neurons are involved in this modulation. The corpora cardiaca (CC) contains interoceptive neuroendocrine cells that release the peptide adipokinetic hormone (AKH), a fly analog of glucagon, during starvation (Kim and Rulifson, 2004). Genetic ablation of these cells using *akh-GAL4* and *UAS-hid* attenuated the starvation-dependent decrease in bitter sensitivity, without affecting sugar sensitivity (Figure $5A_{1-3}$, B_{1-2}, and $S5A_{1-3}$; ablation was confirmed; see Figure $S5B_{1-2}$). Consistent with this result, a hypomorphic mutant in the *AKH receptor* gene (*akhr*) (Hauser et al., 1998; Staubli et al., 2002), $akhr^{EY11371}$ (Bharucha et al., 2008) (Figure S5C), also attenuated the starvation-dependent decrease in bitter sensitivity relative to genetic background-matched controls (Figure $5C_{1-3}$, $5D_2$). In contrast, bitter sensitivity under fed conditions (Figure $5C_1$ and $5D_2$), and sugar sensitivity regardless of starvation level (Figure $5D_1$ and $S5D_{1-3}$) were not affected, similar to the results obtained in the case of sNPF/sNPFR. Normalized-sugar PER assay comparing 1-day WS

flies and unstarved flies revealed that *akhr*^{EY11371} flies showed no change in bitter sensitivity (Figure S5E$_{1-2}$), implying that *akhr* is necessary for the starvation-dependent decrease in bitters sensitivity.

As an independent approach to investigating the role of AKH cells, we asked whether thermogenetic activation of these neuroendocrine cells, using dTrpA1, decreased bitter sensitivity. Because of their low sugar sensitivity, it was difficult to detect a decrease in bitter sensitivity in fed flies. After 18 hrs of wet starvation, flies show an increase in sugar sensitivity but do not yet show a detectable decrease in bitter sensitivity (Figure 1E$_{1-2}$). We reasoned that such partially starved flies might be sensitized to manipulations expected to decrease bitter sensitivity. For this experiment, 18 hr WS flies were pre-incubated at 30 °C for 30 minutes, and gustatory sensitivity was tested at 18 °C immediately following the incubation. Indeed, activation of AKH cells in this manner significantly decreased bitter sensitivity (Figure 5E$_2$ and 5F$_2$). This temperature-dependent decrease in bitter sensitivity was not observed in 18 hr WS genetic control flies (Figure 5E$_1$ and S5F$_{1-4}$) and did not affect sugar sensitivity (Figure 5F$_1$, and S5G$_{1-4}$). Therefore activation of AKH-expressing neuroendocrine cells is sufficient to decrease bitter sensitivity in partially starved flies.

Because both AKH and sNPF regulate bitter sensitivity in the same direction, without interfering with sugar sensitivity, we investigated whether these neuropeptides act in a common pathway. Antibody staining experiments have indicated that AKH-expressing neuroendocrine cells in the CC (Kim and Rulifson, 2004; Lee and Park, 2004) do not co-express sNPF (Kahsai et al., 2010), and expression of sNPF in AKH cells did not rescue the *sNPF* mutant phenotype (Figure S5H). These data suggest that sNPF does not act within AKH-expressing cells. Therefore, we performed a genetic epistasis experiment by asking whether an *sNPF* loss-of-function mutation would suppress the effect of thermogenetic activation of AKH cells to decrease bitter sensitivity. Indeed, thermogenetic activation after 18 hrs of WS was unable to reduce bitter sensitivity in a heterozygous *sNPF*^{c00448} background (cf. Figure 5E$_2$ vs. 5E$_{3-4}$, 5F$_{1-2}$ and S5F$_{1-6}$). Thus a partial reduction of *sNPF* function (which is sufficient to prevent the starvation-induced decrease in bitter sensitivity; Fig. 3B$_2$, green bars) is epistatic to artificial activation of AKH neuroendocrine cells. This suggests that AKH-expressing cells act genetically upstream of sNPF-expressing neurons to control bitter sensitivity, although an indirect, permissive role for sNPF in AKH action is not excluded by these data (Figure 6).

DISCUSSION

Starved animals exhibit an enhanced sensitivity to sweet compounds and a decreased sensitivity to bitter compounds, allowing them to accept food resources in a less selective manner. It has been assumed that the decrease in bitter sensitivity is secondary to the enhanced sugar sensitivity (Moss and Dethier, 1983), implying a unitary mechanism for altering taste sensitivity in response to food-deprivation. Here, we provide genetic evidence for a pathway that contributes to the reduction in bitter sensitivity during starvation, which is independent of the increase in sugar sensitivity, and which occurs with different kinetics during food deprivation. These data suggest that multiple independent neuromodulatory pathways control different physiological responses to food-deprivation in the fly brain, allowing these responses to be implemented at different levels of energy deficit (Figure 6). More generally, these data suggest that the multi-dimensional features of internal states may reflect parallel rather than unitary mechanisms.

Sugar and bitter sensitivities are independently modulated in starved flies

Our data identify independent neuromodulatory cascades that control the increase and decrease in sugar vs. bitter sensitivity, respectively, during starvation. Previously, we demonstrated that dopamine (DA), whose release is increased in starved flies (Inagaki et al., 2012; Marella et al., 2012), acts directly on sugar-sensitive GRNs to enhance calcium influx in response to sweet tastants (Inagaki et al., 2012). Here we show that *npf-GAL4* neurons act genetically "upstream" of DA to promote enhanced sugar sensitivity during starvation. Importantly, manipulations of the NPF-DA pathway had no effect on bitter sensitivity. Conversely, we identified a pathway including the neuropeptides AKH and sNPF and their respective receptors, which promoted decreased bitter sensitivity during starvation without affecting sugar sensitivity. Thus, we observed an independent control of sugar and bitter sensitivity using manipulations of different neuromodulatory systems. Consistent with this genetic independence, we observed a decreased behavioral sensitivity to bitter tastants in food-deprived flies, even when sucrose concentrations in the PER assay were reduced to compensate for the enhanced sugar sensitivity caused by starvation. We also observed that behavioral sensitivity to bitter compounds decreased more slowly than the increase in sugar sensitivity during starvation.

Finally, we observed reduced calcium influx in response to bitter compounds in Gr66 GRNs in starved flies, in the absence of any sweet compounds. Together these data argue strongly for independent regulation of bitter sensitivity during starvation, contrary to the prevailing view.

While the genetic manipulations performed here allowed a double-dissociation of the control of sugar- and bitter-taste sensitivity during starvation, they leave open many questions for future investigation. For example, it is not yet clear whether NPF peptides themselves contribute to the DA-dependent regulation of sweet GRN sensitivity, nor is it known whether NPF neurons act directly on DA neurons, or indirectly via intermediate connections. Similarly, the site at which sNPF reduces the sensitivity of Gr66 GRNs is not clear. Given that sNPF has suggested to be an inhibitory modulator (Shang et al., 2013) (but see (Root et al., 2011)), one possible scenario is that during starvation sNPF inhibits another population of neurons, which lower the activation threshold of Gr66 neurons during the fed state.

The integration of sugar and bitter information occurs at several levels. First, bitter compounds directly inhibit the activation of sugar-sensing GRNs by sweet tastants (Jeong et al., 2013). Second, lateral interpapillar inhibition may occur between sugar-sensing GRNs and bitter-sensing GRNs (Su et al., 2012). Finally, information from sugar- and bitter-sensing GRNs can be integrated in the brain. Genetic inhibition of synaptic transmission from Gr66 GRNs blocked the suppressing effect of bitter in the PER assay (Gordon and Scott, 2009), suggesting that integration occurs downstream of these GRNs in this context. It is possible that the contribution of different mechanisms may change depending on context, as shown recently (Jeong et al., 2013). The independent modulation of both sugar and bitter sensitivities during starvation may ensure that food acceptance thresholds can be modified under a broad range of conditions.

Cost vs. benefit may determine the order of behavioral changes recruited during food-deprivation

Animals continuously compare potential gains and risks to determine their behaviors (Dethier, 1976; Gillette et al., 2000; Itskov and Ribeiro, 2013). Because the benefits of feeding increase with starvation, it is reasonable that the decision to accept or reject a potential food resource is modulated by energy deficit. A comparison of fed vs. 2 days starved flies revealed that sugar sensitivity alone changes 4.6 fold (Figure $1B_2$) and bitter sensitivity alone changes 4.8 fold (Figure $1D_2$), while the relative preference for food containing

both sugar and bitter increases 10.2 fold (Figure $1C_2$). The increased acceptance of unpalatable food during starvation reflects both the "masking" effect of increased sugar sensitivity on the detection of bitter compounds, and, as shown here, an independent decrease in bitter taste sensitivity. This reciprocal tuning of both sugar and bitter sensitivity contributes to a dramatic increase in acceptance of food resources containing potentially toxic compounds, in a starving fly.

Food-deprivation creates a type of "global organismal state change" (LeDoux, 2012) which is multi-dimensional: it involves multiple physiological and behavioral changes. Interestingly, these different changes occur with different kinetics during food deprivation. Some of them, such as the increase in sugar sensitivity (6 hours of starvation; present results), feeding amount (6-12 hours of starvation: (Farhadian et al., 2012; Hergarden et al., 2012), and food-related olfactory sensitivity (several hours of starvation: (Root et al., 2011)) are initiated during mild starvation, while others, such as the decrease in bitter sensitivity (1-2 days of starvation; present results) and increase in locomotion (2days of starvation: (Isabel et al., 2005; Lee and Park, 2004)) are recruited during severe starvation just before death.

Interestingly, changes occurring during mild starvation seem low-risk, in that their implementation is unlikely to kill the animal, whereas changes accompanying severe starvation place the animal at higher-risk for damage or death: e.g., the decrease in bitter sensitivity allows intake of potentially toxic substances, while the increased locomotor activity may deplete energy stores before food is encountered. These considerations may explain why the brain has evolved multiple mechanisms for the adaptive control of behavior in response to organismal state changes. One mechanism first activates lower risk responses, when energy demands are mild, while the other recruits higher risk responses when energy demands are severe and no other options are available.

Strikingly, both of the high-risk changes--the decrease in bitter sensitivity and increase in locomotion--require AKH-producing cells (Isabel et al., 2005; Lee and Park, 2004), while some of the low-risk changes, such as the increase in sugar sensitivity, feeding amount, and food-related memory, are modulated by NPF and DA (Hergarden et al., 2012; Krashes et al., 2009; Riemensperger et al., 2011; Wu et al., 2003). This suggests that the two pathways we have identified may define and coordinate an axis of low- vs. high- risk behavioral changes.

Mechanisms underlying kinetic differences in starvation responses

The early and late responses to starvation, taken together with our genetic data, suggest that that NPF-DA pathway and the AKH-sNPF pathway are engaged with different kinetics. What explains this difference? One possible scenario is that the interoceptive receptors that initiate each pathway have different sensitivities to the extent of energy deficit. In this scenario, the interoceptive receptor activating the NPF-DA pathway would be more sensitive to energy deprivation than that activating the AKH-sNPF pathway. Alternatively, other components in these pathways, such as neuromodulators or modulation targets, may have different sensitivities to their input signals in these pathways. With its ability to detect hemolymph sugar concentration using the ATP-sensitive potassium channels (*sur* and *ir*) (Kim and Rulifson, 2004), AKH cells are likely to be the interoceptors for the AKH-sNPF pathway. Genetic perturbation of recently identified interoceptive receptors (*gr43* (Miyamoto et al., 2012) and *cupcake* (*SLC5A11*) (Dus et al., 2013)) did not affect sugar sensitivity or bitter sensitivity (H.K.I. and D.J.A unpublished results). Therefore, an interoceptive receptor for the NPF-DA pathway has not yet been identified. Once interoceptive receptors for the NPF-DA and AKH-sNPF pathways are identified, it will be interesting to see whether a differential sensitivity of these receptors to energy demands indeed explains the different kinetics of their recruitment during starvation.

AKH homeostatically regulates hemolymph sugar levels, analogous to mammalian glucagon. AKH endocrine cells function as interoceptors to detect a drop in hemolymph sugar during starvation and release AKH to compensate for this drop by promoting sugar release into the hemolymph from fat cells (Bharucha et al., 2008; Kim and Rulifson, 2004; Lee and Park, 2004). AKH has also been indirectly implicated in the increased locomotor activity that accompanies starvation (Isabel et al., 2005; Lee and Park, 2004). Here we show that AKH also suppresses bitter sensitivity during food-deprivation. These data suggest that AKH coordinates multiple responses to starvation.

Recently thermogenetic activation of AKH endocrine cells in starved flies has been shown to increase levels of sugar in the hemolymph (Gruber et al., 2013). Here we have shown that loss-of-function manipulations of the AKH system attenuate the decrease in bitter sensitivity that occurs during food deprivation, and that activation of AKH cells in partially starved flies can potentiate this decrease. We think

that the taste phenotype is unlikely to be secondary to an experimentally induced increase in hemolymph sugar levels, because this increase "pushes" the food-deprived system back towards the fed state, while bitter sensitivity is pushed more towards the starved state. Consistent with this dissociation, loss-of-function manipulations of the AKH system lead to a decrease in hemolymph sugar (Kim and Rulifson, 2004), pushing the system towards the starved state, while we observe an increase in bitter sensitivity, pushing the system towards the fed state, in response to such manipulations. Thus, the homeostatic effects of manipulations of AKH signaling are in opposite directions for hemolymph sugar levels and bitter taste sensitivity, suggesting that they represent independent effects.

Food deprivation recruits neuromodulatory cascades that modify the sensitivities of primary gustatory neurons

In mammals, how the hunger state changes feeding behavior is incompletely understood (Sternson et al., 2013). Our earlier (Inagaki et al., 2012) and present findings suggest that, in *Drosophila*, hunger modulates two classes of primary gustatory neurons to change feeding choices. Modulation of primary sensory neurons enables the state-dependent tuning of each sensory modality before the signal is integrated with other inputs at higher levels in the brain. Interestingly, in mice, it has been reported that multiple neuromodulators and hormones modulate the sensitivity of taste cells (Cai et al., 2013; Elson et al., 2010; Kawai et al., 2000), although whether this modulation causes starvation-dependent behavioral changes is not clear (Sternson et al., 2013). Our observations strengthen the concept that the modulation of primary sensory neurons represents a general mechanism for implementing state-dependent changes in behavioral responses.

In both vertebrates and invertebrates, the neural circuits mediating homeostatic control of behavior remain largely unknown. Our results outline two parallel pathways that translate energy needs into changes in decisions of PER. These data add to a growing body of evidence that neuromodulatory cascades serve as key mediators of state-dependent control (Taghert and Nitabach, 2012). The widespread projections of neuromodulatory neurons allow them to coordinate the activity of multiple sub-circuits in parallel. This property, and the ability of such modulators to alter the response properties of neurons and circuits (Marder and Bucher, 2007; Shang et al., 2013) are well-suited to such a mediating function in state control (LeDoux,

2012). Cascades of neuromodulators afford multiple regulation points, allowing dynamic state control with potential feedback and/or feedforward regulation (Taghert and Nitabach, 2012). Our results may provide entry points to study the dynamics of neuromodulatory cascades and their organismal impact in the future.

EXPERIMENTAL PROCEDURES

Fly Strains

Adult female *Drosophila melanogaster* were used for all experiments. Since genetic background affects the basal sugar and bitter sensitivities, all the comparisons were made within the same genetic background. Flies were backcrossed for at least 6 generations to ensure the same genetic background. Descriptions of detail genotypes are in the Supplemental Experimental Procedures.

PER Assays

For PER assays, 3-7 day-old female flies were wet-starved or fed in vials. Wet starvation was performed by keeping flies in a vial with a water-soaked filter paper. PER was tested as described previously (Inagaki et al., 2012). In brief, 10-20 experimental flies were mounted into pipetman tips. After excluding flies that continually responded to water, fly response to stepwise increasing concentration of sucrose was tested. After testing the sugar sensitivity, the same sets of flies were tested for bitter sensitivity by exposing stepwise increasing concentration of lobeline mixed into 800mM or other concentrations of sucrose. Only full extensions, but not partial extensions, of proboscis were counted. We withdrew the drop as soon as possible after touching it to the labellum, so that flies could not drink the sucrose solution. Different concentration series of sucrose and lobeline were used depending on the genetic background so that the responses are within the dynamic ranges. All the control experiments were performed side by side as blind experiments. Description of sigmoid curve fitting is in the Supplemental Experimental Procedures.

Calcium Imaging

Two-photon imaging was performed on an Ultima two-photon laser-scanning microscope (Prairie Technology) with an imaging wavelength at 940nm. After a brief anesthesia on ice, flies were mounted on a thin plastic plate with wax as shown in Figure 4E. The top side of the plate contained a well made with wax, and the fly head was immersed in saline. In this saline bath, the antennae and cuticle at the anterior side of the fly head capsule were surgically removed with sharp forceps, so that the SOG could be imaged. At the bottom side of the plate, a glass tube was mounted with the opening facing the proboscis of the mounted fly. A piece of twisted Kimwipe was placed just behind the fly. During imaging, water or different concentration of lobeline solutions were delivered from the glass tubing to stimulate gustatory neurons in the proboscis and was removed by the Kimwipe. Detail procedures are in the Supplemental Experimental Procedures.

ACKNOWLEDGEMENTS

Fly stocks were generously provided by the Bloomington Stock Center, the VDRC stock center, Drosophila RNAi Screening Center, Drs. K. Yu, J. W. Wang, P. Shen, J. H. Park, M. J. Pankratz G. M. Rubin, B. Pfeiffer, J. Simpson, L. L Looger, H. Keshishian, K. Scott, C. Montell, H. Amrein, G. S. B. Suh, H. Keshishian, P. A. Garrity, T. Kitamoto, H. Ishimoto, and B. J. Dickson. We also thank Dr. D. R. Nässel for anti-sNPF precursor serum. H.K.I. is supported by the Nakajima Foundation. D.J.A. is an investigator of the Howard Hughes Medical Institute. This work was supported in part by NIH grant 1RO1 DA031389 to D.J. Anderson.

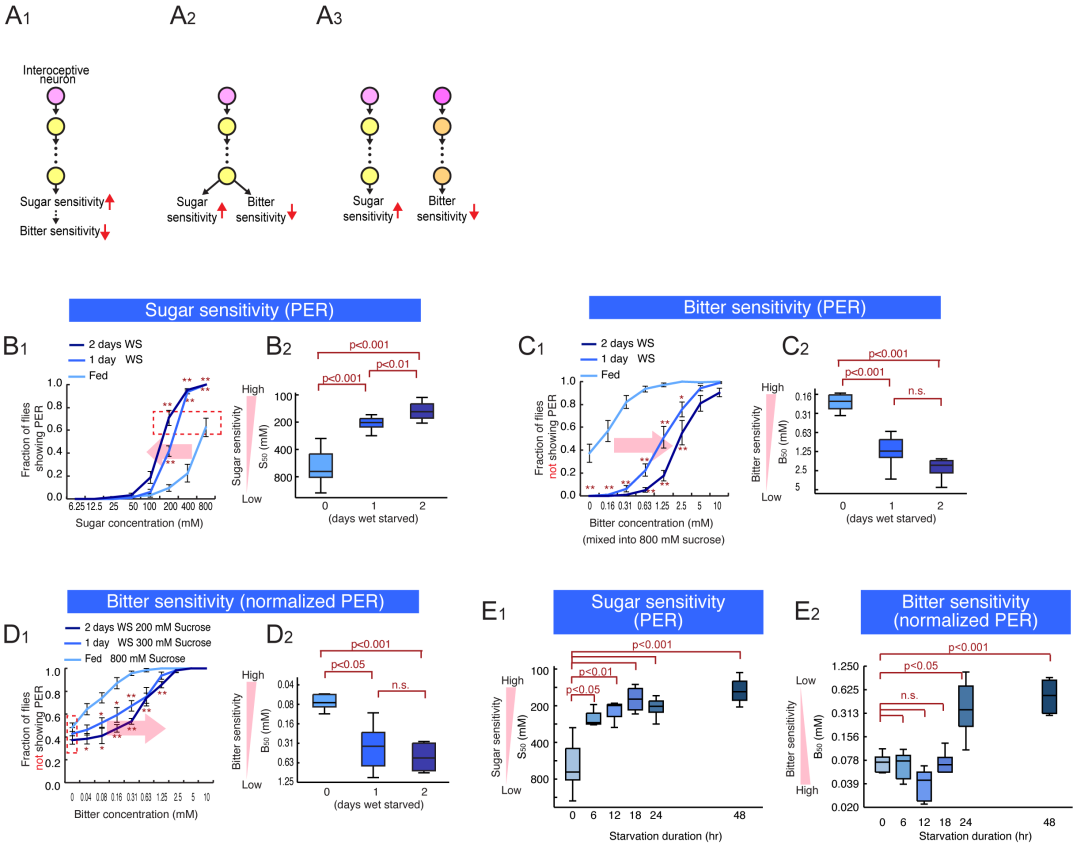
A1
A2
A3
Interoceptive neuron
Sugar sensitivity
Bitter sensitivity
Sugar sensitivity
Bitter sensitivity
Sugar sensitivity
Bitter sensitivity
Sugar sensitivity (PER)
Bitter sensitivity (PER)
B1
B2
C1
C2
2 days WS
1 day WS
Fed
Fraction of flies showing PER
Sugar concentration (mM)
Sugar sensitivity
S50 (mM)
High
Low
(days wet starved)
p<0.001
p<0.01
Fraction of flies not showing PER
Bitter concentration (mM)
(mixed into 800 mM sucrose)
Bitter sensitivity
B50 (mM)
n.s.
Bitter sensitivity (normalized PER)
D1
D2
2 days WS 200 mM Sucrose
1 day WS 300 mM Sucrose
Fed 800 mM Sucrose
p<0.05
E1
E2
Sugar sensitivity (PER)
Bitter sensitivity (normalized PER)
Starvation duration (hr)

Figure 1

Figure 1. Modulation of Sugar and Bitter Sensitivity During Starvation

(A) Schematics illustrating different models to explain the reciprocal control of sugar and bitter sensitivity during starvation. (B) Fraction of flies showing PER to different concentration of sucrose at different starvation levels. (B_1) Average responses. Error bars represent SEM. Two-way ANOVA followed by post hoc t-test with Bonferroni correction at each sugar concentration. *$p<0.05$; **$p<0.005$. $n>5$ for each experimental group. (B_2) S_{50} (the sugar concentration at which 50% of flies show PER) plotted as a function of starvation duration. One-way ANOVA followed by post hoc t-test with Bonferroni correction ($n>9$ for each experimental group). The same plotting and statistical analysis of PER assay are used throughout this paper. Dashed red box indicates the sucrose concentrations that yield the equivalent PER responses at different starvation levels. (C, D) Fraction of flies not showing PER to different concentration of lobeline mixed into 800mM sucrose (C) or different concentrations of sucrose (D). $n>5$ for each experimental group. (E) S_{50} and B_{50} measured and plotted as a function of starvation duration. One-way ANOVA followed by post hoc t-test with Bonferroni correction ($n>5$ for each experimental group). Panels B_1 and B_2 are independent replications of results previously reported in (Inagaki et al, 2012) and are presented here for purposes of comparison. See also Figure S1.

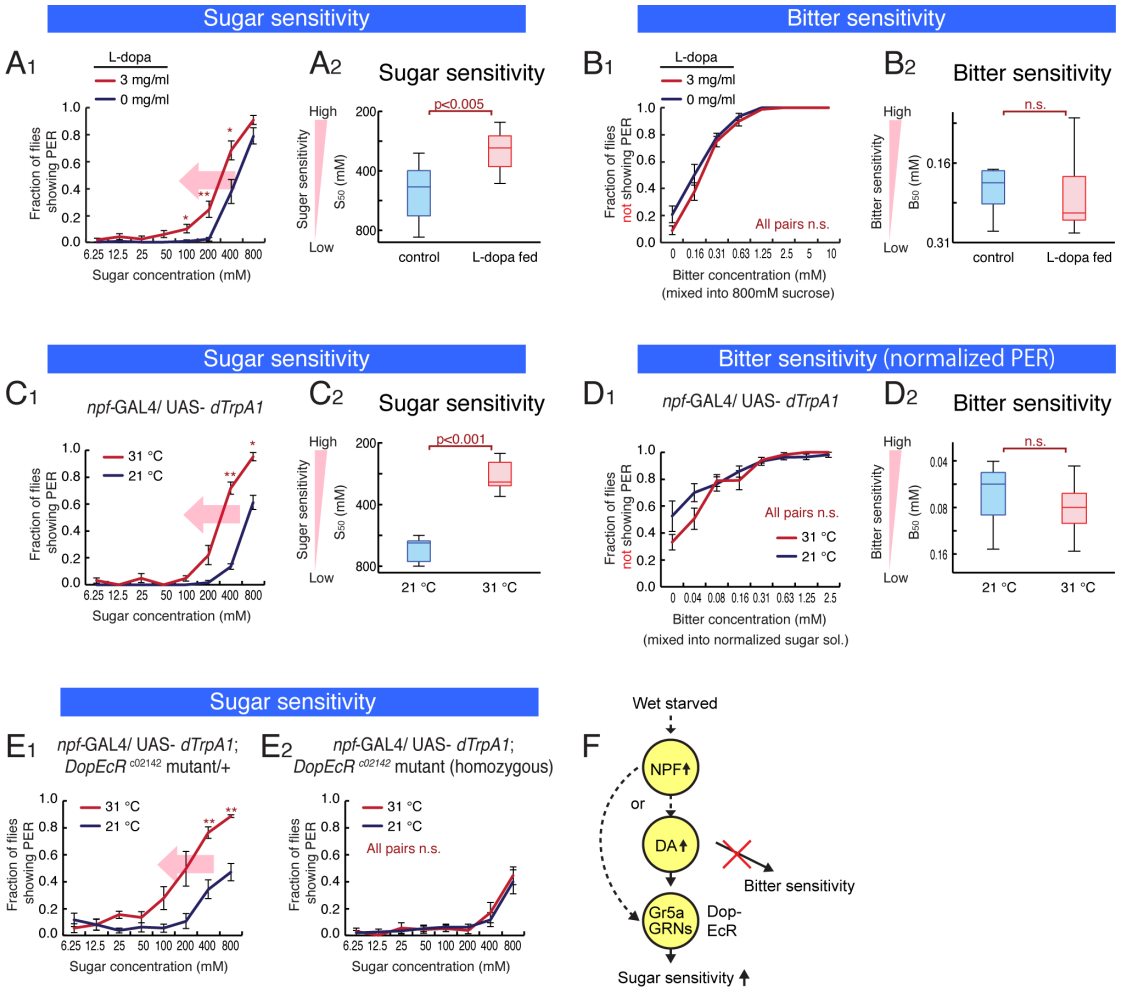
Sugar sensitivity
A1
L-dopa
3 mg/ml
0 mg/ml
Fraction of flies showing PER
Sugar concentration (mM)
A2
Sugar sensitivity
p<0.005
High
Low
Suger sensitivity
S50 (mM)
control
L-dopa fed
Bitter sensitivity
B1
All pairs n.s.
Fraction of flies not showing PER
Bitter concentration (mM)
(mixed into 800mM sucrose)
B2
n.s.
Bitter sensitivity
B50 (mM)
Sugar sensitivity
C1
npf-GAL4/ UAS- dTrpA1
31 °C
21 °C
C2
p<0.001
Bitter sensitivity (normalized PER)
D1
D2
(mixed into normalized sugar sol.)
Sugar sensitivity
E1
npf-GAL4/ UAS- dTrpA1;
DopEcR c02142 mutant/+
E2
DopEcR c02142 mutant (homozygous)
F
Wet starved
NPF
or
DA
Bitter sensitivity
Gr5a GRNs
Dop-EcR
Sugar sensitivity

Figure 2

Figure 2. Neuronal Pathway Regulating Sugar Sensitivity During Starvation

(A-B) Sugar and bitter sensitivity of non-starved wild type flies fed with L-dopa. (C-D) Sugar and bitter sensitivity of flies with thermogenetic activation of NPF neurons (w-; *npf-GAL4* (II) crossed with w-; *UAS-dTrpA1* (II); *UAS-dTrpA1* (III)). For 31 °C experiments, flies were pre-incubated in 31 °C for 30 min. Bitter sensitivity was measured using normalized-sugar PER assay (sucrose concentration used: 800 mM for 21 °C and 400 mM for 31 °C). Data from non-normalized PER response are shown in Figure $S2B_1$. (E) Sugar sensitivity of flies with thermogenetic activation of NPF neurons combined with *DopEcR* mutation (w-; *npf-GAL4* (II); $DopEcR^{c02142}$ crossed with w-; *UAS-dTrpA1* (E_1) or w-; *UAS-dTrpA1* (II); $DopEcR^{c02142}$ (E_2)). (F) Schematic illustrating neuromodulatory pathway regulating sugar sensitivity but not affecting bitter sensitivity. n>5 for all experimental groups. Panels A_{1-2} are independent replications of results previously reported in (Inagaki et al, 2012), and are presented here for purposes of comparison. See also Figure S2.

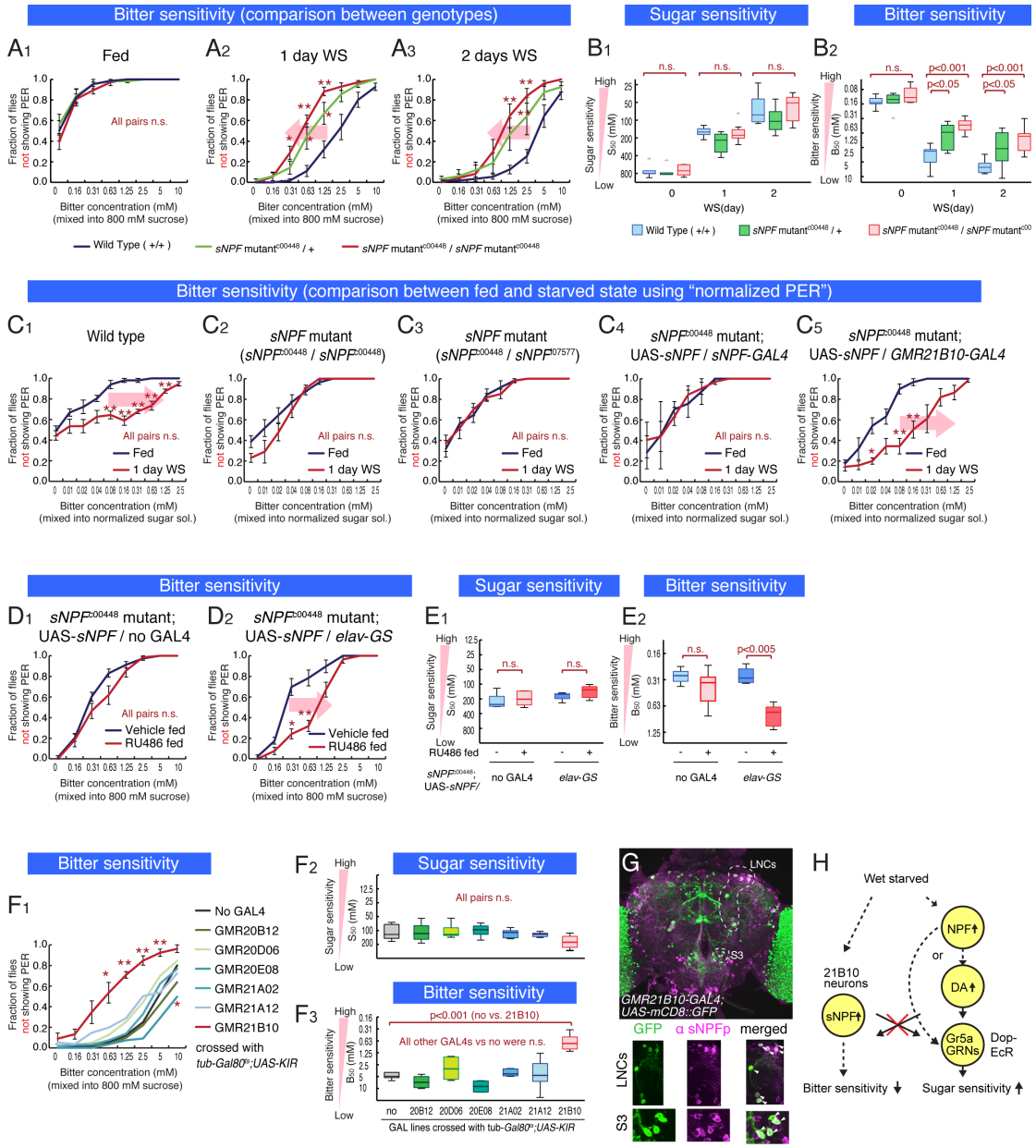
Bitter sensitivity (comparison between genotypes)
Sugar sensitivity
Bitter sensitivity
A1 Fed
A2 1 day WS
A3 2 days WS
B1
B2
All pairs n.s.
Fraction of flies not showing PER
Bitter concentration (mM) (mixed into 800 mM sucrose)
Sugar sensitivity S50 (mM)
Bitter sensitivity B50 (mM)
High
Low
WS(day)
n.s.
p<0.001
p<0.05
Wild Type (+/+)
sNPF mutant c00448 / +
sNPF mutant c00448 / sNPF mutant c00448
Bitter sensitivity (comparison between fed and starved state using "normalized PER")
C1 Wild type
C2 sNPF mutant (sNPF c00448 / sNPF c00448)
C3 sNPF mutant (sNPF c00448 / sNPF 07577)
C4 sNPF c00448 mutant; UAS-sNPF / sNPF-GAL4
C5 sNPF c00448 mutant; UAS-sNPF / GMR21B10-GAL4
Fed
1 day WS
Bitter concentration (mM) (mixed into normalized sugar sol.)
Bitter sensitivity
Sugar sensitivity
D1 sNPF c00448 mutant; UAS-sNPF / no GAL4
D2 sNPF c00448 mutant; UAS-sNPF / elav-GS
E1
E2
Vehicle fed
RU486 fed
p<0.005
sNPF c00448; UAS-sNPF/
no GAL4
elav-GS
Bitter sensitivity
F1
F2
F3
Sugar sensitivity
No GAL4
GMR20B12
GMR20D06
GMR20E08
GMR21A02
GMR21A12
GMR21B10
crossed with tub-Gal80ts;UAS-KIR
All pairs n.s.
p<0.001 (no vs. 21B10)
All other GAL4s vs no were n.s.
no 20B12 20D06 20E08 21A02 21A12 21B10
GAL lines crossed with tub-Gal80ts;UAS-KIR
G
LNCs
S3
GMR21B10-GAL4; UAS-mCD8::GFP
GFP α sNPFp merged
H
Wet starved
21B10 neurons
sNPF
NPF
or
DA
Gr5a GRNs
Dop-EcR
Bitter sensitivity
Sugar sensitivity

Figure 3

Figure 3. sNPF is Necessary and Sufficient for Bitter Sensitivity Control During Starvation

(A-B) Sugar and bitter sensitivity of wild type and *sNPF*^{c00448} mutant flies in the same genetic background. (C) Bitter sensitivity measured with normalized-sugar PER assays in wild type flies (C_1), *sNPF* mutant flies (w-; *sNPF*^{c00448} (C_2) and w-; *sNPF*^{c00448} / *sNPF*^{f07577} (C_3)) and *sNPF* mutant flies with genetic rescue of sNPF expression in different subsets of neurons (w-; *sNPF*^{c00448}; *UAS-sNPF* crossed with w-; *sNPF*^{c00448}; *sNPF-GAL4* (C_4) or w-; *sNPF*^{c00448} ; *GMR21B10-GAL4* (C_5)). Lobeline was mixed into 800 mM sucrose solution for fed flies, or 200 mM sucrose solution for 1-day WS flies. (D-E) Sugar and bitter sensitivity of *sNPF* mutant flies with pan-neuronal, adult rescue of sNPF expression (w-; *sNPF*^{c00448}; *UAS-sNPF* crossed with w-; *sNPF*^{c00448}; + (D_1) or w-; *sNPF*^{c00448} ; *elav-GeneSwitch* (D_2)). Sucrose solution with or wihout 0.5 mM RU486 was fed to flies for 2days before experiments. (F) Sugar and bitter sensitivity of flies with genetic silencing of different subsets of sNPF neurons. For this experiment, w-; *UAS-KIR2.1*; *tub-Gal80*^{ts} flies were crossed with the indicated GAL4 lines or *BDP-GA*L4 flies (No-GAL4). Flies were incubated at 31 °C for 2 days to inactivate Gal80^{ts} before experiments. Only *GMR21B10-GAL4* affected bitter sensitivity (red curve/box) (G) Representative confocal projection of whole mount brains of w- ;; *GMR21B10-GAL4* / *UAS-mCD8::GFP* flies stained with anti-sNPF precursor antibody. Arrowheads indicate neurons with both GFP and anti-sNPF signal. n>5 for all experimental groups. (H) Schematic summarizing results. See also Figure S3.

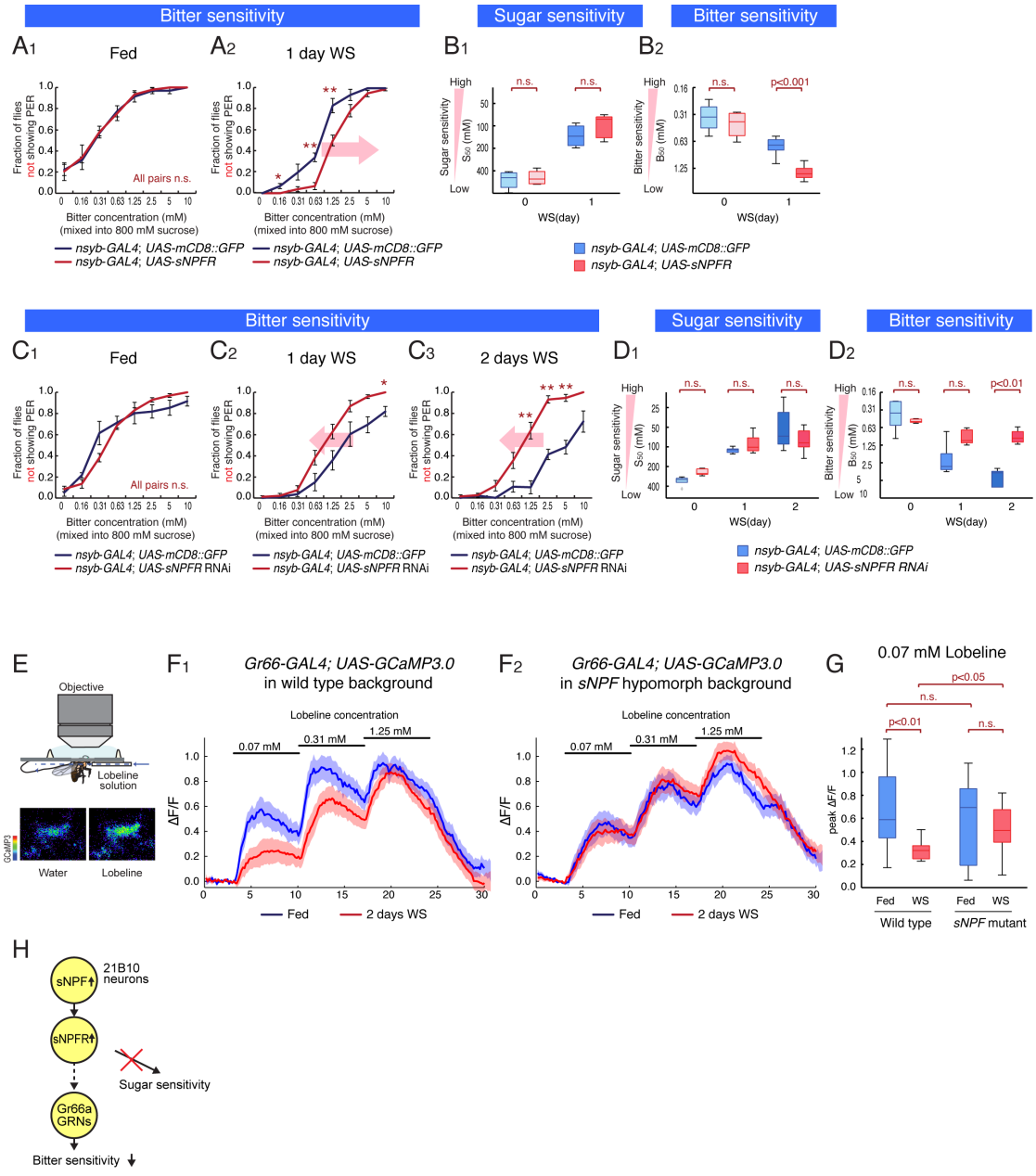
Bitter sensitivity
Sugar sensitivity
Bitter sensitivity
A1
Fed
A2
1 day WS
B1
B2
Fraction of flies not showing PER
All pairs n.s.
Bitter concentration (mM)
(mixed into 800 mM sucrose)
nsyb-GAL4; UAS-mCD8::GFP
nsyb-GAL4; UAS-sNPFR
Sugar sensitivity
Bitter sensitivity
High
Low
n.s.
p<0.001
WS(day)
Bitter sensitivity
Sugar sensitivity
Bitter sensitivity
C1
Fed
C2
1 day WS
C3
2 days WS
D1
D2
All pairs n.s.
Bitter concentration (mM)
(mixed into 800 mM sucrose)
nsyb-GAL4; UAS-mCD8::GFP
nsyb-GAL4; UAS-sNPFR RNAi
p<0.01
WS(day)
E
Objective
Lobeline solution
Water
Lobeline
F1
Gr66-GAL4; UAS-GCaMP3.0
in wild type background
F2
Gr66-GAL4; UAS-GCaMP3.0
in sNPF hypomorph background
Lobeline concentration
0.07 mM
0.31 mM
1.25 mM
ΔF/F
Fed
2 days WS
G
0.07 mM Lobeline
p<0.05
p<0.01
n.s.
peak ΔF/F
Fed
WS
Wild type
sNPF mutant
H
sNPF
21B10 neurons
sNPFR
Sugar sensitivity
Gr66a GRNs
Bitter sensitivity

Figure 4

Figure 4. Modulation Target of sNPF Pathway

(A-B) Sugar and bitter sensitivity of flies with genetic over-expression of *sNPFR* (w-;; *nsyb-GAL4* crossed with *UAS-mCD8::GFP* or *UAS-sNPFR*. *UAS-mCD8::GFP* and *UAS-sNPFR* flies are in the same genetic background). (C-D) Sugar and bitter sensitivity of flies with genetic knock-down of *sNPFR* (UAS-Dicer2 ;; *nsyb-GAL4* crossed with *UAS-mCD8::GFP* or *UAS-sNPFR* RNAi. *UAS-mCD8::GFP* and *UAS-sNPFR* RNAi flies are in the same genetic background). n>5 for each experimental group in A-D. (E) The experimental setup for calcium imaging of bitter-sensing GRNs. Blue arrow indicates direction of flow of bitter solution. The two images below the diagram are representative fields of view showing the GCaMP response of Gr66 GRNs. The fluorescent intensity of GCaMP3 is shown in pseudo-color (scale bar on left). (F) Responses ($\Delta F/F$) to different concentrations of lobeline solution in the central projections of bitter sensing GRNs. The solid lines represent average traces, and envelopes indicate SEM (n>12 for each condition). w-; *Gr66-GAL4*; *UAS-GCaMP3.0* (F_1) and w-; *Gr66-GAL4* / *sNPF*^{c00448}; *UAS-GCaMP3.0* (F_2) were used. (G) Quantification of peak fluorescent changes ($\Delta F/F$) in response to 0.07 mM lobeline solution. One-way ANOVA followed by post hoc t-test with Bonferroni correction. (H) Schematic illustrating neuronal pathway regulating bitter sensitivity. See also Figure S4.

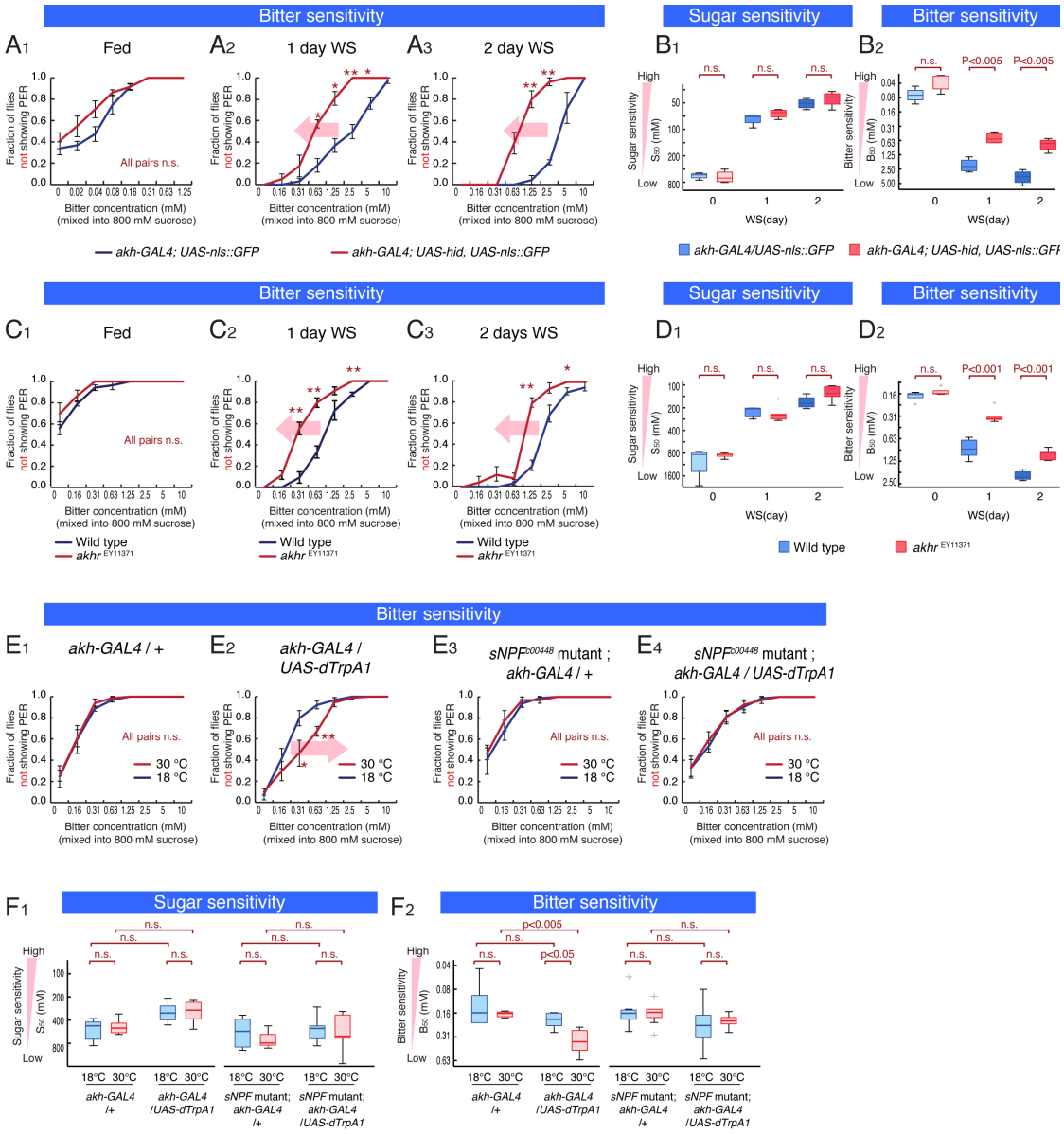
Bitter sensitivity
Sugar sensitivity
Bitter sensitivity
A1
Fed
A2
1 day WS
A3
2 day WS
B1
B2
Fraction of flies not showing PER
All pairs n.s.
Bitter concentration (mM)
(mixed into 800 mM sucrose)
Sugar sensitivity
Bitter sensitivity
High
Low
WS(day)
n.s.
P<0.005
akh-GAL4; UAS-nls::GFP
akh-GAL4; UAS-hid, UAS-nls::GFP
akh-GAL4/UAS-nls::GFP
C1
Fed
C2
1 day WS
C3
2 days WS
D1
D2
P<0.001
Wild type
akhr EY11371
E1
akh-GAL4 / +
E2
akh-GAL4 / UAS-dTrpA1
E3
sNPFc00448 mutant ; akh-GAL4 / +
E4
sNPFc00448 mutant ; akh-GAL4 / UAS-dTrpA1
30 °C
18 °C
F1
F2
p<0.05
18°C 30°C
sNPF mutant; akh-GAL4 /+
sNPF mutant; akh-GAL4 /UAS-dTrpA1

Figure 5

Figure 5. AKH Acts Genetically Upstream of the sNPF Pathway

(A-B) Sugar and bitter sensitivity of flies with or without genetic ablation of AKH neuroendocrine cells (w-; *akh-GAL4* (III) crossed with w-; *UAS-nls::GFP* or w-;*UAS-nls::GFP*, *UAS-hid*). (C-D) Sugar and bitter sensitivity of wild type and $AKHR^{EY11371}$ mutant flies in the same genetic background. (E-F) Sugar and bitter sensitivity of flies with genetic thermoactivation of AKH-producing cells (w-; +; *akh-GAL4* (III) crossed with w-; +; + (E_1) or w-; *UAS-dTrpA1* (II); *UAS-dTrpA1* (III) (E_2). w-; $sNPF^{c00448}$; *akh-GAL4* (III) crossed with w-; +; + (E_3) or w-; *UAS-dTrpA1* (II); *UAS-dTrpA1* (III) (E_4)). Flies were preincubated in 31 °C or 18 °C for 30 min and PER was performed in 18 °C. n>5 for all experimental groups. See also Figure S5.

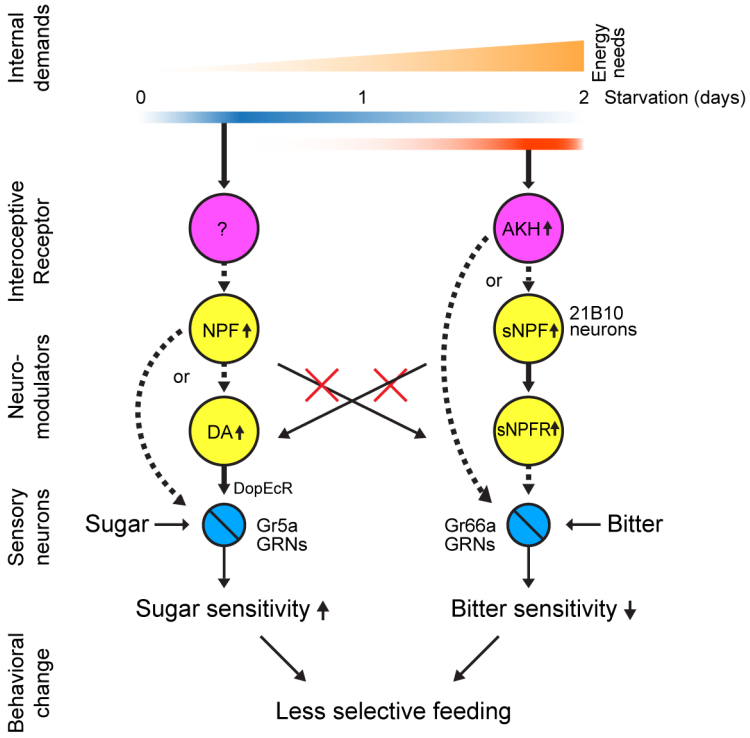

Figure 6

Figure 6. Distinct Neuronal Pathways Modulating Sugar and Bitter Sensitivity During Starvation

Schematic illustrating the two distinct neuronal pathway we identified to control sugar and bitter sensitivity in an independent manner. Dashed arrows indicate genetic interactions that we have not shown to be direct.

REFERENCES

Andrews, Z.B., Liu, Z.W., Walllingford, N., Erion, D.M., Borok, E., Friedman, J.M., Tschop, M.H., Shanabrough, M., Cline, G., Shulman, G.I., *et al*. (2008). UCP2 mediates ghrelin's action on NPY/AgRP neurons by lowering free radicals. Nature *454*, 846-851.

Bainton, R.J., Tsai, L.T., Singh, C.M., Moore, M.S., Neckameyer, W.S., and Heberlein, U. (2000). Dopamine modulates acute responses to cocaine, nicotine and ethanol in Drosophila. Current biology : CB *10*, 187-194.

Berridge, K.C. (1991). Modulation of taste affect by hunger, caloric satiety, and sensory-specific satiety in the rat. Appetite *16*, 103-120.

Beshel, J., and Zhong, Y. (2013). Graded Encoding of Food Odor Value in the Drosophila Brain. The Journal of neuroscience : the official journal of the Society for Neuroscience *33*, 15693-15704.

Bharucha, K.N., Tarr, P., and Zipursky, S.L. (2008). A glucagon-like endocrine pathway in Drosophila modulates both lipid and carbohydrate homeostasis. The Journal of experimental biology *211*, 3103-3110.

Blanchard, R.J., and Blanchard, D.C. (1989). Attack and defense in rodents as ethoexperimental models for the study of emotion. Prog Neuropsychopharmacol Biol Psychiatry *13 Suppl*, S3-14.

Buch, S., Melcher, C., Bauer, M., Katzenberger, J., and Pankratz, M.J. (2008). Opposing effects of dietary protein and sugar regulate a transcriptional target of Drosophila insulin-like peptide signaling. Cell Metab *7*, 321-332.

Cai, H., Cong, W.N., Daimon, C.M., Wang, R., Tschop, M.H., Sevigny, J., Martin, B., and Maudsley, S. (2013). Altered lipid and salt taste responsivity in ghrelin and GOAT null mice. PLoS One *8*, e76553.

Dethier, V.G. (1976). The hungry fly : a physiological study of the behavior associated with feeding (Cambridge, Mass., Harvard University Press).

Dus, M., Ai, M., and Suh, G.S. (2013). Taste-independent nutrient selection is mediated by a brain-specific Na+ /solute co-transporter in Drosophila. Nat Neurosci *16*, 526-528.

Elson, A.E., Dotson, C.D., Egan, J.M., and Munger, S.D. (2010). Glucagon signaling modulates sweet taste responsiveness. Faseb J *24*, 3960-3969.

Farhadian, S.F., Suarez-Farinas, M., Cho, C.E., Pellegrino, M., and Vosshall, L.B. (2012). Post-fasting olfactory, transcriptional, and feeding responses in Drosophila. Physiology & behavior *105*, 544-553.

Feng, G., Reale, V., Chatwin, H., Kennedy, K., Venard, R., Ericsson, C., Yu, K., Evans, P.D., and Hall, L.M. (2003). Functional characterization of a neuropeptide F-like receptor from Drosophila melanogaster. Eur J Neurosci *18*, 227-238.

Gillette, R., Huang, R.C., Hatcher, N., and Moroz, L.L. (2000). Cost-benefit analysis potential in feeding behavior of a predatory snail by integration of hunger, taste, and pain. Proc Natl Acad Sci U S A *97*, 3585-3590.

Gordon, M.D., and Scott, K. (2009). Motor control in a Drosophila taste circuit. Neuron *61*, 373-384.

Grether, M.E., Abrams, J.M., Agapite, J., White, K., and Steller, H. (1995). The head involution defective gene of Drosophila melanogaster functions in programmed cell death. Genes Dev *9*, 1694-1708.

Gruber, F., Knapek, S., Fujita, M., Matsuo, K., Bracker, L., Shinzato, N., Siwanowicz, I., Tanimura, T., and Tanimoto, H. (2013). Suppression of conditioned odor approach by feeding is independent of taste and nutritional value in Drosophila. Current biology : CB *23*, 507-514.

Hamada, F.N., Rosenzweig, M., Kang, K., Pulver, S.R., Ghezzi, A., Jegla, T.J., and Garrity, P.A. (2008). An internal thermal sensor controlling temperature preference in Drosophila. Nature *454*, 217-220.

Hauser, F., Sondergaard, L., and Grimmelikhuijzen, C.J. (1998). Molecular cloning, genomic organization and developmental regulation of a novel receptor from Drosophila melanogaster structurally related to gonadotropin-releasing hormone receptors for vertebrates. Biochem Biophys Res Commun *249*, 822-828.

Hergarden, A.C., Tayler, T.D., and Anderson, D.J. (2012). Allatostatin-A neurons inhibit feeding behavior in adult Drosophila. Proc Natl Acad Sci U S A *109*, 3967-3972.

Inagaki, H.K., Ben-Tabou de-Leon, S., Wong, A.M., Jagadish, S., Ishimoto, H., Barnea, G., Kitamoto, T., Axel, R., and Anderson, D.J. (2012). Visualizing neuromodulation in vivo: TANGO-mapping of dopamine signaling reveals appetite control of sugar sensing. Cell *148*, 583-595.

Isabel, G., Martin, J.R., Chidami, S., Veenstra, J.A., and Rosay, P. (2005). AKH-producing neuroendocrine cell ablation decreases trehalose and induces behavioral changes in Drosophila. Am J Physiol Regul Integr Comp Physiol *288*, R531-538.

Itskov, P.M., and Ribeiro, C. (2013). The dilemmas of the gourmet fly: the molecular and neuronal mechanisms of feeding and nutrient decision making in Drosophila. Front Neurosci *7*, 12.

Jeong, Y.T., Shim, J., Oh, S.R., Yoon, H.I., Kim, C.H., Moon, S.J., and Montell, C. (2013). An odorant-binding protein required for suppression of sweet taste by bitter chemicals. Neuron *79*, 725-737.

Kahsai, L., Kapan, N., Dircksen, H., Winther, A.M., and Nassel, D.R. (2010). Metabolic stress responses in Drosophila are modulated by brain neurosecretory cells that produce multiple neuropeptides. PLoS One *5*, e11480.

Kapan, N., Lushchak, O.V., Luo, J., and Nassel, D.R. (2012). Identified peptidergic neurons in the Drosophila brain regulate insulin-producing cells, stress responses and metabolism by coexpressed short neuropeptide F and corazonin. Cell Mol Life Sci.

Kawai, K., Sugimoto, K., Nakashima, K., Miura, H., and Ninomiya, Y. (2000). Leptin as a modulator of sweet taste sensitivities in mice. Proc Natl Acad Sci U S A *97*, 11044-11049.

Kim, S.K., and Rulifson, E.J. (2004). Conserved mechanisms of glucose sensing and regulation by Drosophila corpora cardiaca cells. Nature *431*, 316-320.

Krashes, M.J., DasGupta, S., Vreede, A., White, B., Armstrong, J.D., and Waddell, S. (2009). A neural circuit mechanism integrating motivational state with memory expression in Drosophila. Cell *139*, 416-427.

Kreneisz, O., Chen, X., Fridell, Y.W., and Mulkey, D.K. (2010). Glucose increases activity and Ca2+ in insulin-producing cells of adult Drosophila. Neuroreport *21*, 1116-1120.

LeDoux, J. (2012). Rethinking the emotional brain. Neuron *73*, 653-676.

Lee, G., and Park, J.H. (2004). Hemolymph sugar homeostasis and starvation-induced hyperactivity affected by genetic manipulations of the adipokinetic hormone-encoding gene in Drosophila melanogaster. Genetics *167*, 311-323.

Lee, K.S., Hong, S.H., Kim, A.K., Ju, S.K., Kwon, O.Y., and Yu, K. (2009). Processed short neuropeptide F peptides regulate growth through the ERK-insulin pathway in Drosophila melanogaster. FEBS Lett *583*, 2573-2577.

Lee, K.S., Kwon, O.Y., Lee, J.H., Kwon, K., Min, K.J., Jung, S.A., Kim, A.K., You, K.H., Tatar, M., and Yu, K. (2008). Drosophila short neuropeptide F signalling regulates growth by ERK-mediated insulin signalling. Nat Cell Biol *10*, 468-475.

Lee, K.S., You, K.H., Choo, J.K., Han, Y.M., and Yu, K. (2004). Drosophila short neuropeptide F regulates food intake and body size. J Biol Chem *279*, 50781-50789.

Luquet, S., Perez, F.A., Hnasko, T.S., and Palmiter, R.D. (2005). NPY/AgRP neurons are essential for feeding in adult mice but can be ablated in neonates. Science *310*, 683-685.

Marder, E., and Bucher, D. (2007). Understanding circuit dynamics using the stomatogastric nervous system of lobsters and crabs. Annu Rev Physiol *69*, 291-316.

Marella, S., Fischler, W., Kong, P., Asgarian, S., Rueckert, E., and Scott, K. (2006). Imaging taste responses in the fly brain reveals a functional map of taste category and behavior. Neuron *49*, 285-295.

Marella, S., Mann, K., and Scott, K. (2012). Dopaminergic modulation of sucrose acceptance behavior in Drosophila. Neuron *73*, 941-950.

Masek, P., and Keene, A.C. (2013). Drosophila Fatty Acid Taste Signals through the PLC Pathway in Sugar-Sensing Neurons. PLoS Genet *9*, e1003710.

Mertens, I., Meeusen, T., Huybrechts, R., De Loof, A., and Schoofs, L. (2002). Characterization of the short neuropeptide F receptor from Drosophila melanogaster. Biochem Biophys Res Commun *297*, 1140-1148.

Meunier, N., Belgacem, Y.H., and Martin, J.R. (2007). Regulation of feeding behaviour and locomotor activity by takeout in Drosophila. J Exp Biol *210*, 1424-1434.

Meunier, N., Marion-Poll, F., Rospars, J.P., and Tanimura, T. (2003). Peripheral coding of bitter taste in Drosophila. Journal of neurobiology *56*, 139-152.

Miyamoto, T., Slone, J., Song, X., and Amrein, H. (2012). A fructose receptor functions as a nutrient sensor in the Drosophila brain. Cell *151*, 1113-1125.

Montell, C. (2009). A taste of the Drosophila gustatory receptors. Curr Opin Neurobiol *19*, 345-353.

Moon, S.J., Lee, Y., Jiao, Y., and Montell, C. (2009). A Drosophila gustatory receptor essential for aversive taste and inhibiting male-to-male courtship. Curr Biol *19*, 1623-1627.

Moss, C.F., and Dethier, V.G. (1983). Central nervous system regulation of finicky feeding by the blowfly. Behav Neurosci *97*, 541-548.

Nassel, D.R., Enell, L.E., Santos, J.G., Wegener, C., and Johard, H.A. (2008). A large population of diverse neurons in the Drosophila central nervous system expresses short neuropeptide F, suggesting multiple distributed peptide functions. BMC Neurosci *9*, 90.

Nassel, D.R., and Wegener, C. (2011). A comparative review of short and long neuropeptide F signaling in invertebrates: Any similarities to vertebrate neuropeptide Y signaling? Peptides *32*, 1335-1355.

Osterwalder, T., Yoon, K.S., White, B.H., and Keshishian, H. (2001). A conditional tissue-specific transgene expression system using inducible GAL4. Proc Natl Acad Sci U S A *98*, 12596-12601.

Page, R.E., Jr., Erber, J., and Fondrk, M.K. (1998). The effect of genotype on response thresholds to sucrose and foraging behavior of honey bees (Apis mellifera L.). J Comp Physiol A *182*, 489-500.

Pauli, A., Althoff, F., Oliveira, R.A., Heidmann, S., Schuldiner, O., Lehner, C.F., Dickson, B.J., and Nasmyth, K. (2008). Cell-type-specific TEV protease cleavage reveals cohesin functions in Drosophila neurons. Dev Cell *14*, 239-251.

Pfeiffer, B.D., Jenett, A., Hammonds, A.S., Ngo, T.T., Misra, S., Murphy, C., Scully, A., Carlson, J.W., Wan, K.H., Laverty, T.R., *et al*. (2008). Tools for neuroanatomy and neurogenetics in Drosophila. Proc Natl Acad Sci U S A *105*, 9715-9720.

Reale, V., Chatwin, H.M., and Evans, P.D. (2004). The activation of G-protein gated inwardly rectifying K+ channels by a cloned Drosophila melanogaster neuropeptide F-like receptor. Eur J Neurosci *19*, 570-576.

Riemensperger, T., Isabel, G., Coulom, H., Neuser, K., Seugnet, L., Kume, K., Iche-Torres, M., Cassar, M., Strauss, R., Preat, T., *et al*. (2011). Behavioral consequences of dopamine deficiency in the Drosophila central nervous system. Proc Natl Acad Sci U S A *108*, 834-839.

Root, C.M., Ko, K.I., Jafari, A., and Wang, J.W. (2011). Presynaptic facilitation by neuropeptide signaling mediates odor-driven food search. Cell *145*, 133-144.

Scott, K., Brady, R., Jr., Cravchik, A., Morozov, P., Rzhetsky, A., Zuker, C., and Axel, R. (2001). A chemosensory gene family encoding candidate gustatory and olfactory receptors in Drosophila. Cell *104*, 661-673.

Sengupta, P. (2013). The belly rules the nose: feeding state-dependent modulation of peripheral chemosensory responses. Current opinion in neurobiology *23*, 68-75.

Shang, Y., Donelson, N.C., Vecsey, C.G., Guo, F., Rosbash, M., and Griffith, L.C. (2013). Short neuropeptide F is a sleep-promoting inhibitory modulator. Neuron *80*, 171-183.

Srivastava, D.P., Yu, E.J., Kennedy, K., Chatwin, H., Reale, V., Hamon, M., Smith, T., and Evans, P.D. (2005). Rapid, nongenomic responses to ecdysteroids and catecholamines mediated by a novel Drosophila G-protein-coupled receptor. J Neurosci *25*, 6145-6155.

Staubli, F., Jorgensen, T.J., Cazzamali, G., Williamson, M., Lenz, C., Sondergaard, L., Roepstorff, P., and Grimmelikhuijzen, C.J. (2002). Molecular identification of the insect adipokinetic hormone receptors. Proc Natl Acad Sci U S A *99*, 3446-3451.

Sternson, S.M., Nicholas Betley, J., and Cao, Z.F. (2013). Neural circuits and motivational processes for hunger. Current opinion in neurobiology *23*, 353-360.

Su, C.Y., Menuz, K., Reisert, J., and Carlson, J.R. (2012). Non-synaptic inhibition between grouped neurons in an olfactory circuit. Nature *492*, 66-71.

Taghert, P.H., and Nitabach, M.N. (2012). Peptide neuromodulation in invertebrate model systems. Neuron *76*, 82-97.

Thibault, S.T., Singer, M.A., Miyazaki, W.Y., Milash, B., Dompe, N.A., Singh, C.M., Buchholz, R., Demsky, M., Fawcett, R., Francis-Lang, H.L., *et al*. (2004). A complementary transposon tool kit for Drosophila melanogaster using P and piggyBac. Nat Genet *36*, 283-287.

Thorne, N., Chromey, C., Bray, S., and Amrein, H. (2004). Taste perception and coding in Drosophila. Curr Biol *14*, 1065-1079.

Tian, L., Hires, S.A., Mao, T., Huber, D., Chiappe, M.E., Chalasani, S.H., Petreanu, L., Akerboom, J., McKinney, S.A., Schreiter, E.R., *et al*. (2009). Imaging neural activity in worms, flies and mice with improved GCaMP calcium indicators. Nat Methods *6*, 875-881.

Wang, Z., Singhvi, A., Kong, P., and Scott, K. (2004). Taste representations in the Drosophila brain. Cell *117*, 981-991.

Weiss, L.A., Dahanukar, A., Kwon, J.Y., Banerjee, D., and Carlson, J.R. (2011). The molecular and cellular basis of bitter taste in Drosophila. Neuron *69*, 258-272.

Wu, Q., Wen, T., Lee, G., Park, J.H., Cai, H.N., and Shen, P. (2003). Developmental control of foraging and social behavior by the Drosophila neuropeptide Y-like system. Neuron *39*, 147-161.

Wu, Q., Zhao, Z., and Shen, P. (2005). Regulation of aversion to noxious food by Drosophila neuropeptide Y- and insulin-like systems. Nat Neurosci *8*, 1350-1355.

Zhang, Y.V., Ni, J., and Montell, C. (2013). The molecular basis for attractive salt-taste coding in Drosophila. Science *340*, 1334-1338.

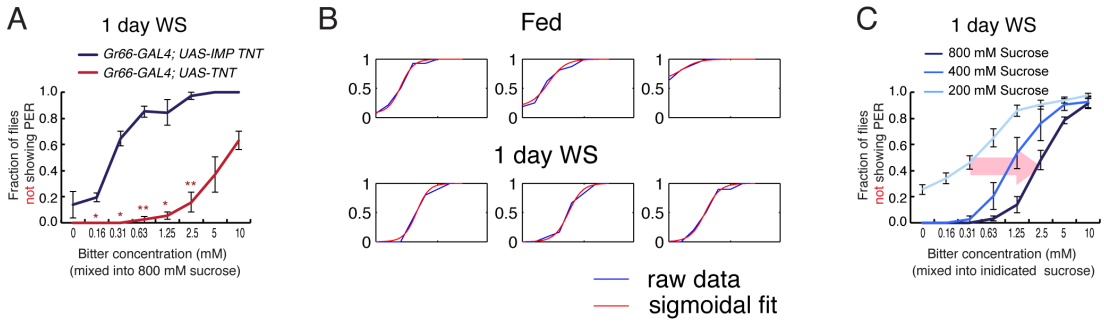

Supplementary Figure 1

Figure S1. Modulation of Bitter Sensitivity During Starvation

(A) Gr66 GRNs is necessary for the bitter-dependent suppression of PER. Fraction of flies not showing PER to different concentrations of lobeline mixed into 800mM sucrose are plotted. (B) Multiple representative examples of sigmoidal fitting (red curves) of fraction of flies not showing PER (raw data in blue curves). See Supplemental Experimental Procedures for sigmoidal fitting. (C) Fraction of flies not showing PER in response to bitter mixed into different concentrations of sucrose solution. (A, C) n>4 for all experimental groups.

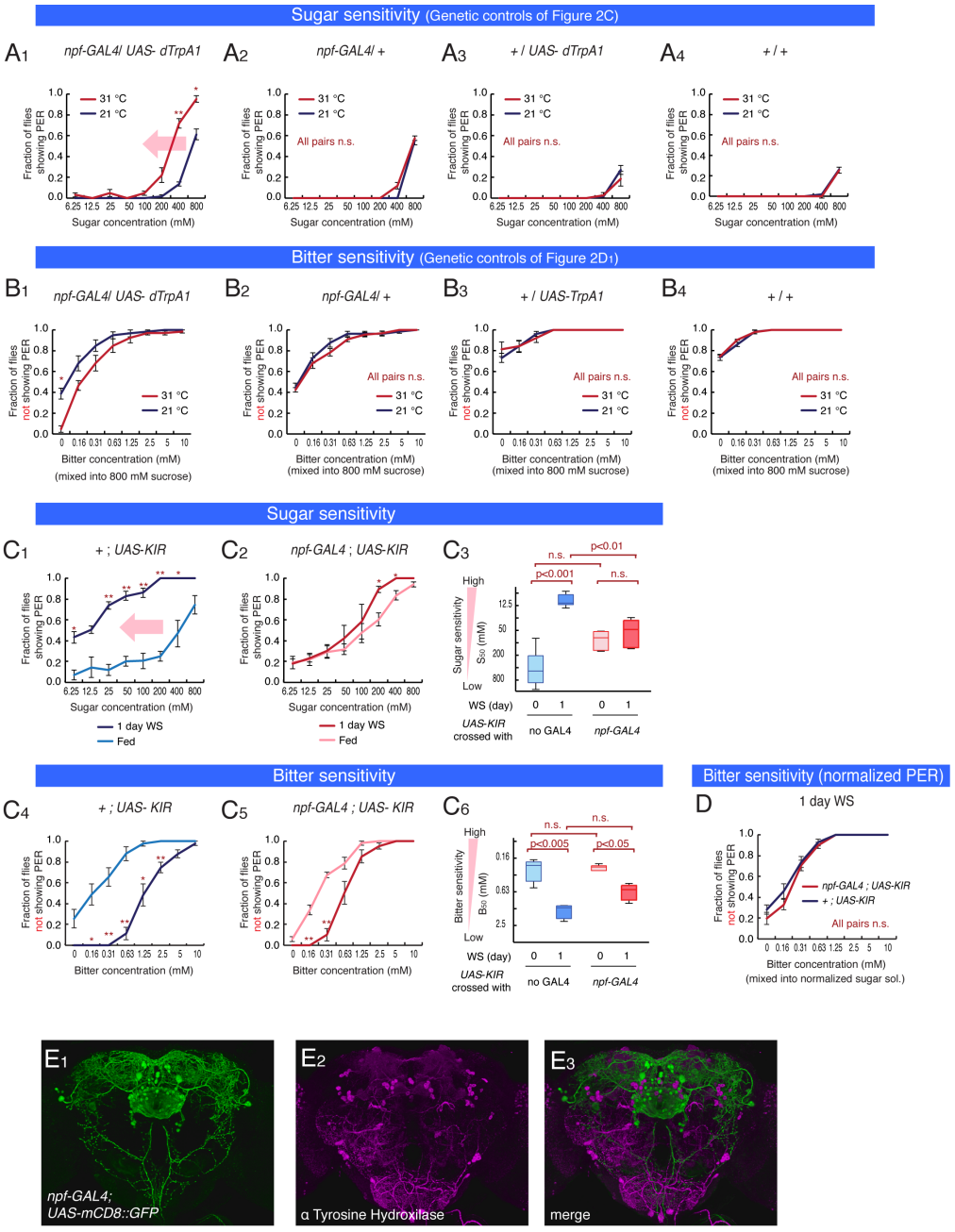

Supplementary Figure 2

Figure S2. Neuronal Pathway Regulating Sugar Sensitivity Does Not Affect Bitter Sensitivity

(A-B) Sugar (A) and bitter (B) sensitivity of flies with thermogenetic activation of NPF neurons. Genotypes: w-; *npf-GAL4* (II) flies were crossed with w-; *UAS-dTrpA1* (II); *UAS-dTrpA1* (III) (A_1 and B_1) or w- flies in the same genetic background (A_2 and B_2); w- flies were crossed with w-; *UAS-dTrpA1* (II); *UAS-dTrpA1* (III) (A_3 and B_3) or w- flies in the same genetic background (A_4 and B_4). A_1 is copied from figure $2C_1$ for purposes of comparison. In (B_1), note that there is statistically significant difference only when bitter is not mixed into sucrose solution (0 mM). Therefore, no difference in bitter sensitivity was observed. (C) Sugar and bitter sensitivity of flies with genetic silencing of NPF neurons. *UAS-KIR2.1* was crossed with either w-; *npf-GAL4* (II) flies (C_2 and C_5) or w- flies in the same genetic background (C_1 and C_4). (D) Comparison of bitter sensitivity of 1-day WS *npf-GAL4; UAS-KIR* flies and *+; UAS-KIR* flies using the sugar-normalized PER assay (200 mM and 100 mM sucrose solution were used, respectively). No difference in bitter sensitivity was observed between two genotypes. (E) Representative confocal projections of whole mount brains from *npf-GAL4*; *UAS-mCD8::GFP* flies (gfp in green: $E_{1,3}$) immunostained with anti-Tyrosine hydroxylase antibody (magenta: E_{2-3}), which labels DA neurons. (A-D) n>4 for all experimental groups.

.

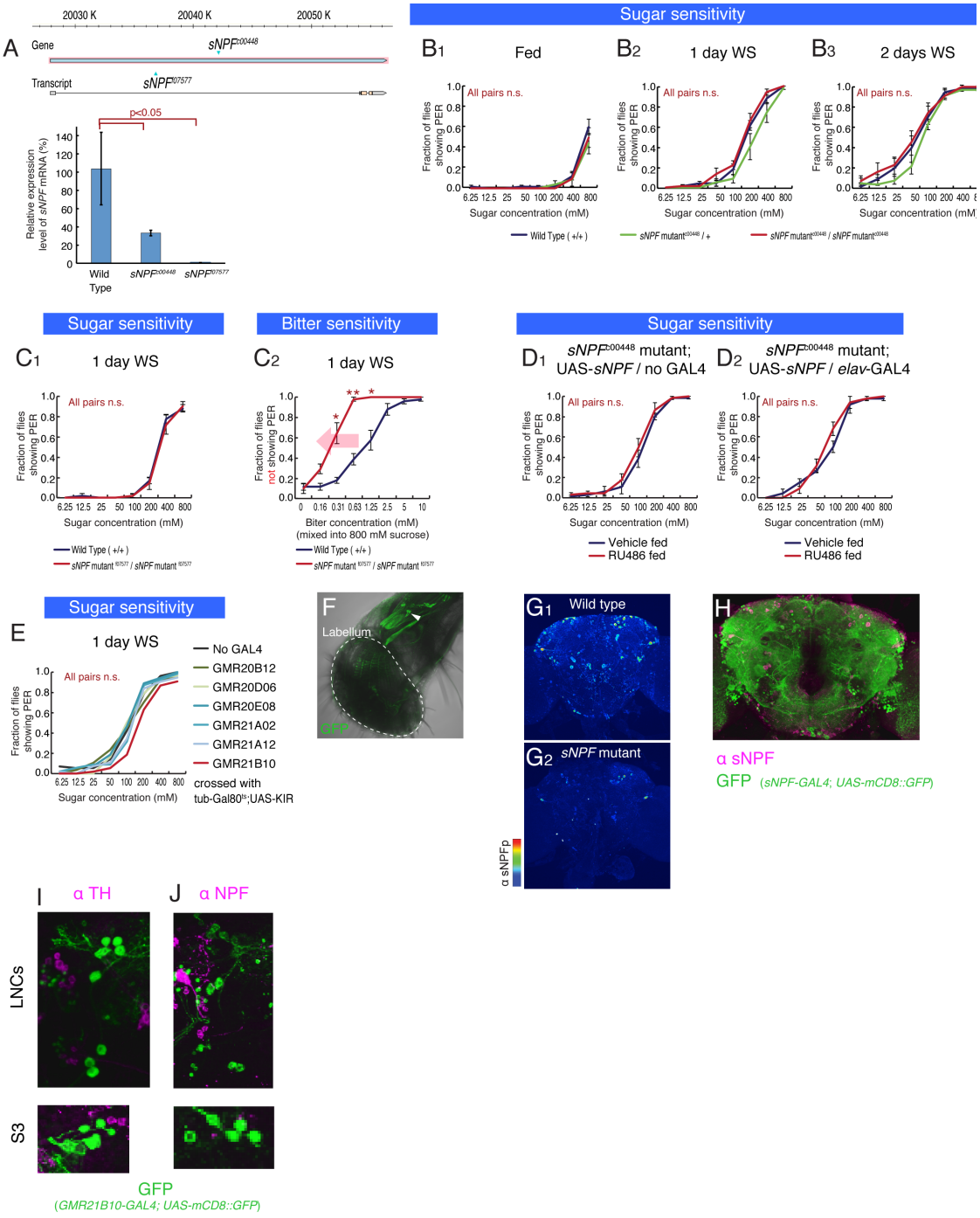

Supplementary Figure 3

Figure S3. Genetic Manipulations of sNPF Do Not Affect Sugar Sensitivity

(A) Insertion of two piggyBac transposons in *sNPF* gene locus (top) and relative *sNPF* mRNA expression level of these strains compared to wild type flies in the same genetic background (bottom) measured by qPCR. One-way ANOVA followed by post hoc t-test with Bonferroni correction (n=3). (B) Sugar sensitivity of wild type and *sNPF* mutant flies. Data is acquired from the same flies that were used in Figure $3A_{1\text{-}3}$. S50 of these experiments are summarized in Figure $3B_1$. (C) Sugar and bitter sensitivity of $sNPF^{f07577}$ flies compared with wild type flies in the same genetic background. (D) Sugar sensitivity of flies with pan-neuronal rescue of sNPF. Data is acquired from the same flies that were used in Figure $3D_{1\text{-}2}$. S50 of these experiments are summarized in Figure $3E_1$. (E) Sugar sensitivity of flies with genetic silencing of different subsets of sNPF neurons. Data is acquired from the same flies that were used in Figure $3F_1$. S50 of these experiments are summarized in Figure $3F_2$. (A-E) n>5 for all experimental groups. (F) Representative confocal projections of the proboscis from *GMR21B10-GAL4*; *UAS-mCD8::GFP* flies (Green: GFP; gray: DIC image of proboscis). Note that there are no cells in labellum where GRNs exist. There are two cells in other parts of labellum (white arrow head). (G) Representative confocal projections of whole mount brains from wild type (G_1) or $sNPF^{c00448}$ (G_2) flies immunostained with anti-sNPF antibody. Scale bar to the left represents relative intensity of immunostaining in pseudocolor. (H) Representative confocal projections of whole mount brains from s*npf-GAL4*; *UAS-mCD8::GFP* flies (GFP: green) immunostained with anti-sNPF antibody (magenta). Note that huge populations of neurons in the brain are labeled by this GAL4. Some of them are sNPF positive. None of the S3 cells are labeled and 3-4 LCNs are labeled by this GAL4 line. (I-J) Representative confocal projections of whole mount brains from *GMR21B10-GAL4*; *UAS-mCD8::GFP* flies immunostained with anti-Tyrosine hydroxylase (TH) (I) or anti-NPF (J) antibodies. Note that neither of LNCs nor S3 cells are TH or NPF positive.

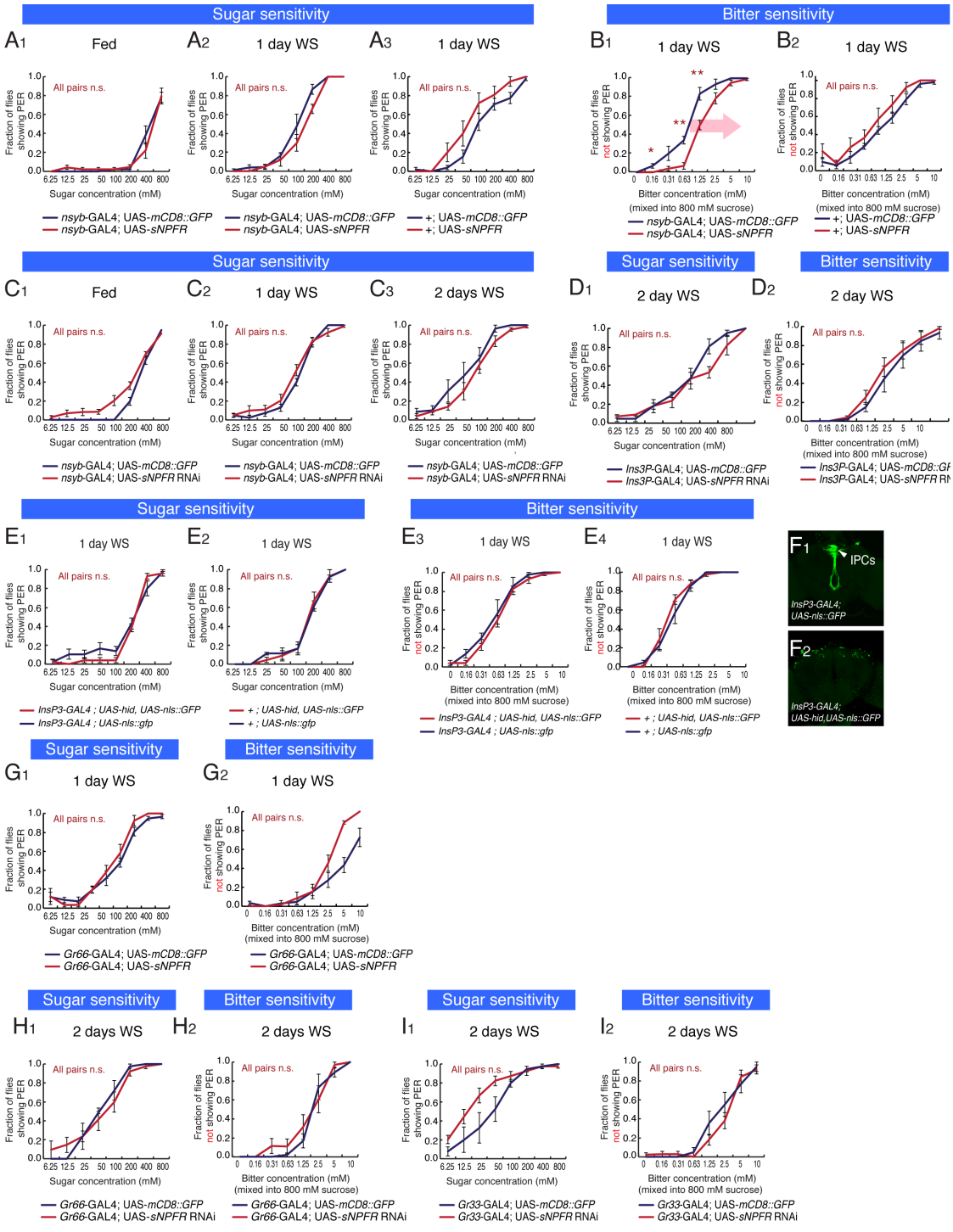

Supplementary Figure 4

Figure S4. Genetic Manipulations of sNPFR Do Not Affect Sugar Sensitivity

(A-B) Sugar and bitter sensitivity of flies with genetic over-expression of sNPFR. Data is acquired from the same flies that were used in Figure $4A_{1-2}$. S50 of these experiments are summarized in Figure $4B_1$. Figure $S4B_1$ is a replicate of Figure $4A_2$ to make comparison easier. (C) Sugar sensitivity of flies with genetic knock-down of sNPFR. Data is acquired from the same flies that were used in Figure $4C_{1-3}$. S50 of these experiments are summarized in Figure $4D_1$. (D) Sugar and bitter sensitivity of flies with genetic knock-down of sNPFR in IPCs by using *InsP3-GAL4*, GAL4 line specifically labeling IPCs, crossed with *UAS-sNPFR RNAi* or *UAS-mCD8::GFP* in the same genetic background. Note that no change was observed in gustatory sensitivities. (E-F) Sugar and bitter sensitivity of flies with genetic cellular ablation of IPCs by using *InsP3-GAL4* (or control wild type flies in the same genetic background) crossed with *UAS-hid* or *UAS-nls::GFP* in the same genetic background. Ablation of IPCs were confirmed as a loss of nls::GFP signal (F). (G-I) Sugar and bitter sensitivity of flies with over-expression or genetic knock-down of sNPFR in bitter-sensing GRNs. Both *Gr66-GAL4* and *Gr33-GAL4* drivers were tested for RNAi also combined with UAS-Dicer2 (*UAS-Dicer2*; *Gr66-GAL4* or *UAS-Dicer2*; *Gr33-GAL4* crossed with *UAS-sNPFR RNAi* or *UAS-mCD8::GFP* in the same genetic background). Similar result (no effect on gustatory sensitivities) was observed for 1-day WS flies (data not shown). n>5 for all experimental groups.

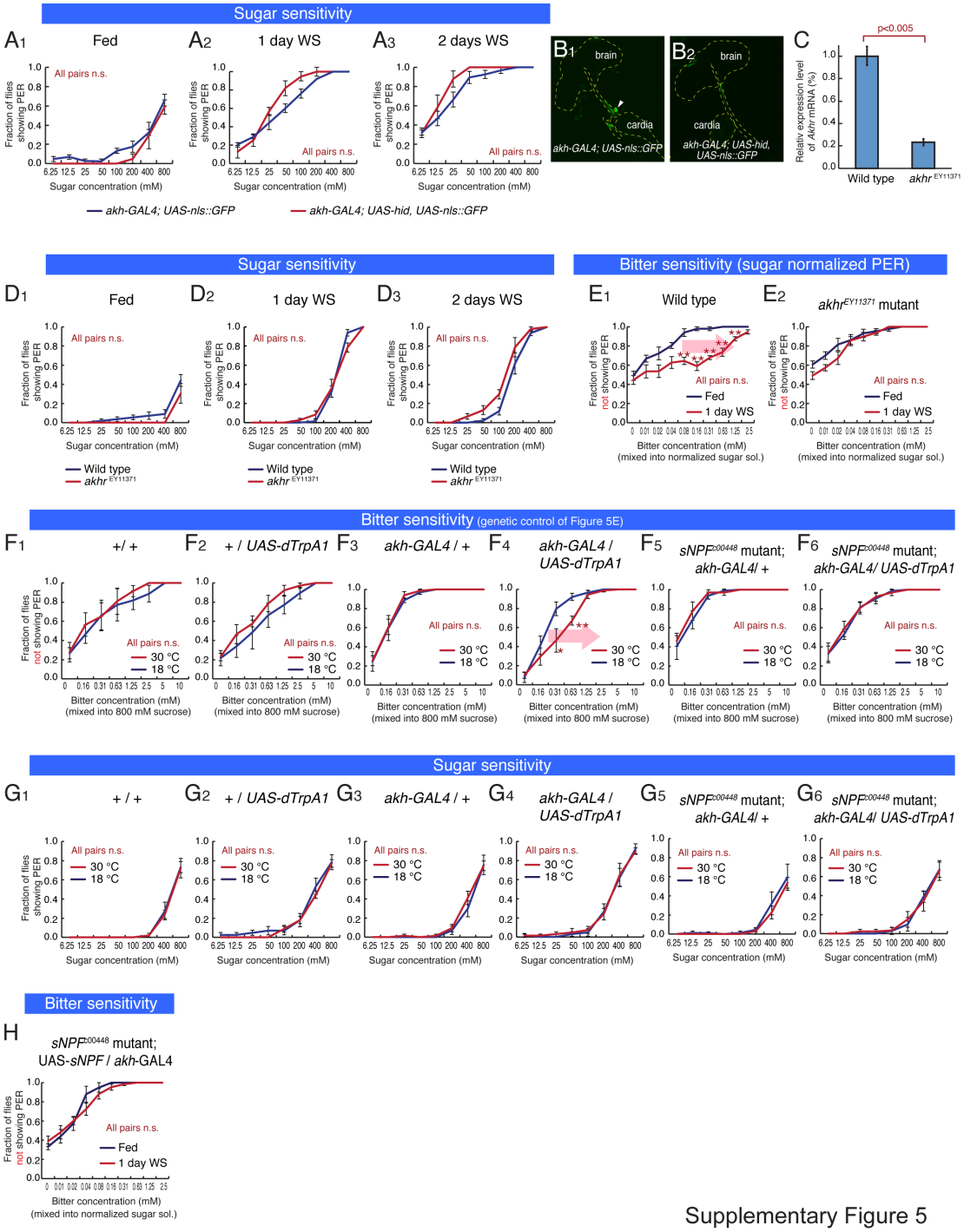

Supplementary Figure 5

Figure S5. Genetic Manipulations of AKH Do Not Affect Sugar Sensitivity

(A-B) Sugar sensitivity of flies with genetic cell-ablation of AKH neuroendocrine cells. Data is acquired from the same flies that were used in Figure $5A_{1-3}$. S50 of these experiments are summarized in Figure $5B_1$. Cell ablation was confirmed with loss of nls::GFP signal (B_{1-2}). (C) Relative *akhr* mRNA expression level of $AKHR^{EY11371}$ compared to wild type flies in the same genetic background (bottom) measured by qPCR. P-value represents t-test (n=3). (D) Sugar sensitivity of wild type and $AKHR^{EY11371}$ mutant flies in the same genetic background. Data is acquired from the same flies that were used in Figure $5C_{1-3}$. S50 of these experiments are summarized in Figure $5D_1$. (E) Results of the sugar-normalized PER assay comparing bitter sensitivity between fed and 1-day WS. Wild type flies (E_1) and $akhr^{EY11371}$ mutant flies (E_2) in the same genetic background were tested. Lobeline was mixed into 800 mM sucrose solution for fed flies, or 200 mM sucrose solution for 1-day WS flies. E_1 is the same as Figure $3C_1$ (duplicated for purposes of comparison). (F-G) Sugar and bitter sensitivity of flies with genetic thermoactivation of AKH-producing cells (w-; +; *akh-GAL4* (III) crossed with w-; +; + (F_3, G_3) or w-; *UAS-dTrpA1* (II); *UAS-dTrpA1* (III) (F_4, G_4). w-; $sNPF^{c00448}$; *akh-GAL4* (III) crossed with w-; +; + (F_5, G_5) or w-; *UAS-dTrpA1* (II); *UAS-dTrpA1* (III) (F_6, G_6)) and its genetic control flies (Wild flies crossed with w-; *UAS-dTrpA1* (II); *UAS-dTrpA1* (III) (F_2, G_2) or wild type flies in the same genetic background (F_1, G_1)). Figure $S3F_{3-6}$ are the same as Figure $5E_{1-4}$ (copied for purposes of comparison). (H) Bitter sensitivity measured with the normalized-sugar PER assay in *sNPF* mutant flies with genetic rescue of sNPF expression in AKH neuroendocrine cells (w-; $sNPF^{c00448}$; *UAS-sNPF* crossed with w-; $sNPF^{c00448}$; *akh-GAL4*). Note that rescuing of *sNPF* expression in AKH neuroendocrine cells does not rescue the starvation-dependent decrease in bitter sensitivity. (A, D-H) n>4 for all experimental groups.

Supplemental Experimental Procedures

Fly strains

sNPF-GAL4, *UAS-sNPF*, and *UAS-sNPFR* (Lee et al., 2008) were generously provided by Drs. Kweon Yu and Jing W. Wang. *npf*-GAL4 (Wu et al., 2003), *akh-GAL4*(Lee and Park, 2004), *InsP3-GAL4* (Buch et al., 2008), *Gr66a-GAL4* (Scott et al., 2001), *Gr33a-GAL4* (Moon et al., 2009), *elav-GenesSwitch* (Osterwalder et al., 2001) were provided by Drs. Ping Shen, Jae H. Park, Michael J. Pankratz, Kristin Scott, Craig Montell, and Haig Keshishian. *BDP-GAL4* (a *GAL4* line with a *Drosophila* synthetic core promoter but no enhancer 5' to this promoter, which has been shown to have no detectable expression in the adult CNS (Pfeiffer et al., 2008)), and *n-synaptobrevin-GAL4* (*nsyb-GAL4*) (Pauli et al., 2008) were obtained from, Barret Pfeiffer, Drs. Gerald M. Rubin, and Julie Simpson, *UAS-mCD8::GFP* (pJFRC2 described in (Pfeiffer et al., 2010)), *UAS-GCaMP3.0* (Tian et al., 2009), *UAS-dTRPA1* (Hamada et al., 2008) were generously provided by Drs. Gerald M. Rubin, Dr. Loren L Looger, and Dr. Paul A. Garrity, respectively. RNAi and related lines (Dietzl et al., 2007) were generously provided by Dr. Barry J. Dickson via the VDRC stock center (*UAS-sNPFR RNAi* (GD661 v9379), *UAS-mCD8::GFP*, and *UAS-Dicer2* (on X chromosome)). $sNPF^{c00448}$, $sNPF^{f07577}$, and $AKHR^{EY11371}$ were obtained from the Bloomington stock center and backcrossed for at least six generation into our wild type background. GMR GAL4 lines (Jenett et al., 2012) and tub-$Gal80^{ts}$ were also obtained from the Bloomington stock center. Other lines used in this research: *UAS-eGFP-KIR2.1*(Baines et al., 2001), *UAS-TeTxLC.TNT* (UAS-TNT), *UAS-TeTxLC.IMPTNT* (UAS-IMPTNT) (Sweeney et al., 1995).

Immunohistochemistry

Dissected brains were fixed in 4% formaldehyde in PEM (0.1M PIPES, pH 6.95, 2mM EGTA, 1mM MgSO4) for 2 hours at 4 °C. After three 15-min rinses with PBS, brains were incubated with primary antibodies overnight. Following three 15-min rinses with PBS, brains were incubated with secondary antibody overnight. Following three rinses, brains were incubated in 50% glycerol in PBS for 2 hours and cleared with VECTASHIELD® (VECTA). All procedures were performed in 4 °C. A Fluoview™ FV1000 Confocal laser scanning biological microscope (Olympus) with a 30×, 1.05 N.A. silicone oil objective (Olympus) was used to obtain confocal serial optical sections. For observation of native fluorescence, incubation with primary and

secondary antibodies was omitted. The antibodies used: Rabbit Anti-sNPF precursor (Nassel et al., 2008) (kind gift by Dr. Dick R Nässel), Rabbit Anti-NPF (RB-19-001: RayBiotech), Mouse Tyrosine Hydroxylase Antibody (ImmunoStar), Alexa Fluor® 568 donkey anti Rabbit IgG(H+L), Alexa Fluor® 568 donkey anti Mouse IgG(H+L) (Invitrogen). Native GFP signal was observed without immunostaining. Fluorender software (Wan et al., 2009) was used to make 3D reconstructed images.

Sigmoidal fitting of data and statistics

In order to fit the data into a sigmoidal curve, sigmoid interpolation was performed. The sigmoid curves were defined as follows:

$$F_S = \frac{1}{1 + e^{(-\alpha_s \log_2 \frac{S_{con}}{S_{50}})}}$$

Where

F_S *: Fraction of flies showing the PER*

S_{con} *: Concentration of sucrose*

S_{50}*: Sucrose concentration where 50% of flies show the PER*

α_S *: slope of the sigmoid curve*

$$F_B = (1 - R_S) + \frac{R_S}{1 + e^{(-\alpha_B \log_2 \frac{B_{con}}{B_{50}})}}$$

Where

F_B *: Fraction of flies not showing the PER*

R_S *: Fraction of flies showing PER when bitter is not mixed (The max PER ratio)*

B_{con} *: Concentration of lobeline*

B_{50}*: Bitter concentration required to inhibit the PER in 50% of flies that showed PER to sugar (without bitter)*

α_B *: slope of the sigmoid curve*

Based on the experimentally measured quantities (S_{con} *or* B_{con} and $F_{S \text{ or } B}$), S_{50} or B_{50} and $\alpha_{S \text{ or } B}$ were chosen to best fit the data. For all experimental data, fitting based on nonlinear regression, which finds the coefficients that fit the data by the Levenberg-Marquardt algorithm for nonlinear least squares, was calculated with Matlab (MathWorks). Goodness-of-fit was tested by two-way ANOVA between the sigmoidal curve and the actual PER response curve, which indicated a good fit for all cases ($p<0.05$. two-way ANOVA) (See supplementary Fig S1B for examples of fitting). Since we are interested in sugar and bitter sensitivity, we used S_{50} or B_{50} for data analysis.

The distribution of values of S_{50} and B_{50} were not significantly distinct from normal distribution among the data acquired from wild-type flies (null hypothesis that distribution is normally distributed was not rejected by Lilliefors test: $p=0.5$ for fed flies, $n=29$, and $p=0.29$ for 1-day WS flies, $n=17$). Thus parametric tests were used for data analysis.

Calcium imaging

The protocol for calcium imaging was modified from that described in (Inagaki et al., 2012; Marella et al., 2006). After a brief anesthesia on ice, flies were mounted on a thin plastic plate with wax as shown in Figure 4E. The top side of the plate contained a well made with wax, and the fly head was immersed in ice-cold Ca^{2+} free saline (108mM NaCl, 5mM KCl, 8.2mM $MgCl_2$, 4mM $NaHCO_3$, 1mM NaH_2PO_4, 15mM Ribose, 5mM HEPES, pH 7.5; note that Ribose, which does not stimulate *Drosophila* sugar-sensing GRNs, is used instead of other sugars). In this saline bath, the antennae and cuticle at the anterior side of the fly head capsule were surgically removed with sharp forceps, so that the SOG could be imaged. The fat body, air sacs, and esophagus were gently removed to give a clear view of the brain and to minimize its movement. At the bottom side of the plate, a glass tube was mounted with the opening facing the proboscis of the mounted fly. A piece of twisted Kimwipe was placed just behind the fly. During imaging, a lobeline solution was delivered from the glass tubing to stimulate gustatory neurons in the proboscis and was removed by the Kimwipe.

Following dissection, the ice-cold Ca^{2+} free saline was removed and the fly brain was immersed in 1 ml of room-temperature imaging saline (108mM NaCl, 5mM KCl, 2mM $CaCl_2$, 8.2mM $MgCl_2$, 4mM $NaHCO_3$, 1mM NaH_2PO_4, 15mM Ribose, 5mM HEPES, pH 7.5). This setup was moved under an Ultima two-photon laser scanning microscope (Prarie Instruments, Inc) with a 40× 0.8 N.A. objective (Olympus, Inc). The glass tubing was connected to four silicon tubes with a plastic manifold (MP-4, Warner Instruments). Each silicon tube was connected to 50 ml syringes filled with either 15 ml of 0, 0.07, 0.31 or 1.25mM lobeline dissolved in water. The flow of lobeline solution was controlled using electrically triggered pinch valves (ALA-VM8, ALA Scientific Instruments) that compressed the silicon tubes between the syringes and the manifold. The timing of valve opening was controlled by the two-photon acquisition system and its software (Prairie view and Trigger Sync, Prairie) so that the timing was linked with the image acquisition. ΔF/F and peak ΔF/F was calculated using Matlab (MathWorks).

qPCR

RNA was extracted from heads of 10 flies (for *sNPF*) and 4 fly whole bodies (for *akhr*). cDNA was synthesized using Super Script® VILO™ cDNA Synthesis kit (Invitrogen). Real Time PCR was performed using EXPRESS SYBR® GreenER™ (Invitrogen) and a 7300 Real Time PCR system (Applied biosystems). *Rp49* was used as a standard. Using melting temperature analysis, each primer pair was confirmed to produce a single PCR product. Primers listed below were used.

RP49-f: CCCGAAAACTTTTAGACTCA

RP49-r: TTTTCAAACATTTCCATCGT

sNPF-f: AGGGTATCGACAACAGAGTG

sNPF-r: CACCAGGAACTTCTTGAATC

AKHR-f: ACAACAATCCGTCGGTGAAC

AKHR-r: CTTCCATTCAGCAGCGAGTT

Baines, R.A., Uhler, J.P., Thompson, A., Sweeney, S.T., and Bate, M. (2001). Altered electrical properties in Drosophila neurons developing without synaptic transmission. The Journal of neuroscience : the official journal of the Society for Neuroscience *21*, 1523-1531.

Buch, S., Melcher, C., Bauer, M., Katzenberger, J., and Pankratz, M.J. (2008). Opposing effects of dietary protein and sugar regulate a transcriptional target of Drosophila insulin-like peptide signaling. Cell Metab *7*, 321-332.

Dietzl, G., Chen, D., Schnorrer, F., Su, K.C., Barinova, Y., Fellner, M., Gasser, B., Kinsey, K., Oppel, S., Scheiblauer, S., *et al*. (2007). A genome-wide transgenic RNAi library for conditional gene inactivation in Drosophila. Nature *448*, 151-156.

Hamada, F.N., Rosenzweig, M., Kang, K., Pulver, S.R., Ghezzi, A., Jegla, T.J., and Garrity, P.A. (2008). An internal thermal sensor controlling temperature preference in Drosophila. Nature *454*, 217-220.

Inagaki, H.K., Ben-Tabou de-Leon, S., Wong, A.M., Jagadish, S., Ishimoto, H., Barnea, G., Kitamoto, T., Axel, R., and Anderson, D.J. (2012). Visualizing neuromodulation in vivo: TANGO-mapping of dopamine signaling reveals appetite control of sugar sensing. Cell *148*, 583-595.

Jenett, A., Rubin, G.M., Ngo, T.T., Shepherd, D., Murphy, C., Dionne, H., Pfeiffer, B.D., Cavallaro, A., Hall, D., Jeter, J., *et al*. (2012). A GAL4-driver line resource for Drosophila neurobiology. Cell Rep *2*, 991-1001.

Lee, G., and Park, J.H. (2004). Hemolymph sugar homeostasis and starvation-induced hyperactivity affected by genetic manipulations of the adipokinetic hormone-encoding gene in Drosophila melanogaster. Genetics *167*, 311-323.

Lee, K.S., Kwon, O.Y., Lee, J.H., Kwon, K., Min, K.J., Jung, S.A., Kim, A.K., You, K.H., Tatar, M., and Yu, K. (2008). Drosophila short neuropeptide F signalling regulates growth by ERK-mediated insulin signalling. Nat Cell Biol *10*, 468-475.

Marella, S., Fischler, W., Kong, P., Asgarian, S., Rueckert, E., and Scott, K. (2006). Imaging taste responses in the fly brain reveals a functional map of taste category and behavior. Neuron *49*, 285-295.

Moon, S.J., Lee, Y., Jiao, Y., and Montell, C. (2009). A Drosophila gustatory receptor essential for aversive taste and inhibiting male-to-male courtship. Current biology : CB *19*, 1623-1627.

Nassel, D.R., Enell, L.E., Santos, J.G., Wegener, C., and Johard, H.A. (2008). A large population of diverse neurons in the Drosophila central nervous system expresses short neuropeptide F, suggesting multiple distributed peptide functions. BMC Neurosci *9*, 90.

Osterwalder, T., Yoon, K.S., White, B.H., and Keshishian, H. (2001). A conditional tissue-specific transgene expression system using inducible GAL4. Proc Natl Acad Sci U S A *98*, 12596-12601.

Pauli, A., Althoff, F., Oliveira, R.A., Heidmann, S., Schuldiner, O., Lehner, C.F., Dickson, B.J., and Nasmyth, K. (2008). Cell-type-specific TEV protease cleavage reveals cohesin functions in Drosophila neurons. Dev Cell *14*, 239-251.

Pfeiffer, B.D., Jenett, A., Hammonds, A.S., Ngo, T.T., Misra, S., Murphy, C., Scully, A., Carlson, J.W., Wan, K.H., Laverty, T.R., *et al*. (2008). Tools for neuroanatomy and neurogenetics in Drosophila. Proc Natl Acad Sci U S A *105*, 9715-9720.

Pfeiffer, B.D., Ngo, T.T., Hibbard, K.L., Murphy, C., Jenett, A., Truman, J.W., and Rubin, G.M. (2010). Refinement of tools for targeted gene expression in Drosophila. Genetics *186*, 735-755.

Scott, K., Brady, R., Jr., Cravchik, A., Morozov, P., Rzhetsky, A., Zuker, C., and Axel, R. (2001). A chemosensory gene family encoding candidate gustatory and olfactory receptors in Drosophila. Cell *104*, 661-673.

Sweeney, S.T., Broadie, K., Keane, J., Niemann, H., and O'Kane, C.J. (1995). Targeted expression of tetanus toxin light chain in Drosophila specifically eliminates synaptic transmission and causes behavioral defects. Neuron *14*, 341-351.

Tian, L., Hires, S.A., Mao, T., Huber, D., Chiappe, M.E., Chalasani, S.H., Petreanu, L., Akerboom, J., McKinney, S.A., Schreiter, E.R., *et al*. (2009). Imaging neural activity in worms, flies and mice with improved GCaMP calcium indicators. Nat Methods *6*, 875-881.

Wan, Y., Otsuna, H., Chien, C.B., and Hansen, C. (2009). An Interactive Visualization Tool for Multi-channel Confocal Microscopy Data in Neurobiology Research. Ieee T Vis Comput Gr *15*, 1489-1496.

Wu, Q., Wen, T., Lee, G., Park, J.H., Cai, H.N., and Shen, P. (2003). Developmental control of foraging and social behavior by the Drosophila neuropeptide Y-like system. Neuron *39*, 147-161.

Chapter III

A NEURAL CORRELATE OF SOCIAL EXPERIENCE REVEALED BY OPTOGENETICS IN FREELY BEHAVING ADULT *DROSOPHILA MELANOGASTER*

SUMMARY

Optogenetics allows the manipulation of neural activity in freely moving animals with millisecond precision, but its application in *Drosophila* has been limited. Here we show that a recently described Red activatable Channelrhosopsin (ReaChR) permits activation of CNS neurons in freely behaving adult flies, at wavelengths that do not interfere with normal visual function. This tool affords the opportunity to control neural activity with millisecond time resolution over a broad dynamic range of stimulation intensities. Using such time-resolved activation, we show that the neural control of male courtship song can be separated into probabilistic/biasing, and deterministic/command-like components. The former, but not the latter, neurons are subject to functional modulation by social experience, supporting the idea that they constitute a locus of state-dependent influence. This separation is not evident using thermogenetic tools, underscoring the importance of temporally precise control of neuronal activation in the functional dissection of neural circuits in *Drosophila*.

Inagaki HK, Jung Y, Hoopfer ED, Wong AM, Mishra N, Lin JY, Tsien RY, Anderson DJ. Optogenetic control of Drosophila using a red-shifted channelrhodopsin reveals experience-dependent influences on courtship. *Nat Methods*. 2013 Dec 22. doi: 10.1038/nmeth.2765.

INTRODUCTION

Drosophila melanogaster is one of the most powerful model organisms available for the genetic dissection of neural circuit function (Luo et al., 2008; Venken et al., 2011) Likewise, the use of light-sensitive microbial opsins, such as channelrhodopsin, has revolutionized the functional dissection of neural circuits in behaving animals (Fenno et al., 2011; Yizhar et al., 2011a) . Unfortunately, with the exception of larval neurons and peripheral sensory neurons in adults (Bellmann et al., 2010; de Vries and Clandinin, 2013; Gordon and Scott, 2009; Inagaki et al., 2012; Pulver et al., 2009; Schroll et al., 2006; Suh et al., 2007; Zhang et al., 2007; Zimmermann et al., 2009) this powerful technology and model organism have been largely incompatible in adult flies (but see refs (de Vries and Clandinin, 2013; Zimmermann et al., 2009)), due to the light-scattering and absorptive properties of the adult fly cuticle. Therefore *Drosophila* researchers have, to a large extent, been unable to exploit the rapidly expanding optogenetic toolkit for neural circuit manipulation. Although P2X2, an ionotropic purinergic receptor, has been used as an optogenetic tool in adult *Drosophila*, this technique requires injection of caged ATP into the brains of individual anesthetized flies (Lima and Miesenbock, 2005). This makes it a relatively cumbersome and invasive technology that is sub-optimal for many applications, including large-scale screening.

In the absence of facile optogenetic manipulation, dTRPA1, a thermosensitive cation channel, has been the preferred method for neuronal activation in freely behaving adult flies (Hamada et al., 2008; Venken et al., 2011). Since this method depends on changes in temperature to control neuronal activity, however, it lacks precision in both the temporal and intensity domains, and enables only constitutive opening of the ion channel, which may inhibit neurons after several seconds due to depolarization block. In contrast, light-activated microbial opsins enable rapid switching of neural activity, pulsatile activation to avoid depolarization block and controlled variation of frequency and intensity parameters. The use of optogenetic tools also avoids the potentially confounding influence of temperature changes on behavior, which accompanies the use of thermogenetic effectors.

Here, we demonstrate that expression of ReaChR in adult CNS neurons enables rapid and temporally precise neuronal activation in freely moving adult *Drosophila*. Using this optogenetic control of behavior, we have separated the control of wing extension, a male-specific courtship behavior, into probabilistic, state-dependent and deterministic, command-like components. Moreover, by combining ReaChR activation with functional calcium imaging, we have also identified a neural correlate of the influence of social experience on male courtship behavior.

RESULTS

Optogenetic vs. thermogenetic control of peripheral gustatory neurons

We reasoned that previously described ChR2 variants do not work well in adult *Drosophila* due, at least in part, to low penetrance of blue light through the cuticle. Indeed, direct measurements *in vivo* indicated that the penetrance of blue light through the cuticle is much weaker (c.a. 1%) than that of longer wavelengths such as green or red light (5-10%) (Fig. 1a). Therefore, we created transgenic flies that express the recently developed red-shifted channelrhodopsins, C1V1(T/T)(Yizhar et al., 2011b) and ReaChR(Lin J.Y.) under the control of the Gal4-UAS system, to test whether red shifted light can penetrate the cuticle sufficiently to activate neurons expressing these channels (Supplementary Table 1 for a listing of all transgenic fly strains created).

We first compared the efficacy with which different opsins elicited the proboscis extension reflex (PER), a feeding behavior triggered by activation of sugar-sensing gustatory receptor neurons (GRNs) that express the receptor Gr5a (Scott et al., 2001). Optogenetic activation of Gr5a neurons using channelrhodopsin-2 (ChR2) has previously been shown to trigger the PER in *Drosophila* (Inagaki et al., 2012; Zhang et al., 2007). All of the blue light-sensitive opsin variants tested (ChR2 (Boyden et al., 2005; Nagel et al., 2003), H134R (Nagel et al., 2005) and C128T (Berndt et al., 2009)) induced PER behavior in response to photostimulation at 470 nm, although only H134R yielded responses in 100% of flies (Fig. 1b). Flies expressing ReaChR in Gr5a GRNs yielded robust PER responses to both red (627 nm) and green (530 nm) light, although the response to the latter wavelength was slightly stronger. In contrast, flies expressing C1V1(T/T) did not exhibit PERs in response to either red or green light (Fig. 1b). Instead, they moved their probosces slightly, albeit in a manner time-locked to photostimulation, suggesting that C1V1(T/T) has only a weak ability to activate Gr5a GRNs.

Surprisingly, in flies expressing dTrpA1 in Gr5a GRNs, we did not observe any behavioral response at an ambient temperature known to activate the ion channel (32ºC) (Hamada et al., 2008; Pulver et al., 2009) (Fig. 1b, TrpA1), or during gradual ramping to this temperature from 22ºC (data not shown). Interestingly, activation of dTrpA1 in Gr5a GRNs using heat pulses from an IR laser (Keene and Masek, 2012) has been reported to induce a PER. We reasoned that if Gr5a neurons are continuously or gradually activated via TrpA1, they may undergo a rapid depolarization block that prevents PER behavior. Consistent with this idea, continuous illumination of Gr5a-ReaChR flies produced only a transient PER reaction (half-time for decay=1.5 sec; Fig. $1c_1$), while pulsatile illumination (1 Hz, 100 msec pulse duration) evoked a train of PERs time-locked to each light pulse (Fig. $1c_2$).

To investigate more directly whether continuous stimulation of Gr5a GRNs indeed causes a depolarization block, we performed electrophysiological recordings from Gr5a GRNs during optogenetic activation using ReaChR. Pulsed light caused continuous bursts of spiking throughout the stimulation period (Fig. $1d_2$, e_2). The latency to the onset of the first spike following illumination was short (5.8±0.19 msec), but increased slightly after successive pulses (12.9±9.5 msec for the 5^{th} pulse; Fig. 1f). In contrast, spiking activity decayed exponentially during continuous light stimulation (half-time for decay, ~1.5 sec; Fig. $1d_1$, e_1). The rapid decay of both spiking and PER behavior during continuous activation of ReaChR (Fig.1g; Pearson's correlation coefficient: r=0.96), suggests that the former likely accounts for the latter.

To test whether constitutive opening of TrpA1 might also cause a depolarization block, we activated this thermosensitive channel using a local heat source while recording from Gr5a GRNs. Indeed, TrpA1 activation triggered only transient spiking in Gr5a GRNs, with a strong decay after several seconds (Fig. 1h), similar to the results obtained using continuous ReaChR activation. Together, these data may explain why PER responses were not induced by constitutive or gradual thermal activation in Gr5a-TrpA1-expressing flies (Fig. 1b). They also reconfirm the importance of pulsed activation of neurons to avoid depolarization block, as reported previously in other systems (Yizhar et al., 2011a).

Activation with ReaChR but not blue light-sensitive opsins in CNS neurons evokes behavioral responses

Only a few studies have reported successful elicitation of behavior in adult *Drosophila* by activating CNS neurons expressing blue light-sensitive opsins (de Vries and Clandinin, 2013; Zimmermann et al., 2009). To determine whether activation using ReaChR would be more effective, we directly compared the behavioral responses of flies expressing blue light- vs. red light- sensitive opsins in GAL4 lines driving expression in different populations of CNS neurons. These lines included: HB9-GAL4, a motor neuron-specific driver (Odden et al., 2002) whose activation induces side walking and, at higher intensities, "knock-out" (loss of postural control and immobility); Corazonin (Crz)-GAL4, which labels male-specific peptidergic interneurons in the abdominal ganglion whose activation induces abdominal bending and ejaculation (Tayler et al., 2012) ;Fru-GAL4 (Stockinger et al., 2005), which labels ~2,000 neurons throughout the brain and whose activation in males induces mating behavior including courtship song (von Philipsborn et al., 2011), which is detectable as wing extension, and abdominal bending; at higher intensities, knock-out is observed; and "P1-GAL4," a split-GAL4 (Luan et al., 2006; Pfeiffer et al., 2010) driver generated from parental GAL4 lines(Jenett et al., 2012) identified in a behavioral screen (E.D.H. and D.J.A., unpublished), that is specifically expressed in ~16-20 male-specific P1 neurons, activation of which elicits wing extension in males (Pan et al., 2012; von Philipsborn et al., 2011). To facilitate the control and monitoring of light-induced behaviors in freely moving adult flies in a high-throughput, cost-effective and flexible manner, we developed a high power LED-based activation system (Fig. 2a-c; Supplementary fig. 1 and Supplementary table 2 and Supplemental Methods).

Strikingly, among all 5 opsins tested using these CNS drivers, ReaChR was the only one whose activation yielded robust behavioral phenotypes in a light-dependent manner (Fig. $2d_{1-4}$). The evoked behaviors were not due to innate responses to light, because control flies lacking *UAS-ReaChR* did not exhibit them (Fig. $2d_{1-4}$, No opsin). The fact that blue-light activated opsins yielded a behavioral response (PER) when expressed in GRNs, but not in the CNS neurons tested here, likely reflects the fact that the peripheral GRNs are located close to the cuticle, where blue light may penetrate more easily. The lack of

responses in C1V1(T/T)-expressing flies cannot, however, be explained in this way. Analysis of C1V1(T/T) expression in CNS neurons revealed that this opsin is expressed weakly in cell somata and not trafficked to arborizations (Supplementary fig. $2a_2$), while ReaChR is strongly expressed in somata and trafficked to arborizations as well (Supplementary fig. $2a_1$, d). This difference likely accounts for the different efficacies of the two red-shifted opsins in this system.

The peak of the ReaChR action spectrum (measured in cultured hippocampal neurons) is ~590 nm (Lin J.Y.). The efficacy of ReaChR activation by different wavelengths in freely behaving flies will, however, reflect a combination of factors including cuticular penetration and intensity, as well as proximity to peak sensitivity. To empirically determine the optimal wavelength of light for behavioral assays, therefore, we compared the ability of blue (470 nm), green (530 nm), amber (590 nm) and red (627 nm) light to induce behavior in flies expressing ReaChR under the control of different CNS GAL4 drivers. When not normalized for intensity, green LEDs had the strongest capacity to elicit ReaChR-dependent behaviors (Fig. $2d_{1-4}$, f, g). Indeed, the efficacy of green light stimulation was so strong that it produced a "knock-out" phenotype at all but the lowest stimulation intensity, with both the HB9-GAL4 and Fru-GAL4 drivers (Fig. 2f, g). In some cases (pIP10 neurons; see below), robust behavioral responses were detected only using green light, and hardly at all using other wavelengths. Although amber light is closest to the peak of the ReaChR action spectrum, commercial LEDs of this wavelength are dimmer than the others and therefore did not elicit strong behavioral responses (Fig. 2f, g).

Although TrpA1-mediated activation of P1 neurons can elicit wing extension (Pan et al., 2012; von Philipsborn et al., 2011), in our direct comparison the fraction of flies showing a wing extension phenotype was much higher using ReaChR and green light, than using TrpA1 (Fig. $2d_4$). This suggests that the intensity of activation obtained using ReaChR (and green light) can be substantially stronger than that achieved using dTrpA1, without subjecting flies to the high temperatures necessary to activate the latter. Nevertheless, although green LEDs elicited the strongest behavioral responses, flies can see this wavelength, whereas their sensitivity to wavelengths > 620 nm is much lower (Stavenga, 2002; Yamaguchi

et al., 2010) (see, however, Hanai (2008)(Hanai et al., 2008)). Therefore we used red LEDs whenever possible to avoid behavioral artifacts caused by strong visual stimulation.

To investigate whether the strength of a given ReaChR-dependent behavioral phenotype can be quantitatively tuned, we tested multiple frequencies and intensities of light pulses using the P1-GAL4 driver. A pulse width of 5 msec was used for all the frequencies tested (10-90 Hz). There was a frequency-dependent increase in the fraction of flies showing wing extension (Fig. $2e_1$: range ~10-80%), as well as in the average number and duration of wing extension bouts per fly (Fig. $2e_2$, and Supplementary fig. 2e), even when correcting for the total duration of illumination (Supplementary fig. $2f_{1-3}$). The fraction of flies showing wing extension responses was also increased over a range of different red light stimulation intensities (0.23-1.11 mW/mm^2), from ~15% to ~80%, (see Fig. 4a and $4c_1$). The HB9 and Fru-GAL4 drivers also yielded an increase in the fraction of flies showing the respective behavioral responses as the intensity of red light was increased, albeit over different ranges (Fig. 2f, g, 627 nm). Together, these data indicate that ReaChR can be used to tune behavioral phenotypes by varying the light intensity and/or pulse frequency, over a relatively broad dynamic range.

Probabilistic vs. deterministic neural control of courtship song can be discriminated using ReaChR

Previous studies of the neural circuitry underlying male courtship behavior in *Drosophila* have used neuronal activation methods, including P2X2 and TrpA1, to identify different neuronal subclasses that control courtship song, including those in the central brain and those in the ventral nerve cord (VNC) (Clyne and Miesenbock, 2008; Kohatsu et al., 2011; Pan et al., 2012; von Philipsborn et al., 2011). In particular, studies using TrpA1 have described two neuronal classes in the central brain controlling this behavior: one, called P1 or pMP4, constitutes a population of interneurons (Kohatsu et al., 2011; Pan et al., 2012; von Philipsborn et al., 2011), while the other, called pIP10, constitutes a small group of descending neurons that project to the VNC (von Philipsborn et al., 2011) (Fig. 3b). The pre-synaptic terminals of P1 neurons overlap the dendrites of pIP10 neurons, suggesting that they may be synaptic partners (von

Philipsborn et al., 2011); however the difference, if any, between the roles of these neurons in controlling courtship song has not been apparent, as similar behaviors are evoked by TrpA1-mediated stimulation of both classes (von Philipsborn et al., 2011).

We exploited the time-resolved control of neuronal activation afforded by ReaChR to compare the temporal patterns of stimulation-evoked behavioral responses in P1 vs. pIP10 neurons. To express ReaChR in the latter cells, we used an intersectional strategy combining a specific GAL4 line (VT40556 (von Philipsborn et al., 2011)) with Fru-FLP (Yu et al., 2010) and a newly generated *UAS>STOP>ReaChR* transgene (where ">" denotes FRT sites, the target of FLP recombinase; see Supplementary fig. 2b,c and Supplementary table 1). Anatomical analysis using a citrine reporter fused to the C-terminus of ReaChR confirmed the restricted expression of ReaChR in flies of the appropriate intersectional genotype (Supplementary fig. 2d).

Surprisingly, we found that the temporal dynamics of wing extension evoked by activation of P1 vs. pIP10 neurons were strikingly different. ReaChR-mediated activation of P1 neurons evoked wing extension in a probabilistic or stochastic manner: the initiation of wing extension was not time-locked to the onset of illumination, but rather occurred with variable latencies throughout the stimulation period (17.7±27.5 sec) (Fig. $3a_1$,c). The average duration of each bout was short (0.99±0.48 sec) relative to the duration of photostimulation (30 sec). Finally, the offset of the behavior was not time-locked to the offset of stimulation; rather, we observed persistent wing extension bouts in the intervals between photostimulation trials (Fig. $3a_1$, e: Pearson's correlation coefficient between stimulation pattern and behavioral response: r=0.004). The stochasticity and persistence of ReaChR-evoked wing extensions were observed regardless of activation wavelength and intensity (Fig. 4a and Supplementary fig.$3a_1$).

In contrast to the results observed with P1 neurons, activation of pIP10 neurons triggered robust wing extension in a deterministic manner time-locked to photostimulation at all but the weakest intensities (Fig. $3a_2$, Fig. 5a and Supplementary fig. $3a_2$). The onset of the behavior was strongly time-locked to the onset of stimulation, with a very short latency (0.08±0.04 sec) (Fig. $3a_2$, c). Once initiated, wing extension continued throughout the photostimulation period, and co-terminated, with few exceptions, with the offset

of photostimulation (Fig. 3a$_2$, d: Pearson's correlation coefficient between stimulation pattern and behavioral response: r=0.993). With weaker intensities of illumination close to threshold ($\leq$0.012 mW/mm^2), wing extension responses were less efficiently evoked, but responses were still restricted to the photostimulation period and no persistent behavior between trials was observed (Fig. 3e, Fig. 5a and Supplementary fig. 3a$_2$).

Therefore, these differences between P1 and pIP10 neurons in the temporal dynamics of ReaChR activation-evoked wing extensions were largely independent of illumination intensity. They did not reflect a higher sensitivity of pIP10 than P1 neurons, because the intensity dependence of pIP10-evoked wing extension by green light was almost identical to that of P1 neurons (Fig. 3f).

Social isolation modulates the threshold of ReaChR-activated male courtship behavior

The probabilistic or biasing nature of the wing extension responses elicited by ReaChR-mediated activation of P1 neurons suggested that these neurons might encode, or be modified by, state-dependent influences on male courtship behavior. To investigate this possibility, we sought a manipulation that influences courtship behavior in an internal state-like manner. One such influence is provided by social experience. Whether immature animals are reared together with conspecifics, or in social isolation, has a profound and lasting effect on numerous behaviors, including social behaviors such as courtship and aggression, in both vertebrates and invertebrates (Dankert et al., 2009; Luciano and Lore, 1975; Matsumoto et al., 2005; Ueda and Wu, 2009; Wang et al., 2008).

Social isolation of male flies for more than several days enhances courtship behavior, including singing, towards females (Dankert et al., 2009). To investigate whether P1 neurons might be modulated by such experience, we first determined whether social isolation lowers the threshold for eliciting wing extension using ReaChR-mediated stimulation of these neurons. Indeed, the intensity of red light that evoked wing extension in 50% of flies expressing ReaChR in P1 neurons was lower in males that were socially isolated for 7 days, than in group-housed males (Fig. 4a-c$_1$). A similar effect was observed using

green light as well (Supplementary fig. 3b). For each of 3 different parameters measured, socially isolated flies exhibited significantly higher values than group housed flies (Fig. $4c_{1-3}$). Thus, social isolation effectively "tuned" the response to ReaChR activation of P1 neurons, such that the probability of a wing extension response was increased. These data suggest that the increased sensitivity to ReaChR activation of wing extension occurs in P1 neurons themselves, or in a functionally downstream population.

Because pIP10 neurons are thought to be functionally "downstream" of P1 neurons (von Philipsborn et al., 2011) (Fig. 3b), we investigated whether ReaChR activation of wing extension via these descending neurons was also sensitive to social experience. Because red light was not strong enough to activate wing extension in male flies expressing ReaChR in pIP10 neurons, we used green light to trigger wing extension. Activation of pIP10 neurons using ReaChR did not reveal any differences between single vs. group-housed flies in the efficiency with which photostimulation evoked wing extension behavior, even at lower intensities that evoked responses in only a subset of flies (Fig. 5a-c). These data indicate that the enhanced sensitivity of ReaChR-evoked wing extension in single-housed flies using the P1-GAL4 driver is likely to occur in P1 neurons themselves (or in other downstream neurons), rather than in pIP10 neurons. They also indicate that the sensitization of the P1 response by social isolation does not reflect a general increase in sensitivity among all neurons involved in wing extension behavior.

Functional calcium imaging reveals a neural correlate of social isolation

To examine directly whether social isolation enhances the sensitivity of P1 neurons to ReaChR activation, we performed calcium imaging experiments using laser-scanning 2-photon microscopy, taking advantage of the relative separation of the action spectrum peaks for ReaChR and GCaMP3.0 (Tian et al., 2009). Importantly, co-expression of GCaMP3.0 in P1 neurons together with ReaChR did not diminish the ability of the latter to mediate light-evoked wing extension in freely moving flies, indicating that the calcium buffering effect of GCaMP3.0 does not interfere with this behavior (data not shown).

An amber LED (590nm) was used for photostimulation during imaging experiments in order to maximize overlap with the peak of the ReaChR action spectrum. Excitation scanning caused an initial increase in baseline GCaMP3.0 fluorescence in flies co-expressing ReaChR in P1 neurons, even in the absence of amber light excitation of ReaChR (Fig. 6a). These increases were not observed in flies lacking *UAS-ReaChR* (Fig. 6a, green trace), implying that they reflect cross-activation of ReaChR by the GCaMP3.0 excitation beam (940 nm). Nevertheless, amber light still evoked a clear increase in the strength of GCaMP3.0 emissions over this background (Fig. 6a). This signal was not observed in flies lacking ReaChR (Fig. 6a, green trace), and therefore was not due to cross-activation of GCaMP3.0 by the amber light used to activate ReaChR (see Methods for filter settings).

Using these conditions, we compared the GCaMP3.0 response of P1 neurons to ReaChR activation of these same neurons, between single-housed (SH) vs. grouped-housed (GH) flies. P1 neurons in SH flies showed larger ReaChR-evoked calcium influxes than those in GH flies, at several different photostimulation frequencies (Fig. 6a,b). Quantitative analysis of ReaChR-citrine expression in these cells indicated that this difference was not due to higher levels of P1-GAL4 expression in SH vs. GH flies (Fig. 6c). Together, these combined behavioral and imaging experiments suggest that the excitability of P1 neurons can be modulated by prior social experience.

DISCUSSION

Here we describe a system for optogenetic activation of behavior in freely moving adult flies using ReaChR, a newly described red-shifted opsin (Lin J.Y.). This system affords temporally precise control of neuronal activation *in vivo* to an extent that is difficult to achieve using thermogenetic tools such as dTrpA1 (but see ref (Keene and Masek, 2012)). The strength of activation obtained using ReaChR, and the broad dynamic range of intensities and frequencies over which stimulation can be delivered, offer a more quantitative and temporally controlled approach to investigating the neuronal control of behavior than is provided by available thermogenetic tools. Moreover, optogenetics permits conditional control of behavior without the temperature increases required by thermogenetic effectors. The use of ReaChR with red light also reduces the confounding influence of strong visual stimulation that occurs when using blue light-activated opsins. Finally, the ability to control activation using LEDs, rather than lasers (Keene and Masek, 2012; Lima and Miesenbock, 2005), permits a relatively inexpensive approach to large-scale, high-throughput screening of GAL4 lines that drive specific behaviors.

Several factors may explain why ReaChR was more effective than other channelrhodopsins tested in intact adult flies. First and foremost, longer wavelengths of light have better penetration through the cuticle. Second, ReaChR has slower off-kinetics (137±7 ms) than the most of other ChR2 variants we tested (c.a. 10-20 ms) (Mattis et al., 2012) , making the channel more light-sensitive (but note that C128T has even longer off-kinetics: 2 sec (Berndt et al., 2009; Yizhar et al., 2011a) ; yet it did not work as well as ReaChR). Finally, the membrane transport or expression of C1V1(T/T) is much lower than that of ReaChR. Although it is possible that ReaChR is simply expressed and/or transported more efficiently than the other opsins tested, a direct comparison is difficult because they are tagged with different fluorescent proteins.

Using ReaChR to monitor both behavioral sensitivity and neuronal activation, we discovered that 1) P1 and pIP10 neurons control male courtship song in a state-like (probabilistic and persistent) vs. command-like (deterministic and time-locked) manner, respectively; and 2) the effect of social isolation to

increase male courtship behavior is mediated, at least in part, through an increase in the excitability of P1 neurons (see Supplementary table 3 for summary). It has been proposed, based on anatomical data, that P1 neurons are part of a circuit integrating multimodal sensory cues that control courtship behavior (Yu et al., 2010). Our observations suggest that P1 neurons also integrate this information with the flies' history of social experience, in a manner that influences the probability that the flies will exhibit courtship behavior. To our knowledge, this represents the first observation of a neural correlate of social experience in *Drosophila*. The mechanisms underlying the influence of social experience on neuronal excitability are not understood, and the identification of P1 neurons as a locus of this influence will facilitate future mechanistic studies.

While ReaChR-based activation of behavior was effective in all the GAL4 lines tested, the optogenetic toolkit in *Drosophila* could benefit from further engineering of red-shifted opsins. The slow off-kinetics of ReaChR may make it difficult to trigger high spiking rates in some neurons. In addition, the action spectrum of ReaChR excitation is broad, creating a non-negligible level of cross-activation by the GCaMP excitation beam during experiments to image calcium transients induced by ReaChR activation. Variants of red-shifted opsins with a narrower action spectrum and faster off-kinetics may overcome these limitations. Finally, the development of red-shifted variants of inhibitory opsins, such as halorhodpsin (Gradinaru et al., 2010) or Arch (Chow et al., 2010), should extend the optogenetic control of neuronal activity in adult flies from excitation to inhibition. Together, such tools would further enhance the applicability of optogenetics to neural circuit dissection in *Drosophila*.

ACKNOWLEDGMENTS

Drs. and/or Mrs. Yonil Jung, Eric D. Hoopfer, Allan M. Wong, Neeli Mishra, John Y. Lin, Roger Y. Tsien, and David J. Anderson are collaborators for this work.

We thank Dr. K. Deisseroth, and B. Pfeiffer for plasmids. Fly stocks were generously provided by the Bloomington Stock Center, Drs. A. Fiala, G. M. Rubin, L. L Looger, P. A. Garrity and B. J. Dickson. We also thank members of the Anderson lab for helpful discussion and sharing of flies. H.K.I. was supported by the Nakajima Foundation. J.Y.L. was funded by Foundation of Research, Science and Technology New Zealand. The project was supported by grants from the National Institutes of Health to R.Y.T. (NS027177) and to D.J.A (R01DA031389-03). D.J.A. and R.Y.T are investigators of the Howard Hughes Medical Institute.

REFERENCES

Bellmann, D., Richardt, A., Freyberger, R., Nuwal, N., Schwarzel, M., Fiala, A., and Stortkuhl, K.F. (2010). Optogenetically Induced Olfactory Stimulation in Drosophila Larvae Reveals the Neuronal Basis of Odor-Aversion behavior. Front Behav Neurosci *4*, 27.

Berndt, A., Yizhar, O., Gunaydin, L.A., Hegemann, P., and Deisseroth, K. (2009). Bi-stable neural state switches. Nat Neurosci *12*, 229-234.

Boyden, E.S., Zhang, F., Bamberg, E., Nagel, G., and Deisseroth, K. (2005). Millisecond-timescale, genetically targeted optical control of neural activity. Nat Neurosci *8*, 1263-1268.

Chow, B.Y., Han, X., Dobry, A.S., Qian, X., Chuong, A.S., Li, M., Henninger, M.A., Belfort, G.M., Lin, Y., Monahan, P.E.*, et al.* (2010). High-performance genetically targetable optical neural silencing by light-driven proton pumps. Nature *463*, 98-102.

Clyne, J.D., and Miesenbock, G. (2008). Sex-specific control and tuning of the pattern generator for courtship song in Drosophila. Cell *133*, 354-363.

Dankert, H., Wang, L., Hoopfer, E.D., Anderson, D.J., and Perona, P. (2009). Automated monitoring and analysis of social behavior in Drosophila. Nat Methods *6*, 297-303.

de Vries, S.E., and Clandinin, T. (2013). Optogenetic stimulation of escape behavior in Drosophila melanogaster. J Vis Exp.

Fenno, L., Yizhar, O., and Deisseroth, K. (2011). The development and application of optogenetics. Annu Rev Neurosci *34*, 389-412.

Gordon, M.D., and Scott, K. (2009). Motor control in a Drosophila taste circuit. Neuron *61*, 373-384.

Gradinaru, V., Zhang, F., Ramakrishnan, C., Mattis, J., Prakash, R., Diester, I., Goshen, I., Thompson, K.R., and Deisseroth, K. (2010). Molecular and cellular approaches for diversifying and extending optogenetics. Cell *141*, 154-165.

Hamada, F.N., Rosenzweig, M., Kang, K., Pulver, S.R., Ghezzi, A., Jegla, T.J., and Garrity, P.A. (2008). An internal thermal sensor controlling temperature preference in Drosophila. Nature *454*, 217-220.

Hanai, S., Hamasaka, Y., and Ishida, N. (2008). Circadian entrainment to red light in Drosophila: requirement of Rhodopsin 1 and Rhodopsin 6. Neuroreport *19*, 1441-1444.

Inagaki, H.K., Ben-Tabou de-Leon, S., Wong, A.M., Jagadish, S., Ishimoto, H., Barnea, G., Kitamoto, T., Axel, R., and Anderson, D.J. (2012). Visualizing neuromodulation in vivo: TANGO-mapping of dopamine signaling reveals appetite control of sugar sensing. Cell *148*, 583-595.

Jenett, A., Rubin, G.M., Ngo, T.T., Shepherd, D., Murphy, C., Dionne, H., Pfeiffer, B.D., Cavallaro, A., Hall, D., Jeter, J.*, et al.* (2012). A GAL4-driver line resource for Drosophila neurobiology. Cell Rep *2*, 991-1001.

Keene, A.C., and Masek, P. (2012). Optogenetic induction of aversive taste memory. Neuroscience *222*, 173-180.

Kohatsu, S., Koganezawa, M., and Yamamoto, D. (2011). Female contact activates male-specific interneurons that trigger stereotypic courtship behavior in Drosophila. Neuron *69*, 498-508.

Lima, S.Q., and Miesenbock, G. (2005). Remote control of behavior through genetically targeted photostimulation of neurons. Cell *121*, 141-152.

Lin J.Y., K.P.M., Muller A., Kleinfeld D. and Tsien R.Y. ReaChR: A red-shifted varinant of channelrhodopsin enables deep transcranial optogenetic excitation.

Luan, H., Peabody, N.C., Vinson, C.R., and White, B.H. (2006). Refined spatial manipulation of neuronal function by combinatorial restriction of transgene expression. Neuron *52*, 425-436.

Luciano, D., and Lore, R. (1975). Aggression and social experience in domesticated rats. J Comp Physiol Psychol *88*, 917-923.

Luo, L., Callaway, E.M., and Svoboda, K. (2008). Genetic dissection of neural circuits. Neuron *57*, 634-660.

Matsumoto, K., Pinna, G., Puia, G., Guidotti, A., and Costa, E. (2005). Social isolation stress-induced aggression in mice: a model to study the pharmacology of neurosteroidogenesis. Stress *8*, 85-93.

Mattis, J., Tye, K.M., Ferenczi, E.A., Ramakrishnan, C., O'Shea, D.J., Prakash, R., Gunaydin, L.A., Hyun, M., Fenno, L.E., Gradinaru, V.*, et al.* (2012). Principles for applying optogenetic tools derived from direct comparative analysis of microbial opsins. Nat Methods *9*, 159-172.

Nagel, G., Brauner, M., Liewald, J.F., Adeishvili, N., Bamberg, E., and Gottschalk, A. (2005). Light activation of channelrhodopsin-2 in excitable cells of Caenorhabditis elegans triggers rapid behavioral responses. Curr Biol *15*, 2279-2284.

Nagel, G., Szellas, T., Huhn, W., Kateriya, S., Adeishvili, N., Berthold, P., Ollig, D., Hegemann, P., and Bamberg, E. (2003). Channelrhodopsin-2, a directly light-gated cation-selective membrane channel. Proc Natl Acad Sci U S A *100*, 13940-13945.

Odden, J.P., Holbrook, S., and Doe, C.Q. (2002). Drosophila HB9 is expressed in a subset of motoneurons and interneurons, where it regulates gene expression and axon pathfinding. J Neurosci *22*, 9143-9149.

Pan, Y., Meissner, G.W., and Baker, B.S. (2012). Joint control of Drosophila male courtship behavior by motion cues and activation of male-specific P1 neurons. Proc Natl Acad Sci U S A *109*, 10065-10070.

Pfeiffer, B.D., Ngo, T.T., Hibbard, K.L., Murphy, C., Jenett, A., Truman, J.W., and Rubin, G.M. (2010). Refinement of tools for targeted gene expression in Drosophila. Genetics *186*, 735-755.

Pulver, S.R., Pashkovski, S.L., Hornstein, N.J., Garrity, P.A., and Griffith, L.C. (2009). Temporal dynamics of neuronal activation by Channelrhodopsin-2 and TRPA1 determine behavioral output in Drosophila larvae. J Neurophysiol *101*, 3075-3088.

Schroll, C., Riemensperger, T., Bucher, D., Ehmer, J., Voller, T., Erbguth, K., Gerber, B., Hendel, T., Nagel, G., Buchner, E.*, et al.* (2006). Light-induced activation of distinct modulatory neurons triggers appetitive or aversive learning in Drosophila larvae. Curr Biol *16*, 1741-1747.

Scott, K., Brady, R., Jr., Cravchik, A., Morozov, P., Rzhetsky, A., Zuker, C., and Axel, R. (2001). A chemosensory gene family encoding candidate gustatory and olfactory receptors in Drosophila. Cell *104*, 661-673.

Stavenga, D.G. (2002). Colour in the eyes of insects. J Comp Physiol A Neuroethol Sens Neural Behav Physiol *188*, 337-348.

Stockinger, P., Kvitsiani, D., Rotkopf, S., Tirian, L., and Dickson, B.J. (2005). Neural circuitry that governs Drosophila male courtship behavior. Cell *121*, 795-807.

Suh, G.S., Ben-Tabou de Leon, S., Tanimoto, H., Fiala, A., Benzer, S., and Anderson, D.J. (2007). Light activation of an innate olfactory avoidance response in Drosophila. Curr Biol *17*, 905-908.

Tayler, T.D., Pacheco, D.A., Hergarden, A.C., Murthy, M., and Anderson, D.J. (2012). A neuropeptide circuit that coordinates sperm transfer and copulation duration in Drosophila. Proc Natl Acad Sci U S A *109*, 20697-20702.

Tian, L., Hires, S.A., Mao, T., Huber, D., Chiappe, M.E., Chalasani, S.H., Petreanu, L., Akerboom, J., McKinney, S.A., Schreiter, E.R.*, et al.* (2009). Imaging neural activity in worms, flies and mice with improved GCaMP calcium indicators. Nat Methods *6*, 875-881.

Ueda, A., and Wu, C.F. (2009). Effects of social isolation on neuromuscular excitability and aggressive behaviors in Drosophila: altered responses by Hk and gsts1, two mutations implicated in redox regulation. J Neurogenet *23*, 378-394.

Venken, K.J., Simpson, J.H., and Bellen, H.J. (2011). Genetic manipulation of genes and cells in the nervous system of the fruit fly. Neuron *72*, 202-230.

von Philipsborn, A.C., Liu, T., Yu, J.Y., Masser, C., Bidaye, S.S., and Dickson, B.J. (2011). Neuronal control of Drosophila courtship song. Neuron *69*, 509-522.

Wang, L., Dankert, H., Perona, P., and Anderson, D.J. (2008). A common genetic target for environmental and heritable influences on aggressiveness in Drosophila. Proc Natl Acad Sci U S A *105*, 5657-5663.

Yamaguchi, S., Desplan, C., and Heisenberg, M. (2010). Contribution of photoreceptor subtypes to spectral wavelength preference in Drosophila. Proc Natl Acad Sci U S A *107*, 5634-5639.

Yizhar, O., Fenno, L.E., Davidson, T.J., Mogri, M., and Deisseroth, K. (2011a). Optogenetics in neural systems. Neuron *71*, 9-34.

Yizhar, O., Fenno, L.E., Prigge, M., Schneider, F., Davidson, T.J., O'Shea, D.J., Sohal, V.S., Goshen, I., Finkelstein, J., Paz, J.T.*, et al.* (2011b). Neocortical excitation/inhibition balance in information processing and social dysfunction. Nature *477*, 171-178.

Yu, J.Y., Kanai, M.I., Demir, E., Jefferis, G.S., and Dickson, B.J. (2010). Cellular organization of the neural circuit that drives Drosophila courtship behavior. Curr Biol *20*, 1602-1614.

Zhang, W., Ge, W., and Wang, Z. (2007). A toolbox for light control of Drosophila behaviors through Channelrhodopsin 2-mediated photoactivation of targeted neurons. Eur J Neurosci *26*, 2405-2416.

Zimmermann, G., Wang, L.P., Vaughan, A.G., Manoli, D.S., Zhang, F., Deisseroth, K., Baker, B.S., and Scott, M.P. (2009). Manipulation of an innate escape response in Drosophila: photoexcitation of acj6 neurons induces the escape response. PLoS One *4*, e5100.

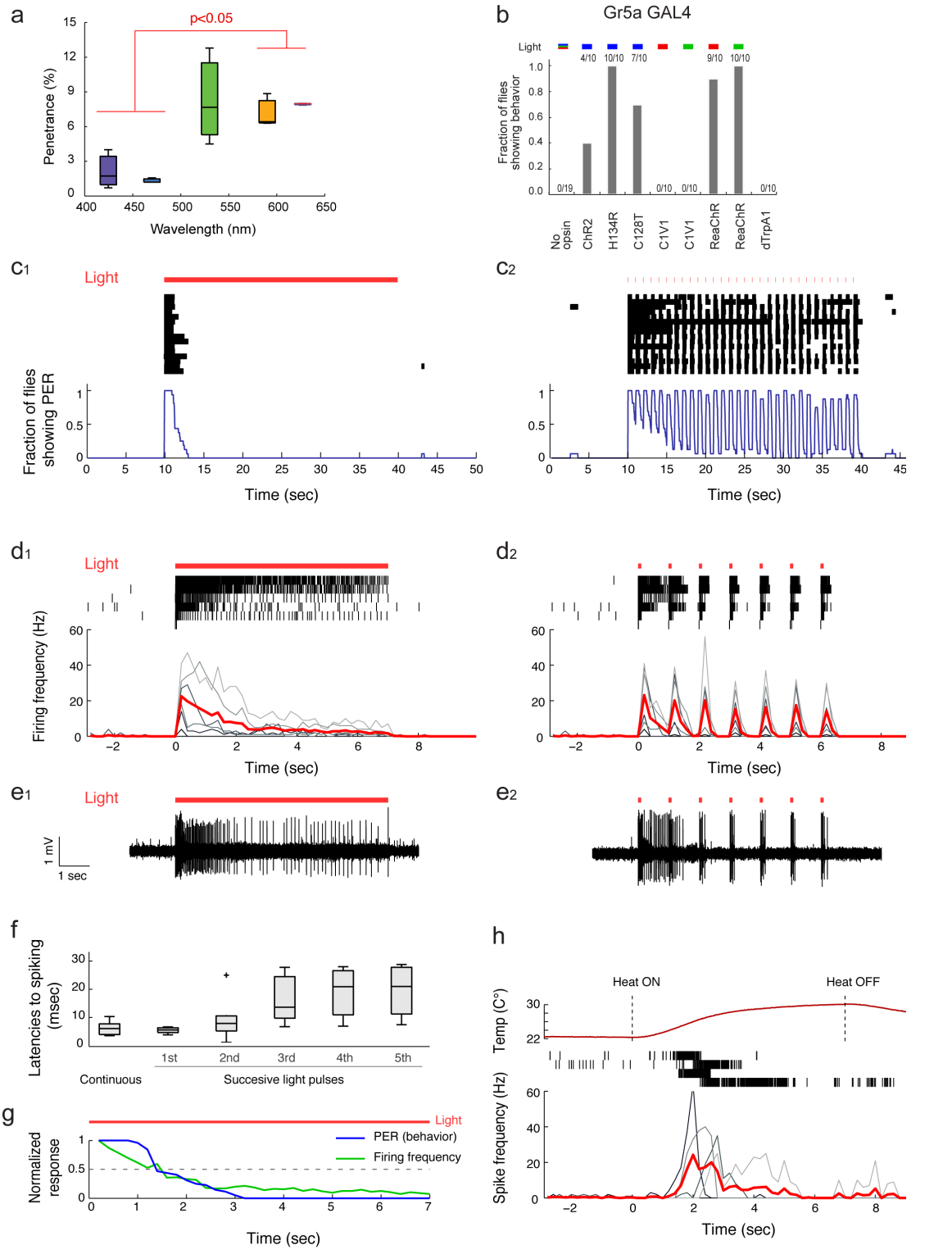
a
p<0.05
Penetrance (%)
Wavelength (nm)
b
Gr5a GAL4
Light
Fraction of flies showing behavior
No opsin
ChR2
H134R
C128T
C1V1
C1V1
ReaChR
ReaChR
dTrpA1
c1
Light
Fraction of flies showing PER
Time (sec)
c2
Time (sec)
d1
Light
Firing frequency (Hz)
Time (sec)
d2
Time (sec)
e1
Light
1 mV
1 sec
e2
f
Latencies to spiking (msec)
1st
2nd
3rd
4th
5th
Continuous
Succesive light pulses
g
Light
PER (behavior)
Firing frequency
Normalized response
Time (sec)
h
Heat ON
Heat OFF
Temp (C°)
Spike frequency (Hz)
Time (sec)

Figure. 1

Figure 1 Optogenetic vs. thermogenetic control of Gr5a GRNs.

(a) Penetrance of light through the cuticle of adult *Drosophila*. n=3. p-value represents one-way ANOVA (p=0.0046) followed by t-test with Bonferroni correction (b) Comparison of fraction of flies showing PER triggered by different opsins expressed in Gr5a GRNs (Gr5a-Gal4; *UAS-opsins*). Fractions at top indicate number of responders/number of flies tested. Activation wavelengths are represented as blue (470 nm), green (530 nm), red (627 nm) bars. (c-e) Behavioral (c) and electrophysiological (d, e) responses of flies expressing ReaChR in Gr5a GRNs. Red lines (c-e): photostimulation pattern (627 nm, 1.1 mW/mm^2); pulsed photostimulation (c_2-e_2) was delivered at 1 Hz, with a 100 msec pulse width; photostimulation in (c_1-e_1) was continuous. Raster plots (c): PER bouts. Blue curves (c): Fraction of flies showing PER (time bins: 1sec; n=16). Raster plots (d): Gr5a GRNs spikes. Lower plots: Average spiking rate (red lines) based on raster plots; spiking rates for individual flies are overlaid (gray lines; time bins: 200 msec; n=6). (e) Sample traces from electrophysiological recordings. (f) Latencies to first spike following photostimulation onset, from (d_1) and (d_2). Boxplots: lower and upper whiskers represent 1.5 inter-quartile range of the lower and upper quartiles, respectively; boxes indicate lower quartile, median, and upper quartile, from bottom to top. (g) Overlay of normalized PER responses and firing frequencies during continuous photostimulation (red line) based on data in (c_1) and (d_1). (h) Top row: Measured temperature change caused by a heat source placed near the labellum. Middle row: Raster plots representing spikes in Gr5a GRNs expressing dTrpA1. Bottom row: spiking responses plotted as in (d). n=4.

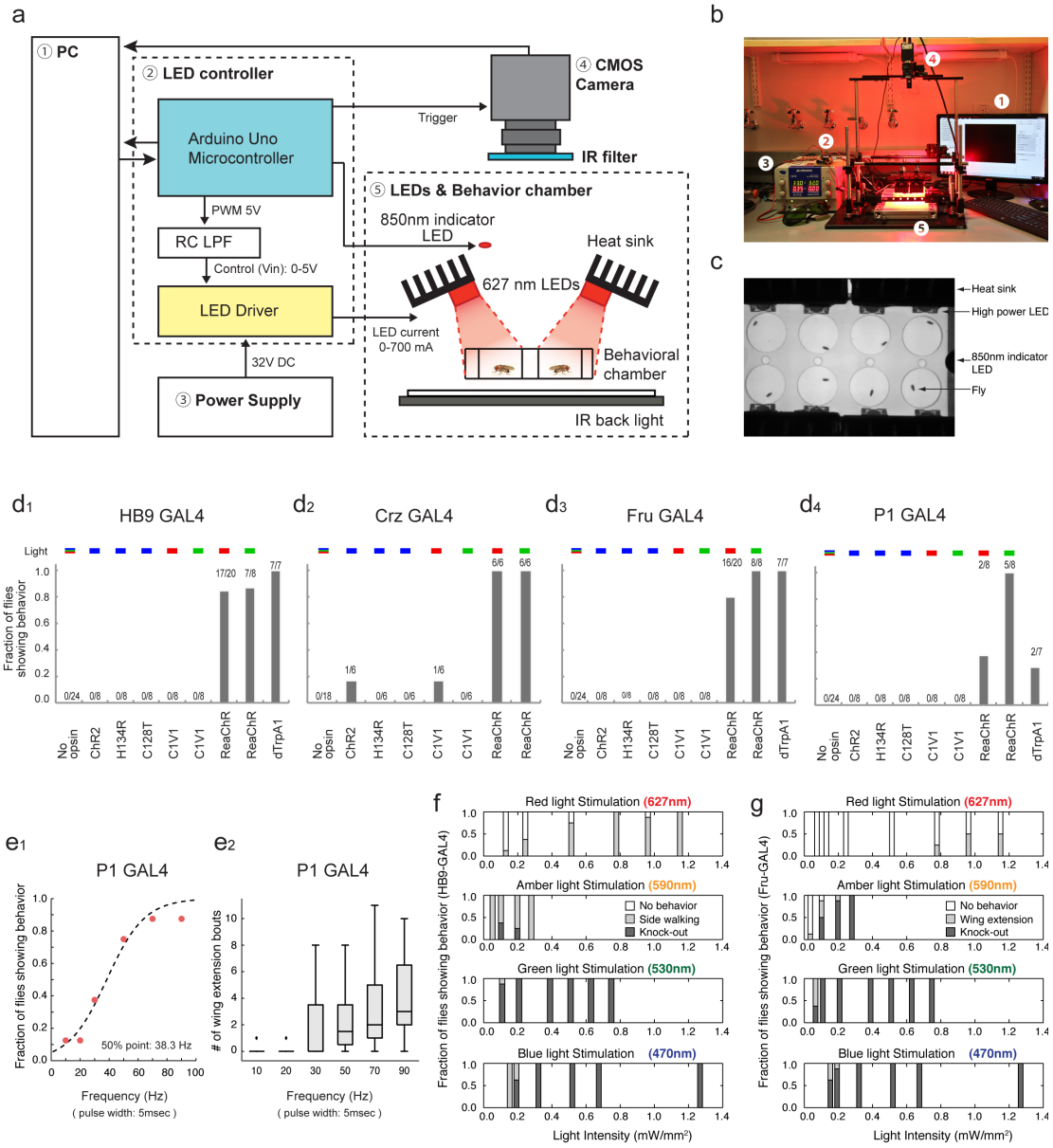
a
① PC
② LED controller
Arduino Uno Microcontroller
PWM 5V
RC LPF
Control (Vin): 0-5V
LED Driver
32V DC
③ Power Supply
④ CMOS Camera
Trigger
IR filter
⑤ LEDs & Behavior chamber
850nm indicator LED
Heat sink
627 nm LEDs
LED current 0-700 mA
Behavioral chamber
IR back light
b
c
Heat sink
High power LED
850nm indicator LED
Fly
d1 HB9 GAL4
d2 Crz GAL4
d3 Fru GAL4
d4 P1 GAL4
Light
Fraction of flies showing behavior
No opsin
ChR2
H134R
C128T
C1V1
C1V1
ReaChR
ReaChR
dTrpA1
e1 P1 GAL4
Fraction of flies showing behavior
50% point: 38.3 Hz
Frequency (Hz)
(pulse width: 5msec)
e2 P1 GAL4
# of wing extension bouts
Frequency (Hz)
(pulse width: 5msec)
f
Red light Stimulation (627nm)
Amber light Stimulation (590nm)
Green light Stimulation (530nm)
Blue light Stimulation (470nm)
No behavior
Side walking
Knock-out
Fraction of flies showing behavior (HB9-GAL4)
Light Intensity (mW/mm²)
g
Red light Stimulation (627nm)
Amber light Stimulation (590nm)
Green light Stimulation (530nm)
Blue light Stimulation (470nm)
No behavior
Wing extension
Knock-out
Fraction of flies showing behavior (Fru-GAL4)
Light Intensity (mW/mm²)

Figure. 2

Figure 2 ReaChR enables light-dependent activation of the CNS neurons in *Drosophila*.

(a-b) Experimental setup for high power LED-based activation system. Each number in the diagram (a) corresponds to a number in the photograph (b). See supplementary fig.1 and table 2 for detail. (c) View from the CMOS camera. (d) Comparison of behavioral responses of flies expressing different channelrhodopsin variants in distinct CNS subpopulations. Plot properties as in Fig. 1b. "Fraction of flies showing behavior" indicates: (d_1) side walking or knock-out phenotype; (d_2) ejaculation; (d_3) wing extension or knock-out; or (d_4) wing extension, and was quantified for each GAL4 line. No opsin: empty promoter GAL4 (BFP-GAL4. See methods) crossed with *UAS-ReaChR*. Flies showing any of the characteristic behaviors during 1 min of continuous photostimulation were scored as responders. (e) ReaChR-mediated activation of P1 neurons using different frequencies of red light pulses (627 nm, 1.1 mW/mm^2, 1 min) (P1-GAL4; *UAS-ReaChR* (attP40)). The fraction of flies showing wing extension during 1 min photostimulation trials was fitted by a sigmoidal function to calculate the 50% point (e_1). n=8. (f-g) Fraction of flies exhibiting characteristic behaviors at different photostimulation intensities and wavelengths, in animals expressing HB9 GAL4 (f) or Fru GAL4 (g), and *UAS-ReaChR*. n=8.

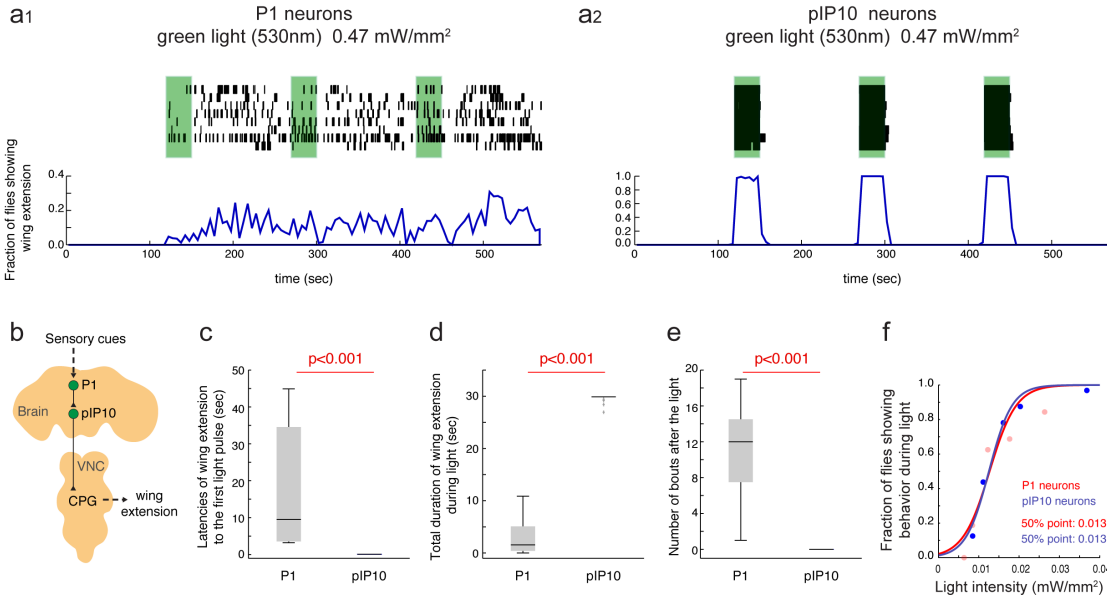
a1
P1 neurons
green light (530nm) 0.47 mW/mm2
Fraction of flies showing wing extension
time (sec)
a2
pIP10 neurons
green light (530nm) 0.47 mW/mm2
time (sec)
b
Sensory cues
P1
Brain
pIP10
VNC
CPG
wing extension
c
p<0.001
Latencies of wing extension to the first light pulse (sec)
P1
pIP10
d
p<0.001
Total duration of wing extension during light (sec)
P1
pIP10
e
p<0.001
Number of bouts after the light
P1
pIP10
f
Fraction of flies showing behavior during light
P1 neurons
pIP10 neurons
50% point: 0.013
50% point: 0.013
Light intensity (mW/mm2)

Figure. 3

Figure 3 Probabilistic vs. deterministic optogenetic control of courtship song.

(a) Activation of P1 neurons (P1-Gal4; *UAS-ReaChR*(VK5)) (a_1) and pIP10 neurons (VT40556/*UAS>stop>ReaChR* (attP40); *fru*-FLP) (a_2) with green light (530 nm, 0.47 mW/mm^2). Top: Raster plot representing wing extension bouts (n=8 flies per genotype). Green bars represent 30 sec continuous photostimulation trials with 120 sec inter-trial intervals. Bottom: Fraction of flies showing wing extension (time bins: 5 sec). Note different y-axis scales in (a_1) and (a_2). P1 responses during trials 2 and 3 are more clearly phased to the onset of photostimulation at lower light intensities (Supplementary fig. 3a1). (b) Schematic illustrating neuronal circuit control of courtship song, simplified from ref (von Philipsborn et al., 2011). (c) Latency to first wing extension after onset of the first photostimulation. (d) Total duration of wing extension during photostimulation. (e) Number of wing extension bouts during 30 sec following photostimulation offset. Plots in (c-e) are based on data in (a_1) and (a_2). p-values represent Mann-Whitney U tests. (f) Fraction of flies showing wing extension during a single photostimulation trial as a function of light intensity (green light: 530 nm, continuous, 30 sec). The data were fitted by a sigmoidal function to calculate the 50% point. n=32 for both P1 neurons, and pIP10 neurons.

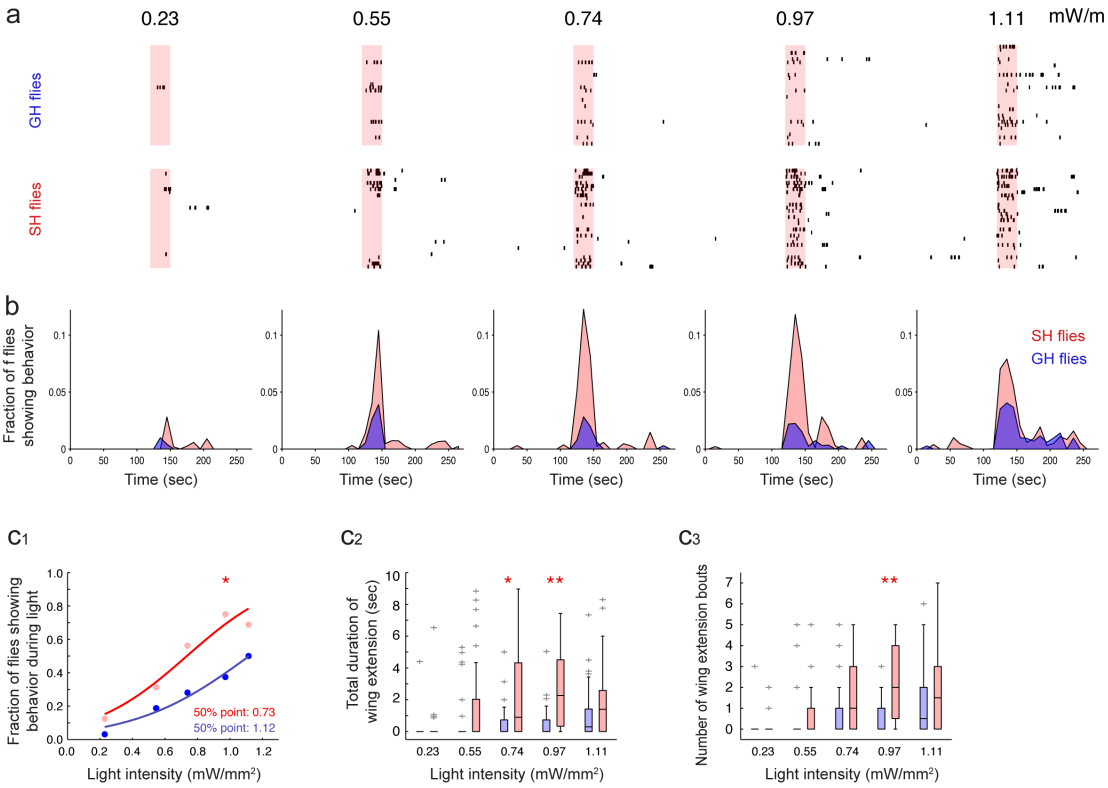
a
0.23
0.55
0.74
0.97
1.11
mW/m
GH flies
SH flies
b
Fraction of f flies showing behavior
Time (sec)
SH flies
GH flies
c1
Fraction of flies showing behavior during light
50% point: 0.73
50% point: 1.12
Light intensity (mW/mm²)
c2
Total duration of wing extension (sec)
Light intensity (mW/mm²)
c3
Number of wing extension bouts
Light intensity (mW/mm²)

Figure. 4

Figure 4 Social isolation lowers the threshold for ReaChR-activated male courtship behavior.

(a) Raster plots representing wing extension bouts from group-housed (GH: top row) or single-housed (SH: bottom row) flies expressing ReaChR in P1 neurons (P1-GAL4/ *UAS-ReaChR* (VK5)). Flies were activated with different intensities of red light (627 nm). Light red bars in raster plots indicate photostimulation trials (30 sec continuous light), with different intensities indicated above the bars. n=32 flies per intensity. (b) Fraction of flies showing wing extension based on the raster plots in (a). Data was binned every 10 sec. Time scale is the same in (a) and (b). In this and in Fig. 5, red or blue points/traces/boxplots represent data from single-housed or group-housed flies, respectively. (c_{1-3}) Different parameters were extracted from the raster plots in (a). Properties of boxplots in this and in Fig. 5 are as in Fig. 1f; "+" indicates outlier data bigger than the upper whisker. *:$p<0.05$; **:$p<0.005$. p-values in (c_1) represent Friedman's test comparing SH vs. GH ($p=6.3 \times 10^{-28}$) followed by Fisher's exact test with Bonferroni correction comparing SH vs. GH at each intensity of light. p-values in (c_{2-3}) represent Krusukal-Wallis one-way ANOVA followed by Mann-Whitney U tests with Bonferroni correction. P-values for Krusukal-Wallis one-way ANOVA: (c_2) $p=6.4 \times 10^{-11}$; (c_3) $p=8.2 \times 10^{-12}$.

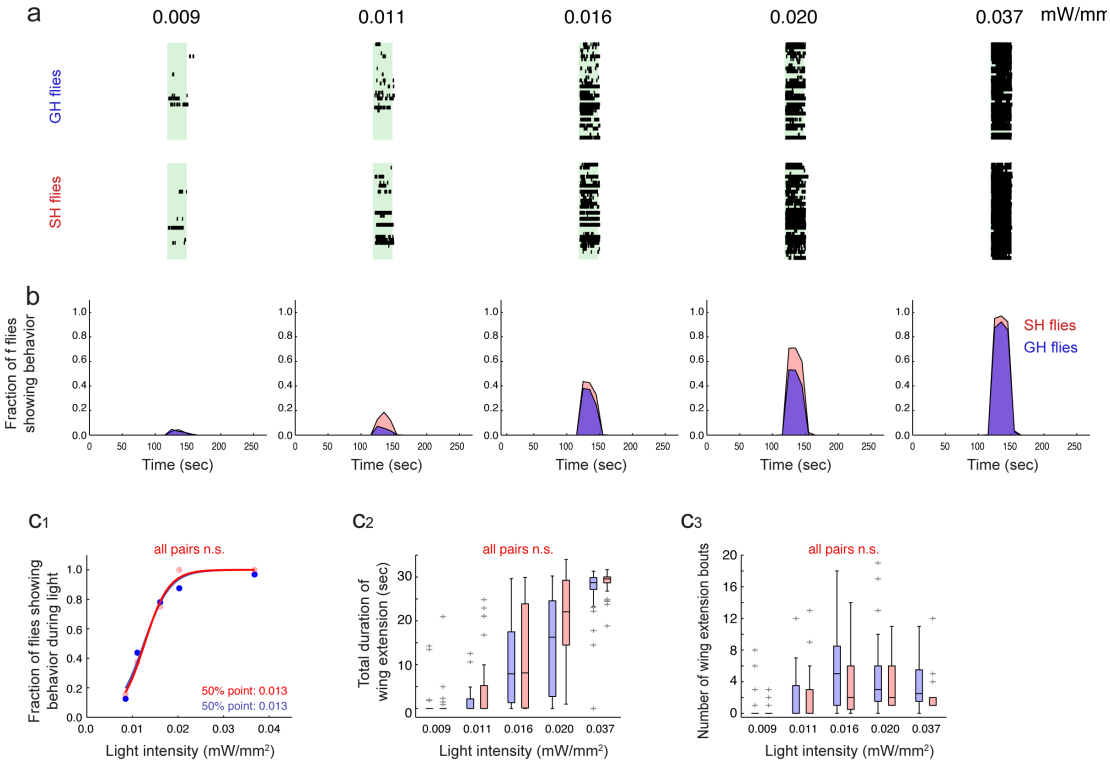
a
0.009
0.011
0.016
0.020
0.037 mW/mm
GH flies
SH flies
b
Fraction of f flies showing behavior
Time (sec)
SH flies
GH flies
c1
all pairs n.s.
Fraction of flies showing behavior during light
50% point: 0.013
50% point: 0.013
Light intensity (mW/mm²)
c2
all pairs n.s.
Total duration of wing extension (sec)
Light intensity (mW/mm²)
c3
all pairs n.s.
Number of wing extension bouts
Light intensity (mW/mm²)

Figure. 5

Figure 5 Optogenetic activation of pIP10 neurons is not modulated by social isolation.

(a) Raster plot representing wing extension bouts from group-housed (GH: top row) or single-housed (SH: bottom row) flies expressing ReaChR in pIP10 neurons (VT40556-GAL4^{24}/ *UAS>stop>ReaChR*(attP40); *fru*-FLP). Flies were activated with different intensities of green light (530 nm). Green bars indicate photostimulation trials (30sec continuous light), with different intensities indicated above the bars. n=32 flies per intensity. (b) Fraction of flies showing wing extension based on the raster plot in (a). Time scale is the same in (a) and (b). ($c_{1\text{-}3}$) Different parameters extracted from the raster plots in (a). The GH data in (c_1) (blue points) are the same as those used in Fig. 3f, and are replotted here for purposes of comparison. (c_1) Friedman's test comparing SH vs. GH followed by Fisher's exact test with Bonferroni correction comparing SH vs. GH at each light intensity. ($c_{2\text{-}3}$) Krusukal-Wallis one-way ANOVA followed by Mann-Whitney U tests with Bonferroni correction. All statistical tests yielded p-values > 0.05.

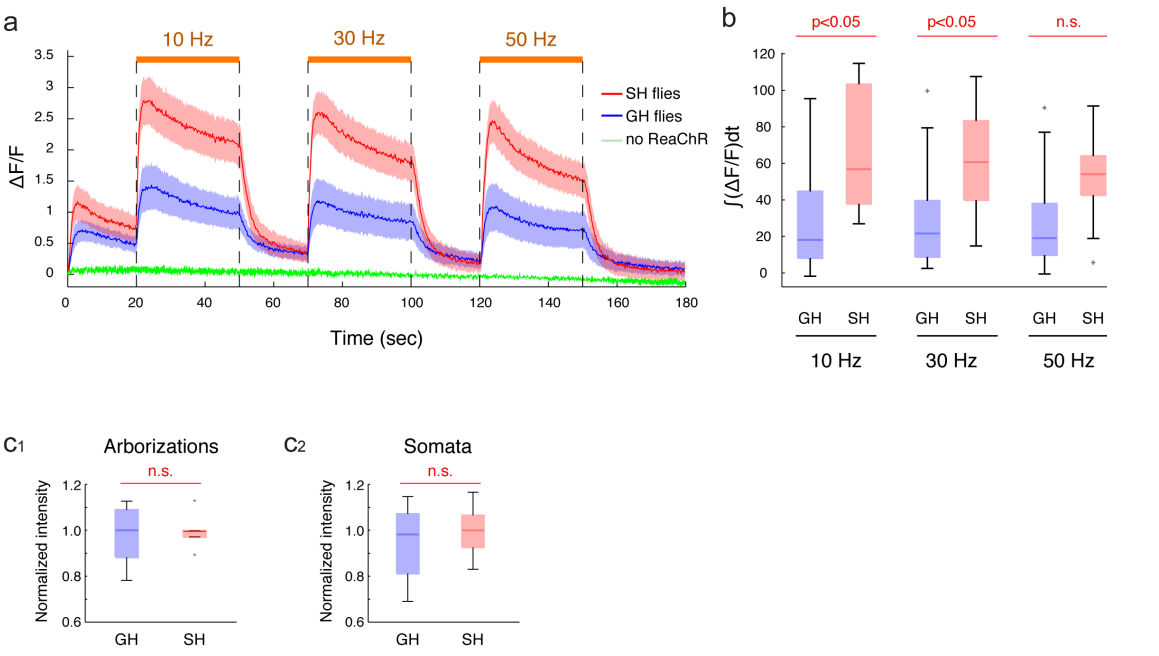

Figure. 6

Figure 6 Functional calcium imaging of P1 neurons.

(a) Responses of P1 neurons (ΔF/F) to ReaChR activation were monitored using 2-photon LSM. Flies expressing both ReaChR and GCaMP3 in P1 neurons (P1-GAL4/ *UAS-ReaChR*(attP40); *UAS-GCaMP3*(VK5)) were single-housed (SH: red line) or group-housed (GH: blue line) and imaged (n>10 brains for each curve). Amber light (590 nm, 1.7 mw/mm^2) with a 5 msec pulse-width was delivered at the indicated frequencies in 30 sec consecutive trials (ornge lines above traces). GCaMP3.0 emissions were monitored in the arborizations of P1 neurons. Flies expressing GCaMP3.0 but not ReaChR in P1 neurons (P1-GAL4; *UAS-GCaMP3*(VK5)) were used as negative controls (green line) (n=3). Solid red and blue lines represent average traces, and envelopes indicate SEMs. (b) Quantification of fluorescent changes. ∫ΔF/Fdt, integrated ΔF/F during 30 sec of light activation. Data were analyzed from (a). (c) Expression level of ReaChR at the arborizations and somata of P1 neurons were quantified using a citrine tag fused to the C-terminus of ReaChR. P-values represent Mann-Whitney U tests with Bonferroni correction.

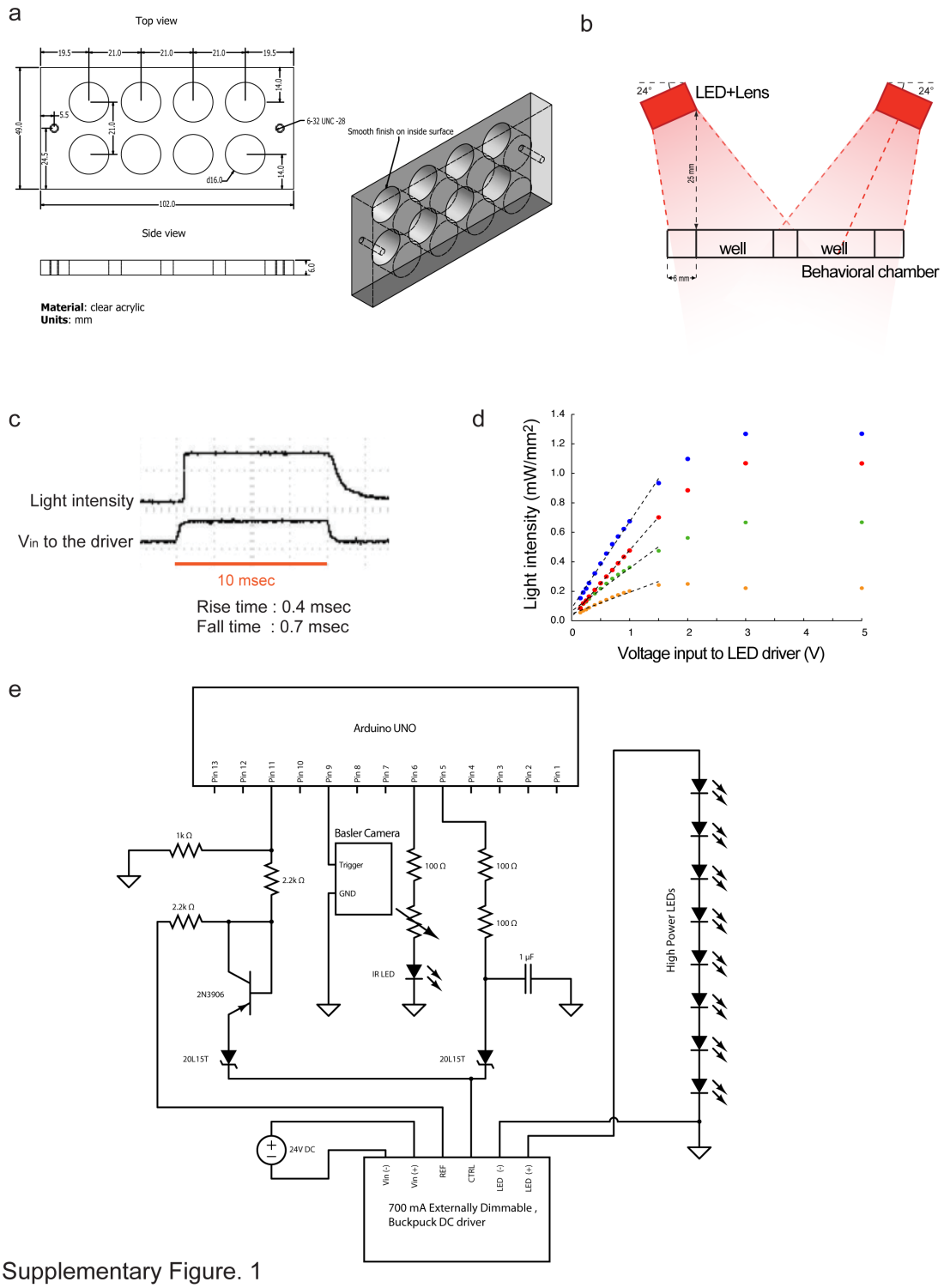

Supplementary Figure. 1

Supplementary Figure 1 | Detail of the behavioral experimental setup.

(a) Design of the behavioral chamber. A top plate with holes to introduce flies into the chambers, and a bottom plate, are attached with screws to the behavioral chamber. (b) Alignment of LEDs with the behavioral chamber. Light beams are angled towards the center of the behavioral wells. Each LED delivers light to each well. (c) Light intensity of the LED and voltage input from the Arduino UNO board (Smart Projects, Italy) to the LED driver were simultaneously monitored. Start-up delay of LED is 0.4 msec and turn-off delay of LED is approximately 0.7 msec. (d) Relationship of light intensity inside the behavioral chamber and voltage input to the LED driver. Points with different color represent LEDs of different wavelengths (Red: 627 nm, Amber: 590 nm, Green: 530 nm, Blue: 470 nm). Dotted lines indicate linear dynamic ranges for each type of LED. (e) Electric circuit diagram for the LED controller. This circuit was built on a custom Arduino shield. With the Arduino program, this electric circuit controls high power LEDs. Intensity, pulse width, pulse frequency, length of pulse train, and the number of and interval between repeated pulse trains are controllable for up to 8 × 700mA LEDs in parallel.

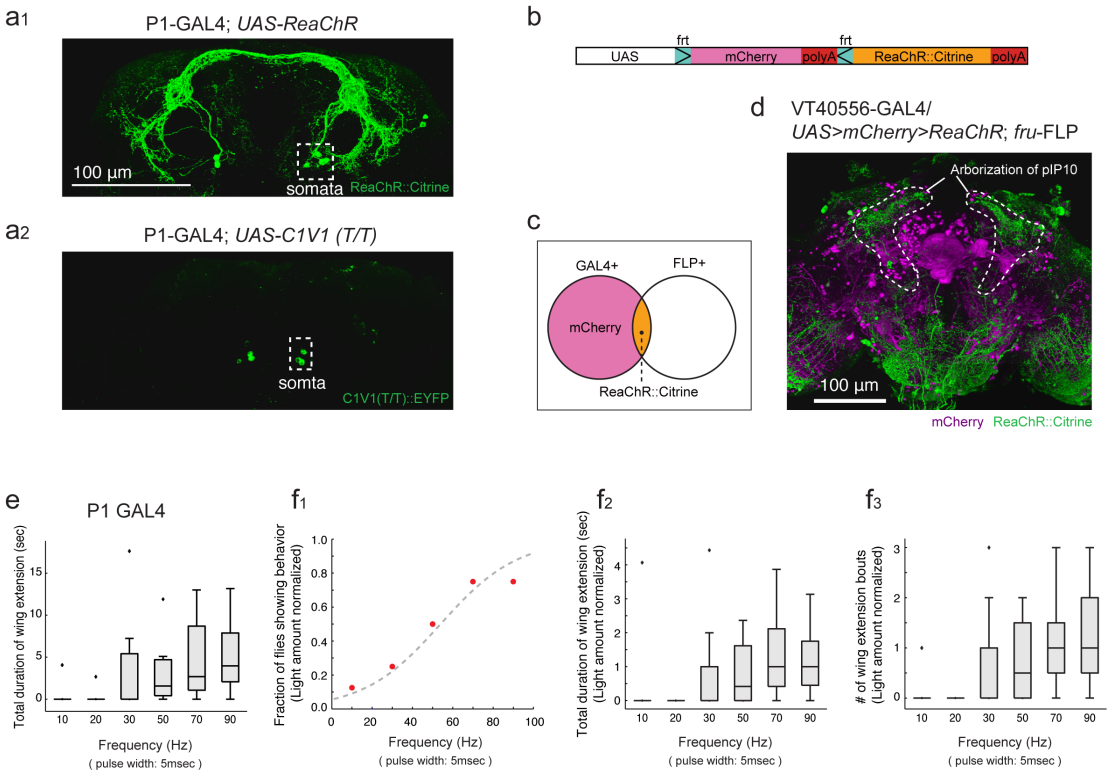

Supplementary Figure. 2

Supplementary Figure 2 | Expression of ReaChR in the brain and ReaChR-based activation of behaviors with different frequencies. (a) Expression and trafficking of ReaChR (a1) and C1V1(T/T) (a2) in P1 neurons in adult flies. Note that both opsins are expressed at cell somata (box with a white dotted line), but only ReaChR is trafficked to the arborizations. Both of the opsins are visualized with a citrine or YFP tag immunostained with anti-GFP antibody. (b) Design of the *UAS-frt-mCherry-frt-ReaChR* transgene (Note that ReaChR is tagged with citrine). (c) Diagram representing the intersectional approach for labeling pIP10 neurons. (d) Representative confocal projection of whole-mount brain from VT40556 (GAL4) / *UAS-frt-mCherry-frt-ReaChR* (*UAS>stop>ReaChR*) (attP40); *fru*-FLP flies. (e) Relationship between pulse stimulation frequencies and total duration of UWEs in flies expressing ReaChR in P1 neurons (P1-GAL4; *UAS-ReaChR* (VK5)). Parameters are extracted from the same data used for Fig. 2e. Boxplot properties are as in Fig.2. (f) Relationships of frequencies of light pulses and behavior in flies expressing ReaChR in P1 neurons, after normalization for the total amount of light delivered at different frequencies. For normalization purpose, behaviors during different durations of light activation were counted (first 60, 30, 20, 12, 8.57, and 6.67 sec during the activation for 10, 20, 30, 50, 70, 90 Hz, respectively). Parameters are extracted from the same data used for Fig. 2e. Boxplot properties are as in Fig. 2.

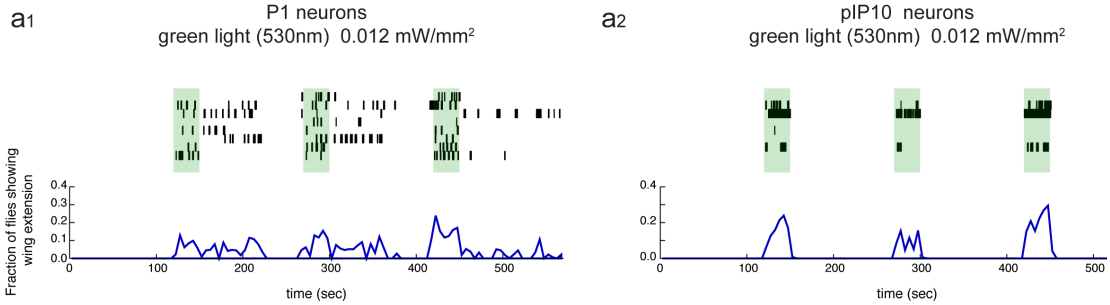

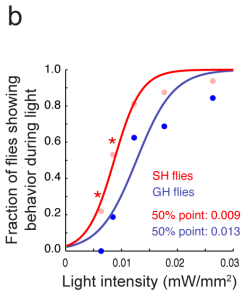

Supplementary Figure. 3

Supplementary Figure 3| ReaChR- based activation of P1 neurons.

Activation of P1 neurons (P1-Gal4; *UAS-ReaChR*(VK5) (a_1) and pIP10 neurons (VT40556/*UAS>stop>ReaChR* (attP40); *fru*-FLP) (a_2) with green light (530 nm, 0.012 mW/mm^2). Top: Raster plot representing wing extension bouts (n=8 flies per genotype). Green bars represent 60 sec continuous photostimulation with 300 sec inter-trial intervals. Bottom: Fraction of flies showing wing extension (time bins: 5 sec). Note that regardless of photostimulation conditons (see also Fig. 3,4), ReaChR-based activation of P1 neurons triggers stochastic and persistent wing extensions. (b) Fraction of P1-Gal4; *UAS-ReaChR*(VK5) flies showing wing extension during a single photostimulation trial as a function of light intensity (green light: 530 nm, continuous, 30 sec). The data were fitted by a sigmoidal function to calculate the 50% point. n=32 for each intensity. (blue points) are the same as red point used in Fig. 3f, and are replotted here for purposes of comparison *: $p<0.05$. p-values represent Friedman's test comparing SH vs. GH ($p=0.02$) followed by Fisher's exact test with Bonferroni correction comparing SH vs. GH at each intensity of light.

Supplementary Table 1 | List of transgenic flies created for this paper

#	Name	Opsin	tag	plasmid	attP landing site
1	UAS-ReaChR	ReaChR	Citrine	pJFRC2 (10x UAS with IVS)	attP40 (II)
2	UAS-ReaChR	ReaChR	Citrine	pJFRC2 (10x UAS with IVS)	attP5 (II)
3	UAS-ReaChR	ReaChR	Citrine	pJFRC2 (10x UAS with IVS)	VK5 (III)
4	LexAop-ReaChR	ReaChR	Citrine	pJFRC19 (10x LexAop with IVS)	attP40 (II)
5	LexAop-ReaChR	ReaChR	Citrine	pJFRC19 (10x LexAop with IVS)	attP5 (II)
6	LexAop-ReaChR	ReaChR	Citrine	pJFRC19 (10x LexAop with IVS)	VK5 (III)
7	UAS-frt-mCherry-frt-ReaChR	ReaChR	Citrine	pJFRC2 (10x UAS with IVS) with frt cassette	attP5 (II)
8	UAS-frt-mCherry-frt-ReaChR	ReaChR	Citrine	pJFRC2 (10x UAS with IVS) with frt cassette (	VK5 (III)
9	LexAop-frt-mCherry-frt-ReaChR	ReaChR	Citrine	pJFRC19 (10x LexAop with IVS) with frt cassette	attP5 (II)
10	LexAop-frt-mCherry-frt-ReaChR	ReaChR	Citrine	pJFRC19 (10x LexAop with IVS) with frt cassette	VK5 (III)
11	UAS-C1V1	C1V1 (T/T)	EYFP	pJFRC2 (10x UAS with IVS)	attP5 (II)
12	UAS-C1V1	C1V1 (T/T)	EYFP	pJFRC2 (10x UAS with IVS)	VK5 (III)
13	LexAop-C1V1	C1V1 (T/T)	EYFP	pJFRC19 (10x LexAop with IVS)	attP5 (II)
14	LexAop-C1V1	C1V1 (T/T)	EYFP	pJFRC19 (10x LexAop with IVS)	VK5 (III)

#	Name	X	II	III
15	UAS-frt-mCherry-frt-ReaChR ; *fru*-flp	w-	UAS-frt-mCherry-frt-ReaChR (attP5)	*fru*-flp
16	UAS-ReaChR; UAS-GCaMP3	w-	UAS-ReaChR (attP40)	UAS-GCaMP3 (VK5)

Supplementary Table 2 | List of materials to build LED-based high-throughput screening system
This list is provided for the convenience of readers who wish to build similar setups. We are listing the company and product names that we used, but alternatives may be used.

#	Category	Number	Note (company, ordering info, etc.)
	Camera related (①,④&⑤ in Fig. 2a,b)		
1	**Camera**	1	We used Basler A622FM 2/3" CMOS FireWire.A Monchrome Camera (640 x 480 pixels up to 100 fps) (Basler Inc. Exton, PA USA. http://www.baslerweb.com/).
2	**Lens for camera**	1	Varifocal Video Lens 12mm - 36mm 1:2.8 Focal Length 2/3" C mount (compar) (Edmund Optics, Barrington, NJ 08007-1380 USA, http://www.edmundoptics.com/)
3	**IR filter**	1	A long-pass filter on the lens of the camera to remove the light from high power LEDs. We used longpass filter (pass wavelengths longer than 780nm). LP780-M40.5 (Midwest Optical Systems, Inc. Palatine, IL USA. http://www.midopt.com/)
4	**IR backlight**	1	Backlight to visualize flies in behavioral chamber. We used SOBL-200-150-IR 850nm(Smart Vision Lights. Muskegon, MI, USA. http://smartvisionlights.com/)
5	**PC**	1	
6	**Software and driver to record movies from the camera**	1	We used CMU 1394 Dedgital camera driver (http://www.cs.cmu.edu/~iwan/1394/index.html) with gVision (http://gvision-hhmi.sourceforge.net/) or a custom made Matlab software (Mathworks).
7	**Bread board, optical, posts and connectors to assemble the behavioral rig**	N.A.	Acquired from Thorlab, Inc (Newton, New Jersey, USA. http://www.thorlabs.com/index.cfm).
	LED related and its controller (②,③&⑤ in Fig. 1a&b)		
8	**High power LED (blue)**	8	Blue (470 nm) Rebel LED, mounted on a 10 mm square cool base- 70 lm @ 700mA (LUXEON® STAR LEDs: SR-05-B0040). Spectral half-width (spectral width at ½ of the peak intensity) is 20nm. (8-15 are acquired from Quadica Developments Inc.

			Ontario N3T 5L7 Canada. http://www.luxeonstar.com/default.asp)
9	**High power LED (green)**	8	Green (530 nm) Rebel LED, mounted on a 10 mm square cool base- 161 lm @ 700 mA (LUXEON® STAR LEDs: SR-05-M0100). Spectral Half-width is 30nm.
10	**High power LED (amber)**	8	Amber (590 nm) Rebel LED, mounted on a 10 mm square cool base- 77 lm@ 700mA (LUXEON® STAR LEDs: SR-05-L0040). Spectral Half-width is 20nm.
11	**High power LED (red)**	8	Red (627 nm) Rebel LED, mounted on a 10 mm square cool base- 102 lm @ 700 mA (LUXEON® STAR LEDs: SR-05-D2050) Spectral Half-width is 20nm.
12	**Optics for LEDs**	32	All of the LEDs were used with optics. 29.8° 10mm Frosted optic with integrated mounting legs (Carclo)
13	**Heat conductive seal**	32	To seal LEDs to the heat sink (LUXEON® STAR LEDs: LXT-R-10)
14	**Heat sink for LEDs**	16	All the LEDs were attached to heat sinks to avoid overheat (LUXEON® STAR LEDs: N50-25B)
15	**LED driver**	1	700 mAExternally dimmable, Buckpuck DC driver with leads (LUXEON® STAR LEDs: 3023-D-E-700)
16	**Power supply**	1	Any power driver that is capable of supplying 700mA 32V DC.
17	**850nm indicator LED**	1	Because IR filter filters out the light from high power LEDs, the only way to know when the light is on is information from the LED controller. We placed one IR LED whose on/off is synchronized to the high power LED so that we can easily tell when LEDs are on in the movie.
18	**Arduino Uno**	1	Microcontroller to control camera and LEDs (Smart Projects, Italy. http://www.arduino.cc/)
19	**Electric parts to build an Arduino shield to control the LEDs**	N.A.	See Supplementary fig. 1e for the circuit designs and parts.
20	**Code to control Arduino UNO board**	1	
21	**Behavioral chamber**		The design of the chamber and the alignment of chamber and LEDs are described in Supplementary Fig. 1a,b. Any kind of chamber can be used but it is necessary to measure light intensity and to make sure uniform illumination.

Supplementary Table 3 | Summary of properties of courtship controlling neuron

	P1 neuron	pIP10 neuron
Probability of response	Stochastic	Deterministic
Timing of response	variable onset/offset	Time-locked to stimulus onset/offset
Modulation by social state	Yes	No
Class of neuron	State control / Biasing neuron	Command neuron

METHODS

Construction of transgenic animals

Plasmids were constructed by standard DNA cloning and PCR methods. All PCR reactions were performed using PrimeStar® HS DNA polymerase (Takara). Following amplification all sequences were verified by DNA sequencing.

UAS-ChR2(H134R)::EYFP-2A-ChR2(H134R)::EYFP

A DNA fragment containing the ChR2(H134R) coding sequence kindly provided by Dr. Karl Deisseroth was amplified by PCR and subcloned into pUAST vector in a tandem manner with an intervening F2A sequence[12] (Donnelly et al., 2001). Several transgenic flies were created with different insertion sites. We picked the line that exhibited the strongest induction of PER when crossed to Gr5a-GAL4.

UAS-C1V1(T/T)

A DNA fragment containing the coding sequence of C1V1(E122T/E162T)-TS-eYFP kindly provided by Dr. Karl Deisseroth was amplified by PCR and subcloned into the vector pJFRC2[29]. This vector was injected and integrated into attP40 and VK5 sites[29].

UAS-ReaChR, LexAop-ReaChR, UAS-frt-mCherry-frt-ReaChR, and LexAop-frt-mCherry-frt-ReaChR

A DNA fragment containing the ReaChR::citrine coding sequence was amplified by PCR and subcloned into pJFRC2 and pJFRC19[29] for UAS-, and LexAop-driven versions, respectively. For the version containing an frt-mcherry-stop-frt cassette, the frt sequences (GAAGTTCCTATTCTCTAGAAAGTATAGGAACTTC) and ReaChR DNA fragments were subcloned into pJFRC2 and pJFRC19 using SLIC cloning (Li and Elledge, 2007). These vectors were injected and integrated into attP40, attP5 and VK5 sites[29].

Fly strains

UAS-ChR2[5], UAS-dTrpA1[15], UAS-GCaMP3.0[43], Gr5a-GAL4[18], and BDP-GAL4 (Pfeiffer et al., 2008) (empty promoter Gal4: an enhancer-less GAL4 containing a *Drosophila* basal promoter) were generously

provided by Dr. André Fiala, Dr. Paul A. Garrity, Dr. Loren L. Looger, Dr. Kristin Scott and Dr. Gerald M. Rubin, respectively. Fru-GAL4[26], Fru-flp[37] and VT40556 GAL4[27] were kindly provided by Dr. Barry J. Dickson. HB9-gal4 was obtained from Bloomington Stock Center (BL #32555). Crz-Gal4[25] and UAS-C128T[12] were previously created in the lab. All the transgenic flies created for this paper are summarized in supplementary table 1. These flies are available on request.

All experimental flies were maintained on a 12/12 hour day-night cycle. Newly eclosed male flies were CO2 anesthetized and allowed to recover for more than 3-7 days prior to behavioral tests at 25°C. For dTrpA1 experiments, flies were raised at 18°C. For experiments with Gr5a-GAL4, female flies were used, and for all the other experiments male flies were used.

Feeding of retinal

All *trans*-retinal powder (Sigma) was stored in -20°C as a 40 mM stock solution dissolved in DMSO (x100). 400 μl of sugar-retinal solution (400 μM all *trans*-retinal diluted in 89mM sucrose) was directly added to surface of solid food in food vials when larvae were at the first or second instar stage. After collecting newly eclosed flies, they were transferred into a vial containing food with 400 μM all *trans*-retinal (food was heated and liquefied to mix the retinal evenly in the food).

Behavioral setup

See supplementary table 2 for a list of components used to assemble the behavioral setup. See supplementary figure 1 for details of the setup and the behavioral chamber. In brief, high power LEDs mounted on heat sinks were placed above the behavioral chamber to provide an illumination source (Fig. 2a and Supplementary fig 1a,b). The range of available light intensities in our setup is approximately 0.001 -1 mW/mm^2 (note that intensity ranges are different for different LEDs; see Supplementary fig 1d). LED units were designed to be switchable to facilitate testing of different photostimulation wavelengths. The LEDs were controlled by an externally dimmable LED driver (700 mA; Externally dimmable, Buckpuck DC driver with leads) and its output was adjusted using custom software controlling an Arduino UNO board (Smart Projects, Italy). The Arduino digital PWM output was converted into analogue voltage using an RC-filter (electronic low-pass

filter composed of resistor and capacitor. RC LPF in Fig. 2a) containing a 200 Ω resistor and 1 μF capacitor to control the output current of the LED driver. Fly behavior was monitored using a CMOS camera equipped with an IR long-pass filter to avoid detection of light from the high power LEDs. IR back-light was used to visualize the behaving flies. Video capture and LED control were time-locked using the Arduino UNO board. To time-stamp photostimulation trials in the videos, we placed an IR indicator LED, whose illumination was synchronized to that of the photostimulation LEDs, in the field of view of the camera. The temperature inside the behavioral chamber was minimally affected by the high intensity photostimulation. After illumination using the highest available intensities of blue, green or red LEDs (1.1, 0.67 and 1.27 mW/mm^2, respectively) for 1 minute, the biggest change in ambient temperature, detected using a thermocouple inserted into the chamber, was 0.7 °C.

Behavioral experiments and quantification of behaviors

For experiments to activate Gr5a-GRNs, flies were mounted into 200 μl pipetman tips as described previously[12]. Mounted flies were placed beneath high power LEDs and PERs were monitored using a videocamera. Mounted flies were not placed in the behavioral chamber, but placed at the same location as the wells of behavioral chamber in supplementary figure 1b. Bouts of PER were counted manually. Definition of bouts: a bout starts when flies start extending their proboscis, and ends when they retract the proboscis. Incomplete proboscis extensions were not counted. LEDs were used at maximum intensities in Figs. 1b, c and 2d, e (Red: 1.1 mW/mm^2, Amber: 0.22 mW/mm^2, Green: 0.67 mW/mm^2, and Blue: 1.27 mW/mm^2). For Fig.1b, 100msec photostimulation trials (1 Hz) were delivered (3 trials) and flies showing more than one PER during this activation period were counted as responders. Fly genotype: w-;Gr5a(II);GR5a(III)/*UAS-ReaChR*(VK5) (Fig. 1b-g); w-;Gr5a(II)/*UAS-dTrpA1*(II);GR5a(III)/*UAS-dTrpA1* (III) (Fig. 1h).

To activate Crz neurons (Fig. 2 d_2), males expressing each opsin in crz-GAL4 neurons were mounted dorsal side down on a glass slide as previously described[25]. Flies were illuminated using the maximum available intensity of light for each type of LED, continuously for 1 minute, while monitoring them from the ventral side using a video camera. The number of flies exhibiting ejaculation during light stimulation was manually

counted.

For all other behavioral experiments, we used acrylic behavioral chambers (16mm diameter) in a 2 x 4 array (Fig. 2 and Supplementary Fig. S1) to monitor fly behavior. Unless otherwise indicated, chambers were photostimulated using the maximum intensity available for each LED, for 1 minute using continuous illumination, while monitoring them with the camera from above. The number of flies showing continuous side-walking during stimulation using the HB9-GAL4 driver was manually counted (Fig. 2 d_1,f). Fru-GAL4 neurons were activated in the same manner, and flies showing wing extension or knock-out phenotypes were counted manually (Fig. 2 d_3,g). Knock-out was defined as the cessation of locomotion and loss of postural control. Flies that showed a weaker behavioral phenotypes (HB9, side walk; Fru, wing extension) at the onset of photostimulation, but that were knocked out before the 1 minute stimulation was terminated, were counted as knock-out flies (Fig. 2f, g).

Wing extension evoked by activation of P1 or pIP10 neurons was manually scored (Fig. 3-5). Grooming (rapid wing movements while touching with hind leg) was excluded. Definition of bouts: a bout starts when flies begin to increase the wing angle, and ends when they stop decreasing it.

Measurement of light intensity

A photodiode power sensor (Thorlab, Inc: S130VC) was placed at the location of the behavioral chamber. The peak wavelength of each LED (Red: 627 nm, Amber: 590 nm, Green: 530 nm, Blue: 470 nm) was measured at different voltage inputs. Measurements were repeated 4 times and averaged. The baseline intensity of each wavelength before LED illumination was subtracted. Note that light intensity can drop during stimulation at high input voltages. In this study, intensity after 10 sec of stimulation was measured.

Measurement of penetrance of different wavelengths of light through the fly cuticle

A 400 μm multimode optic fiber (N.A. 0.48. Thorlab, Inc) was inserted into the fly abdomen. The amount of light entering the optic fiber inside or outside the fly was measured using a power meter (Model 1931, New port). Penetrance was calculated as the amount of light that entered the optic fiber inside the fly, divided by

the amount of light measured outside the fly. The long axis of the optic fiber was always aligned with the light source. Different wavelengths of high power LEDs (470 nm, 530 nm, 590 m, 627 nm) and mercury lamp combined with band-pass filters (Leica, 425/40 nm (center wavelength/band width)) were used as light sources.

Fly histology

All fixation and staining procedures were performed at 4 °C in PBS, unless otherwise specified. Dissected brains were fixed in 4% formaldehyde in PEM (0.1M PIPES, pH 6.95, 2mM EGTA, 1mM MgSO4) for 2 hours. After three 15 min rinses with PBS, brains were incubated with primary antibodies overnight. Following three 15 min rinses with PBS, brains were incubated with secondary antibody overnight. Following three 15 min rinses, brains were incubated in 50% glycerol in PBS for 2 hours and cleared with VECTASHIELD® (VECTA). All procedures were performed at 4 °C. A Fluoview™ FV1000 Confocal laser scanning biological microscope (Olympus) with a 30×, 1.05 N.A. silicone oil objective (Olympus) was used to obtain confocal serial optical sections. The antibodies used for Supplementary fig. 2a,d were: anti-GFP, rabbit polyclonal antibody unconjugated (invitrogen) and Alexa Fluor® 488 donkey anti Rabbit IgG(H+L) (invitrogen). Both of the antibodies were diluted to 1/300. Expression of mCherry in Supplemental figure 2d was monitored using native fluorescence without antibody staining.

Fluorender software (Wan et al., 2009) (http://www.sci.utah.edu/software/13-software/127-fluorender.html) was used to make 3D image reconstructions. To measure the expression levels of ReaChR::citrine in P1 neurons in fig. 6c, the native fluorescence of citrine in different specimens was monitored using the same intensity of laser power (470 nm) and PMT voltage. Signal intensity was quantified in imageJ (http://rsbweb.nih.gov/ij/).

Calcium imaging

Two-photon imaging was performed on an Ultima two-photon laser scanning microscope (Prairie Technology) with an imaging wavelength of 925nm (Fig. 6). To filter out auto-fluorescence of the brain and light from the amber stimulation LED (for ReaChR activation), we used a 500/20 nm (center wavelength/band

width) band-pass filter (Chroma) in the emission pathway to detect the GCaMP3 fluorescence. The scanning resolution was 128 × 128 pixels, dwell time per pixel was 8 μsec, and the optical zoom was ×4. The scanning speed was ca.10 Hz. The excitation intensity of the 2-photon laser was varied among samples depending on the level of GCaMP3, but always lower than 20 mW/mm^2.

In both cases, a 40×, 0.80 N.A. water-immersion objective (Olympus) was used for imaging. A high power amber LED (590 nm) collimated with an optic fiber (Thorlab: M590F1) was used as a light source to activate ReaChR. To narrow the band width of the LED output, we connected the optic fiber to a fiber optic filter holder (World Precision Instruments) equipped with 589/10 nm (center wavelength/band width) bandpass filter (Edmund optics). A ⌀200 μm core multimode optic fiber (N.A. 0.39) (Thorlab: FT200EMT) was used to deliver the light from the fiber optic holder to the brain. One side of the optic fiber was custom-made to be a bare tip (Thorlab) and was dipped into the saline imaging bath and placed 430 μm away from the brain. A 10×, 0.30 N.A. water-immersion objective (Olympus) was used to locate the brain and align the optic fiber. The distance between brain and the fiber was measured with an objective micrometer (Olympus). We set the light intensity to be 170 μW at the tip of optic fiber. Thus, at a distance of 430 μm from the tip of a 0.39 N.A. optic fiber, the light power is calculated to be approximately 1.7 mW/mm^2 at the brain surface (the size of light spot should be approximately 0.10 mm^2 at the brain). In addition to the PMT used to monitor GCaMP emissions, we used another PMT to monitor the 590 nm ReaChR activation light. This was to ensure that the intensities of 590 nm light were comparable between samples.

To prepare the brain for imaging, an ex-vivo prep was used. After a brief anesthesia on ice, the brain was dissected out using a sharp forceps into a 35 mm plastic petri dish (FALCON®, 35 3001) containing Drosophila *imaging* saline (108mM NaCl, 5mM KCl, 2mM $CaCl_2$, 8.2mM MgCl2, 4mM NaHCO3, 1mM NaH2PO4, 5mM Trehalose, 10mM Sucrose, 5mM HEPES, pH 7.5)(Wong et al., 2002). The fat body, air sacs, and esophagus were gently removed to give a clear view of the brain and to minimize its movement. The brains were attached to the bottom of the plate by static. The saline was changed once after dissection to remove debris. Calcium imaging was performed within 10-15 minutes after the dissection to ensure that the brains were healthy.

Electrophysiology

The tip recording method was used to record the electrophysiological responses of labellar taste neurons (Hodgson et al., 1955Hodgson et al., 1955). Briefly, the fly was mounted and immobilized for recording by inserting a pulled glass capillary (BF150-86-10, Sutter instruments) from the dorsal surface of the thorax to the tip of the labellum, passing through the cervical connective and the head. The mounting glass capillary was filled with recording solution (7.5 g/L NaCl, 0.35 g/L KCl, 0.279 g/L CaCl2·2H2O and 11.915 g/L HEPES (Sigma-Aldrich)) and served as a ground electrode. Another glass capillary, pulled to a tip diameter of 10 to 20 micrometers and filled with 30 mM tri-choline chloride (TCC; Sigma-Aldrich), as an electrolyte, was used for recording the electrophysiological responses of the gustatory neurons innervating this sensillum. All the recordings were obtained from L7 sensilla. The recordings were made using a MultiClamp 700B amplifier and Digidata 1440A A/D converter (Molecular Devices). The recorded data was sampled at a rate of 10 kHz, filtered (band pass filter between 100 Hz and 3 kHz) and stored on a PC hard drive using Clampex 10 software (Molecular Devices). The data were analyzed by sorting the action potentials and measuring their frequency within the indicated time windows using Clampfit software (Molecular Devices).

For PER activation experiments, a high power amber LED (590 nm) collimated with an optic fiber (Thorlab: M590F1) was used as a light source to activate ReaChR. To deliver light to the labellum a ⌀200 μm core multimode optic fiber with bare end (N.A. 0.39) (Thorlab) was used. The distance of optic fiber from the labellum was set to be 540 μm using a micrometer. The estimated light intensity at the labellum was approximately 1.0 mW/mm^2.

To activate TrpA1 (Fig. 1h), a custom-made heat source was used. In brief, the heat source is a small piece of thermistor (2K Bead Thermistor, Fenwal), which emits heat in proportion to the electrical current passed through it. The distance of the heat source from the labellum was set to be 540 μm using micrometer. The temperature at this distance was measured using a thermocouple (Omega) (top panel in Fig. 1h).

Donnelly, M.L., Hughes, L.E., Luke, G., Mendoza, H., ten Dam, E., Gani, D., and Ryan, M.D. (2001). The 'cleavage' activities of foot-and-mouth disease virus 2A site-directed mutants and naturally occurring '2A-like' sequences. J Gen Virol *82*, 1027-1041.

Hodgson, E.S., Lettvin, J.Y., and Roeder, K.D. (1955). Physiology of a primary chemoreceptor unit. Science *122*, 417-418.

Li, M.Z., and Elledge, S.J. (2007). Harnessing homologous recombination in vitro to generate recombinant DNA via SLIC. Nat Methods *4*, 251-256.

Pfeiffer, B.D., Jenett, A., Hammonds, A.S., Ngo, T.T., Misra, S., Murphy, C., Scully, A., Carlson, J.W., Wan, K.H., Laverty, T.R.*, et al.* (2008). Tools for neuroanatomy and neurogenetics in Drosophila. Proc Natl Acad Sci U S A *105*, 9715-9720.

Wan, Y., Otsuna, H., Chien, C.B., and Hansen, C. (2009). An Interactive Visualization Tool for Multi-channel Confocal Microscopy Data in Neurobiology Research. Ieee T Vis Comput Gr *15*, 1489-1496.

Wong, A.M., Wang, J.W., and Axel, R. (2002). Spatial representation of the glomerular map in the Drosophila protocerebrum. Cell *109*, 229-241.